

Copyright

by

Rebecca Leigh Leonard

2014

**The Thesis Committee for Rebecca Leigh Leonard  
Certifies that this is the approved version of the following thesis:**

**A First-Principles Directional Drilling Simulator for Control Design**

**APPROVED BY  
SUPERVISING COMMITTEE:**

**Supervisors:**

---

Eric van Oort

---

Mitchell Wayne Pryor

**A First-Principles Directional Drilling Simulator for Control Design**

**by**

**Rebecca Leigh Leonard, B.S.M.E.**

**Thesis**

Presented to the Faculty of the Graduate School of

The University of Texas at Austin

in Partial Fulfillment

of the Requirements

for the Degree of

**Master of Science in Engineering**

**The University of Texas at Austin**

**December 2014**

## **DEDICATION**

For my MeMe.

## ACKNOWLEDGEMENTS

Few people are capable of encouraging and inspiring others the way in which Dr. van Oort can those around him. His enthusiasm for academia and the oil and gas industry fueled my passion for this field – from the very first day of his Introduction to Well Construction course in January of 2012. This was the first day of class at The University of Texas for each of us, and it is incredible to look back at everything that has been accomplished since that day. Thank you, Dr. van Oort, for your unwavering support while I “created myself” over the past three years. I look forward to building upon our work for many years to come.

Mitch, I cannot thank you enough for your continuous availability and willingness to contribute to my perpetual state of improvement over the past few years. I appreciate all of your input and assistance in making my thesis one of which we are all proud. Your patience and flexibility got me through it. Thank you.

A million “thanks” to Mark Dykstra for the countless hours he spent coaching me in his field of study. I think I learn something new every time we sit down to talk, and I am still amazed at your ability to stifle “I told you so” after I insist on doing things my way. Thank you so much for your patience and guidance.

Paul Daley and Mark Anderson – thank you for giving me the freedom to set my own priorities while I worked to earn my graduate degree. The work environment you both worked to create is quite conducive to striking a balance between industry and academia. Thank you for all of the opportunities to develop myself.

Thank you to Joey Roth for getting me into this mess and making it so much fun. To Olivier Hoffman and Yongsong Cai – I appreciate your mentorship more than you know. Jason, Tex, Chad, and Dion – what can I say? Thank you for reminding me not to take myself so seriously and for your never-ending patience with my incessant requests for data. Your coaching helped me keep everything in perspective.

Most importantly, thank you to my family. No words could express the reasons.

## **ABSTRACT**

### **A First-Principles Directional Drilling Simulator for Control Design**

Rebecca Leigh Leonard, M.S.E.

The University of Texas at Austin, 2014

Supervisors: Eric van Oort and Mitchell Wayne Pryor

A directional drilling simulator was constructed using a re-formulation of first-principles classical mechanics in order to serve as a platform for advanced control design. Dedicated focus was placed on building a modular solution that would interface with an existing Supervisory Control And Data Acquisition (SCADA) architecture. Model complexity was restricted to include only the features required to make an immediate step change in tool face control performance through more accurate determination of torsional dead time and time constant values. Development of this simulator advanced the art of drilling automation by building a foundation upon which developers may design novel control schemes using big data gathered in the modern oilfield.

This first-principles model is supported by theoretical formulation of equations of motion that capture fundamental behavior of the drill string during both rotary and slide drilling operations. Wellbore trajectory was interpolated between survey points using the Minimum Curvature Method, and a semi-soft-string drill string model was assumed. Equations of motion were derived using energy methods captured in both Hamiltonian

and Lagrangian mechanics and solved using the finite-element method. Transient dynamic solutions were obtained using Newmark integration methods.

A sensitivity analysis was conducted to determine which parameters played the most influential roles in dynamic drill string behavior for various operational scenarios and to what extent those parameters influenced torsional dead time and time constant calculations. The torsional time constant was chosen as a measure of correlation between case studies, due to the significant role this value plays in state-of-the-art tool face control algorithms. Simulation results were validated using field data collected from rigs using a SCADA system to operate in various shale plays in North America. Results from field tests were used to compare torsional time constant values calculated using manually-determined, simulation-based, and analytical methods and investigate directional drilling performance over a range of operational scenarios.

Simulation-based time constant calculation results were consistently more accurate than analytically-determined values when compared to manually-tuned values. The first-principles directional drilling simulator developed for this study will be adopted by the existing SCADA system in order to standardize and improve slide drilling performance.

# TABLE OF CONTENTS

<b>DEDICATION</b>	<b>iv</b>
<b>ACKNOWLEDGEMENTS</b>	<b>v</b>
<b>ABSTRACT</b>	<b>vi</b>
<b>TABLE OF CONTENTS</b>	<b>viii</b>
<b>LIST OF TABLES</b>	<b>xii</b>
<b>LIST OF FIGURES</b>	<b>xiv</b>
1 Introduction.....	1
1.1 Background Information.....	1
1.1.1 Motivation.....	1
1.1.2 Slide Drilling vs. Rotary Drilling.....	2
1.1.3 Conventional Drilling vs. Automated Drilling .....	6
1.2 Research Objectives.....	9
1.3 Approach.....	9
1.4 Deliverables .....	10
1.5 Thesis Outline .....	11
2 Literature Review.....	12
2.1 Physical Principles .....	12
2.1.1 Drill String Loads .....	12
2.1.2 Dynamic Drill String Behavior.....	14
2.1.2.1 Axial Drill String Dynamics .....	14
2.1.2.2 Torsional Drill String Dynamics.....	15
2.1.2.3 Lateral Drill String Dynamics.....	16
2.1.2.4 Coupled Drill String Dynamics.....	17
2.2 Drilling Engineering Concepts .....	19
2.2.1 Modeling Techniques.....	19
2.2.1.1 Wave Equation .....	19

2.2.1.2	Finite Differences .....	21
2.2.1.3	Boundary Elements .....	21
2.2.1.4	Finite Elements.....	21
2.2.2	Torque and Drag Analysis .....	23
2.2.3	Engineering Tools and Methods .....	26
2.3	Drilling Automation: The State of the Art .....	27
2.3.1.1	Research Initiatives .....	28
2.3.1.2	Service Company Technologies.....	29
2.3.1.3	Operator Technologies .....	32
2.4	Summary .....	35
3	Theoretical Development.....	37
3.1	Model Input Parameters .....	38
3.1.1	Surface Equipment.....	39
3.1.1.1	Hoisting Equipment.....	39
3.1.1.2	Rotary Equipment .....	41
3.1.1.3	Circulating Equipment .....	42
3.1.2	The Drill String .....	42
3.1.3	Down-Hole Motor.....	45
3.1.4	Bit .....	48
3.1.5	Drilling Fluid .....	50
3.1.6	Casing and Formation Characteristics .....	52
3.2	Well Trajectory .....	53
3.2.1	Survey Data Inputs.....	53
3.2.2	Wellbore Interpolation via Minimum Curvature Method.....	55
3.3	Finite Element Discretization .....	59
3.3.1	Physical Explanation.....	59
3.3.2	Mass Matrix .....	64
3.3.3	Stiffness Matrix.....	64
3.3.4	Damping Matrix.....	65
3.3.5	External Force Vector .....	65

3.4	Summary .....	65
4	Numerical Analysis.....	68
4.1	Boundary Conditions .....	68
4.1.1	Surface Contributions .....	68
4.1.2	Wellbore Constraints .....	69
4.1.3	Bit Boundary Conditions - Off-Bottom .....	71
4.1.4	Bit Boundary Conditions - On-Bottom.....	71
4.2	Drill String Discretization.....	73
4.3	Drill String /Wellbore Interaction.....	75
4.4	Internal Forces .....	76
4.5	Torque and Drag Loads .....	77
4.6	Newmark Beta Integration.....	79
4.7	Model Characteristics and Sensitivities .....	83
4.7.1	Static Analysis .....	83
4.7.2	Step Change Analyses.....	85
4.7.2.1	Block Speed.....	85
4.7.2.2	Top Drive RPM.....	86
4.7.2.3	Pump Rate .....	87
4.7.3	Model Sensitivities.....	88
4.7.3.1	Drill String Composition.....	88
4.7.3.2	Well Trajectory .....	92
4.7.3.3	Operating Parameters .....	96
4.7.3.4	Viscosity and Friction Effects .....	101
4.7.3.5	Formation Characteristics .....	102
4.8	Summary.....	102
5	Experimental Results and Discussion.....	104
	Overview .....	104
5.1	Appalachia Case Study .....	105
5.2	Groundbirch Case Study .....	113
5.3	Key Performance Indicators and Value Assessment .....	125

5.4	Summary .....	127
6	Conclusions and Recommendations for Future Work .....	130
	Overview .....	130
	6.1 Summary of Work.....	131
	6.2 Future Work .....	134
	Appendix A.....	136
	Vertical Well Trajectory .....	136
	Build Well Trajectory .....	136
	Slant Well Trajectory.....	136
	Lateral Well Trajectory.....	136
	Appalachia .....	137
	Groundbirch F4-15.....	137
	Groundbirch E4-15 .....	138
	Appendix B.....	140
	Groundbirch F4-15 Long-Lateral, Slim-Hole Design .....	141
	Groundbirch F4-15 BHA Summary.....	142
	Appendix C.....	146
	Nomenclature.....	148
	References.....	151
	Vita .....	164

## LIST OF TABLES

Table 3.1:	Drill string elements are defined using a standard set of parameters. ....	43
Table 3.2:	Drill string dynamics are influenced by a set of parameters that are calculated using parameters found in Table 3.1.....	44
Table 3.3:	Bit aggressiveness varies according to bit type and formation characteristics. [SIEP, 2009].....	50
Table 3.4:	Experimentally-determined friction coefficients characterize casing-tool joint interaction for various drilling fluid compositions. [Bol, “Effect of mud composition on wear and friction...” 1986] .....	52
Table 3.5:	Khulief and Al-Naser used simplified drill string configuration specifications to conduct modal and dynamic response analysis using the finite-element method. [Khulief and Al-Naser, 2005].....	66
Table 4.1:	Uniform drill pipe and motor assembly – 1,000’ total in length. ....	83
Table 4.2:	Drill String #1: Uniform Drill Pipe and Motor Assembly .....	89
Table 4.3:	Drill String #2: Drill Pipe, Drill Collars, and Motor Assembly.....	90
Table 4.4:	Drill String #3: Drill Pipe, HWDP, Drill Collars, and Motor Assembly.....	91
Table 4.5:	Rate of penetration and top drive RPM set-point changes were made over a 60-second time interval.....	96
Table 5.1:	This drill string composition was used to simulate transient behavior for the Appalachia case study.....	107
Table 5.2:	Simulation-based time constant calculations generally fall between analytically-determined and manually-entered values.....	108

Table 5.3:	This table includes key components of the F4-15 directional plan and relevant comments for each section of the well. The highlighted sections are included in this analysis. A comprehensive, interpolated directional plan can be found in Appendix A.....	116
Table 5.4:	Groundbirch wells F4-15 and E4-15 were compared using key performance indicators to assess tool face control performance metrics.....	127
Table B.1:	This table outlines the BHA model used in the Appalachia case study.....	140

## LIST OF FIGURES

- Figure 1.1: A bent-housing mud motor is used to orient the tool face and turn the bit during slide drilling operations. [Mitchell & Miska, 2011].....2
- Figure 1.2: Free-body diagrams are shown to compare forces acting upon a drill string element during slide and rotary drilling operations. Note the absence of axial drag ( $w_d$ ) in the free-body diagram for rotating pipe. [Mitchell & Miska, 2011] .....3
- Figure 1.3: Rotary vs. slide drilling ROP is compared for various shale formations in North America. Best-in-class wells in the Marcellus shale are drilled with 165 ft/hr rotating ROP and 70 ft/hr sliding ROP. [Shell, 2014] .....4
- Figure 1.4: System dead time ( $T_d$ ) and time constant ( $\tau$ ), are calculated through analysis of system response to a step change in system input ( $Y$ ). .....5
- Figure 1.5: Data shows that the torsional time constant increases with measured depth, especially in lateral sections of the wellbore. This chart presents data collected on Shell Rig-1 while drilling in the Marcellus. [Shell, 2013] .....6
- Figure 1.6: Real-time drilling data trends compare tool face controller performance while using an analytically-determined time constant (bad slide) vs. the manually-tuned time constant (good slide). The magenta and red lines mark the time at which the dead time and time constant are altered within the system – noting the transition from bad to good control performance. ....7
- Figure 1.7: A three-tiered path to drilling automation was presented by Aldred et al. in 2012. This demonstrates the potential for advancement in the field of drilling automation, where Tier 3 is the ultimate industry goal.....8

Figure 2.1: A schematic comparison between Euler-Bernoulli Beam Theory and Timoshenko Beam Theory highlights the absence of shear forces in the Euler-Bernoulli force diagram. [paulino.cee.illinois.edu] .....13

Figure 2.2: Rate of penetration improvements on the order of 200% (sliding) and 25% (rotating) were achieved using the NOV Drilling Agitator Tool (DAT). [NOV, 2014] .....15

Figure 2.3: Richard et al. represent the drilling system using a discrete model characterized by the axial and torsional degrees of freedom. [Richard et al., 2005] .....18

Figure 2.4: Dareing and Livesay modeled the drill string as an elastic wire cable. [Dareing and Livesay, 1968].....20

Figure 2.5: A mesh sensitivity analysis is required to achieve convergence for various drill string components. Results published by Ghasemloonia demonstrate that the pipe section requires a finer mesh to converge than the collar section, due to the geometrical characteristics of the material. [Ghasemloonia et al., 2013] .....22

Figure 2.6: Florence et al. published a timeline of auto-driller development, which highlights the evolution of braking equipment and control system technology. [Florence et al., 2009] .....27

Figure 2.7: Schlumberger’s Slider is a torque rocking technology that increases sliding rate of penetration by breaking friction forces along the drill string. This graphic demonstrates the difference between sliding ROP while drilling manually (5.8 ft/hr) vs. while drilling with Slider (16.1 ft/hr). [Schlumberger, 2014] .....30

Figure 2.8: CANRIG's ROCKIT technology uses a position-based top drive control algorithm to oscillate the drill string and deliver more weight to the bit, which facilitates faster drilling rates. [CANRIG, 2014] .....	31
Figure 2.9: NOV's IntelliServ technology delivers increased rate of penetration through integration of rig instrumentation systems and high-speed telemetry. [NOV, 2014] .....	32
Figure 2.10: Shell's SCADAdrill system (Blue) has evolved to the point at which it is capable of drilling faster than a manual driller/directional driller (Red). .....	33
Figure 2.11: Shell's SCADAdrill system uses a 4 degree-of-freedom rotary drilling system model, where the top drive and bottom-hole assembly are represented using damped, lumped masses that are connected via a spring with axial and torsional compliance. ....	34
Figure 2.12: The Shell SCADAdrill drilling system simulator uses a 3D lookup table to interpolate rate of penetration using bit speed (RPM) and axial load (WOB) values. ....	35
Figure 3.1: The drilling system model developed for this study incorporates various sub-systems. ....	38
Figure 3.2: The draw-works model used in this study is a simplified representation of a drilling rig hoisting system. [Bommer, 2008].....	39
Figure 3.3: An axial velocity (ROP) command is issued to the draw-works. The block and hook is modeled as a point mass, and a proportional-integral controller characterizes hoisting response.....	40
Figure 3.4: The top drive is suspended from the traveling block, and axial position is set through manipulation of the block speed. [Bommer, 2008] .....	41

Figure 3.5: A rotary speed (RPM) command is issued to the top drive. The top drive is modeled as a point mass, and a proportional-integral controller characterizes rotary compliance.....	42
Figure 3.6: A bent sub is placed above the down-hole motor to create a deflection assembly by applying a side-force at the bit. Unconstrained and constrained drill string configurations are shown in (a) and (b), respectively. [Mitchell and Miska, 2009] .....	45
Figure 3.7: This cross-section of down-hole motor highlights dimensions that affect motor torque and speed.....	46
Figure 3.8: Physical motor characteristics can be used to build power curves that are referenced during drilling operations. [Mitchell and Miska, 2009].....	47
Figure 3.9: This comparison illustrates how bit aggressiveness varies by bit type.....	48
Figure 3.10: Bit-rock interaction is modeled as a cylinder pressing against a flat plate...49	
Figure 3.11: Cased- and open-hole friction factors are assigned based on the measured depth of each drill string node. ....	53
Figure 3.12: Measured depth, inclination, and azimuth values characterize a three-dimensional well trajectory and dogleg severity values along the wellbore.	54
Figure 3.13: The Minimum Curvature Method uses adjacent survey points to interpolate the well trajectory using a circular arc formulation. ....	55
Figure 3.14: The Minimum Curvature Method uses a coordinate reference frame based on North, East, and Vertical coordinates. ....	56
Figure 3.15: Dogleg severity is a function of the changes in inclination and azimuth between two points at known depths. ....	57
Figure 3.16: The position vector of a subsequent survey point is a function of the measured depth and unit tangent vectors that characterize those points. ....	58

Figure 3.17: Distributed gravitational forces act upon a drill string element in an inclined wellbore.....	61
Figure 3.18: A drill string element is defined by 2 nodes, and each node has 2 degrees-of-freedom. ....	62
Figure 3.19: Generalized displacements define coefficients that are used to interpolate degrees-of-freedom between nodes. ....	63
Figure 4.1: ROP and RPM set points are system inputs that govern hook load and surface torque inputs, respectively, based on PI controller characteristics...69	
Figure 4.2: In the semi-soft-string drill string model, the drill string lies on the low side of the wellbore, where tool joints mark points of contact.....	70
Figure 4.3: An illustration of the off-bottom scenario demonstrates how bit boundary conditions are defined. ....	71
Figure 4.4: An illustration of the on-bottom scenario demonstrates how bit boundary conditions are defined. ....	72
Figure 4.5: This illustration of the drill string discretization process shows how component length, discretization length, element count, node count, and element length are defined. ....	74
Figure 4.6: Example of a scenario in which a drill string component length is not a multiple of the discretization length. ....	74
Figure 4.7: Geometrical characteristics of a tubular drill string component. ....	75
Figure 4.8: Internal tension and torsion forces acting on drill string elements. ....	76
Figure 4.9: Gravitational ( $F_G$ ), normal ( $F_N$ ), torque ( $T$ ), and drag ( $F_D$ ) loads act on a drill string component in an inclined wellbore while internal tension forces ( $F_T$ ) affect normal force contributions.....	77

Figure 4.10: Johancsik et al. calculated friction coefficients from surface torque and drag data for several wells. [Johancsik et al., 1984] .....	79
Figure 4.11: The simulation routine uses survey data, drill string composition, formation characteristics, and auxiliary system parameters to calculate well trajectory and analyze system loads and dynamic behavior at each time step.....	82
Figure 4.12: Drill pipe stretch at various locations is verified analytically in a vertical wellbore. This graph shows the displacement between surface and bit nodes for the drill string configuration described in Table 4.1. ....	84
Figure 4.13: Drill pipe velocity and accelerations match first-principles analytical solutions at various points along the drill string. ....	84
Figure 4.14: A block speed step test was performed to tune hoisting equipment controllers and validate the finite-element drill string model in the axial domain.....	85
Figure 4.15: A top drive RPM step test was performed to tune rotary equipment controllers and validate the finite-element drill string model in the torsional domain. Figure 4.16 shows the region of interest in greater detail.....	86
Figure 4.16: The region of interest for transient torsional response is located at the time at which the step change is introduced. ....	87
Figure 4.17: This model does not capture transient behavior for fluid dynamics initiated at the mud pumps. Instead, changes in flow rate immediately manifest pressure effects at the down-hole motor, which affects bit RPM. ....	88
Figure 4.18: Axial displacement and torque transmission vs. time for Drill String #1- described in Table 4.2. ....	89
Figure 4.19: Axial displacement and torque transmission vs. time for Drill String #2- described in Table 4.3. ....	90

Figure 4.20: Axial displacement and torque transmission vs. time for Drill String #3- described in Table 4.4. ....	91
Figure 4.21: Drill string composition affects transient torsional response.....	92
Figure 4.22: Vertical, build, slant, and lateral well plans are compared to demonstrate how well trajectory affects dynamic simulation results.....	93
Figure 4.23: Wellbore orientation affects static drill string forces. These plots compare gravitational, tension, and normal forces for vertical, build, slant, and lateral wells. ....	94
Figure 4.24: Wellbore orientation affects transient torsional response.....	95
Figure 4.25: Axial and torsional dynamics are affected by changes in operating parameters and boundary conditions. ....	97
Figure 4.26: Torque transmission behavior is dependent upon the magnitude of the disturbance and boundary conditions.....	98
Figure 4.27: Step changes in axial and angular velocity set-points affect the system differently as boundary conditions change. ....	98
Figure 4.28: Weight-on-bit is a key factor that affects the torsional time constant. This parameter is controlled using hook load measurements. Notice that the two values mirror each other when on-bottom. ....	99
Figure 4.29: Rate of penetration is a function of weight- and torque-on-bit.....	99
Figure 4.30: Excessive wellbore friction factors lead to system instability. ....	101
Figure 5.1: Appalachia well plans include vertical, build, hold, and lateral section.....	106
Figure 5.2: Analytical calculations generally under-estimate the torsional time constant value that produces satisfactory tool face control results in the lateral section of Appalachia wells.....	110

Figure 5.4: Projected torsional dead time and time constant values for Groundbirch F4-15 match the trend uncovered during the Appalachia case study.....	117
Figure 5.5: Experimental results from the Groundbirch case study were consistent with trends uncovered during the Appalachia case study, i.e. the simulation-based torsional time constant generally fell in-between the analytical and manually-entered values. ....	119
Figure 5.6: Tool face control performance comparison between two wells at the first kick-off point. ....	121
Figure 5.7: Tool face control performance comparison between two wells in the tangent section. ....	122
Figure 5.8: Tool face control performance comparison between two wells at the second kick-off point. ....	123
Figure 5.9: Tool face control performance comparison between two wells in the tangent section. ....	124
Figure B.1: Groundbirch elected to drill long, slim-hole laterals with open-hole completions on the 4-15 pad.....	141
Figure B.2: Groundbirch F4-15 required an extra bit trip and aggressive build rate near the heel, due to directional issues encountered while drilling the build and turn section.....	143
Figure B.3: F4-15 and E4-15 were drilled using the same bit model but different motor bends (1.5 degrees compared to 1.83 degrees, respectively) to approximately 1,850 m MD. Then, F4-15 drilled the heel with a less aggressive bit. ....	144
Figure B.4: The Halliburton MegaForce bit is a more aggressive, matrix-body bit used to drill upper-well sections on both F4-15 and E4-15. This bit was also used to drill the lower-well section on E4-15. ....	145

Table B.5: The less-aggressive, conventional Halliburton FX bit was used to drill the lower-build section on F4-15.....	145
Figure C.1: The Stribeck friction model calculates TOB as a function of bit RPM.....	146
Figure C.2: This plot shows how a lower Rayleigh damping constant affects axial response to a step change.....	147
Figure C.3: This plot shows how a lower Rayleigh damping constant affects torsional response to a step change.....	147

# **1 Introduction**

One of the biggest challenges in the field of drilling automation is the development of control algorithms that manipulate operational parameters to drill a prescribed well trajectory quickly and efficiently. Automation engineers lack a physically-meaningful model and simulation platform for use in developing improved control algorithms. This thesis presents a physics-based, directional drilling simulator that may be used as a test bed for the development of control algorithms to ultimately achieve the following objectives:

1. Decrease the amount of time it takes to orient the tool face while sliding.
2. Improve the ability to maintain the desired tool face while sliding.

Simulation results are validated against field data using a state-of-the-art Supervisory Control And Data Acquisition (SCADA) drilling system. An emphasis is placed on the investigation of the torsional time constant and its relationship with the principles of tool face control – comparing simulation results to conventional prediction analytics and manually-tuned control parameters.

## **1.1 BACKGROUND INFORMATION**

### **1.1.1 Motivation**

Implementation of best practices through drilling automation offers a way to maximize efficiency, safety, and reliability of drilling operations – enabling well delivery teams to drive down costs and improve performance. In an industry generally reluctant to change, it can be difficult to convince key stakeholders that it is worth the disruption of the status quo to adopt novel technologies. One of the easiest ways to prove that drilling technology is worth the investment is through demonstration of decreased cost per foot to deliver a well using that tool or process. Increased Rate Of Penetration (ROP) is one way

to quantify success. Cost savings as a function of ROP improvement is calculated using the following relationship:

$$\text{ROP Improvement (\%)} \times \text{On-Bottom Drilling Time (days)} \times \text{Spread Rate} \left( \frac{\$}{\text{day}} \right) = \text{Savings (\$)}$$

Onshore, improvements in drilling performance could generate savings on the order of \$1M/year (CANRIG, 2014). Offshore, the value of comparable performance improvement gains increases exponentially, due to the increased operational costs associated with operating in an offshore environment.

### 1.1.2 Slide Drilling vs. Rotary Drilling

In *rotary drilling* operations, the top drive transmits torque to the bit via the drill string in order to maintain the current well trajectory. In *slide drilling* operations, wellbore inclination and azimuth is controlled using a bent-housing mud motor to rotate the bit without rotating the drill string from surface. Figure 1.1 shows a typical steerable motor configuration.

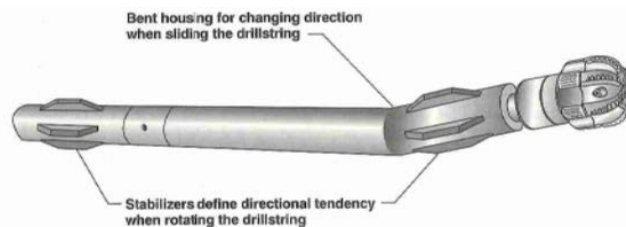


Figure 1.1: A bent-housing mud motor is used to orient the tool face and turn the bit during slide drilling operations. [Mitchell & Miska, 2011]

In rotary drilling mode, drill string rotation causes axial friction forces to diminish, minimizing drag effects along the wellbore. Friction forces are more detrimental while slide drilling than while rotary drilling, due to the absence of drill string rotation. Figure 1.2 presents free-body diagrams for sliding and rotating pipe elements to illustrate this phenomenon.

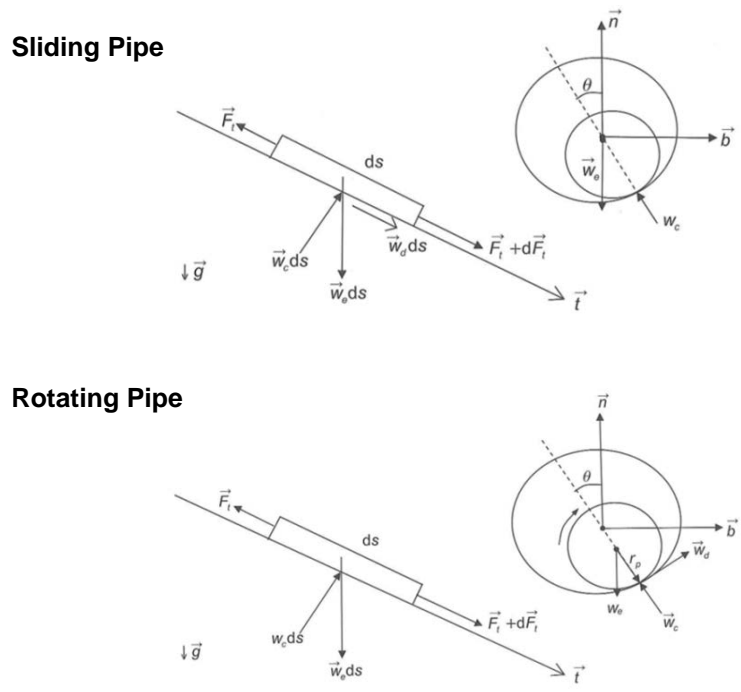


Figure 1.2: Free-body diagrams are shown to compare forces acting upon a drill string element during slide and rotary drilling operations. Note the absence of axial drag ( $w_d$ ) in the free-body diagram for rotating pipe. [Mitchell & Miska, 2011]

Axial force is transferred to the bit more effectively in the absence of drag loads while rotary drilling. Because ROP is a function of Weight On Bit (WOB), rotary drilling ROP is generally greater than slide drilling ROP. On a typical land well in North America, approximately 5-10% of the total well footage is spent sliding [Shell, 2014]. However, the time spent sliding may exceed 20% of the total drilling time on a single well [CANRIG, 2005-2010]. Figure 1.3 shows a comparison of rotary vs. slide drilling ROP for various shale formations in North America.

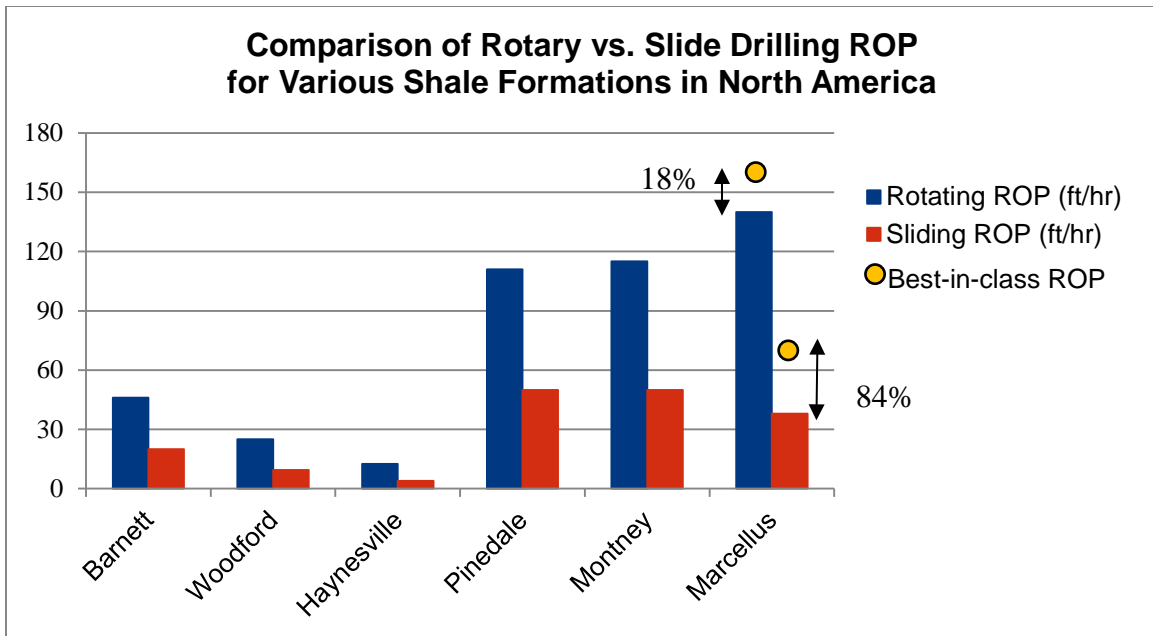


Figure 1.3: Rotary vs. slide drilling ROP is compared for various shale formations in North America. Best-in-class wells in the Marcellus shale are drilled with 165 ft/hr rotating ROP and 70 ft/hr sliding ROP. [Shell, 2014]

In order to increase slide drilling ROP, the driller may oscillate the top drive, introducing surface torque sufficient to rotate the drill string just enough to break friction forces along the wellbore without altering tool face. This method becomes increasingly useful as the depth and lateral step-out of a well increases. However, the success of the implementation relies on the driller's understanding of the torsional dead time and time constant.

*Dead Time ( $T_d$ )* is defined as the time delay between top drive rotation and tool face rotation. A dead time of 4 seconds means that if the top drive starts rotating, the tool face should start rotating 4 seconds later. The *Time Constant ( $\tau$ )* is the time that it takes the tool face to reach 63% ( $1 - 1/e$ ) of its final value, where  $e$  is a mathematical constant representing the base of the natural logarithm. For example, if the torsional time constant is 8 seconds, and the tool face is commanded to rotate 10 degrees, it will take 8 seconds

for the tool face to rotate 6.3 degrees after the top drive starts rotating. Figure 1.4 illustrates this concept as it relates to angular velocity.

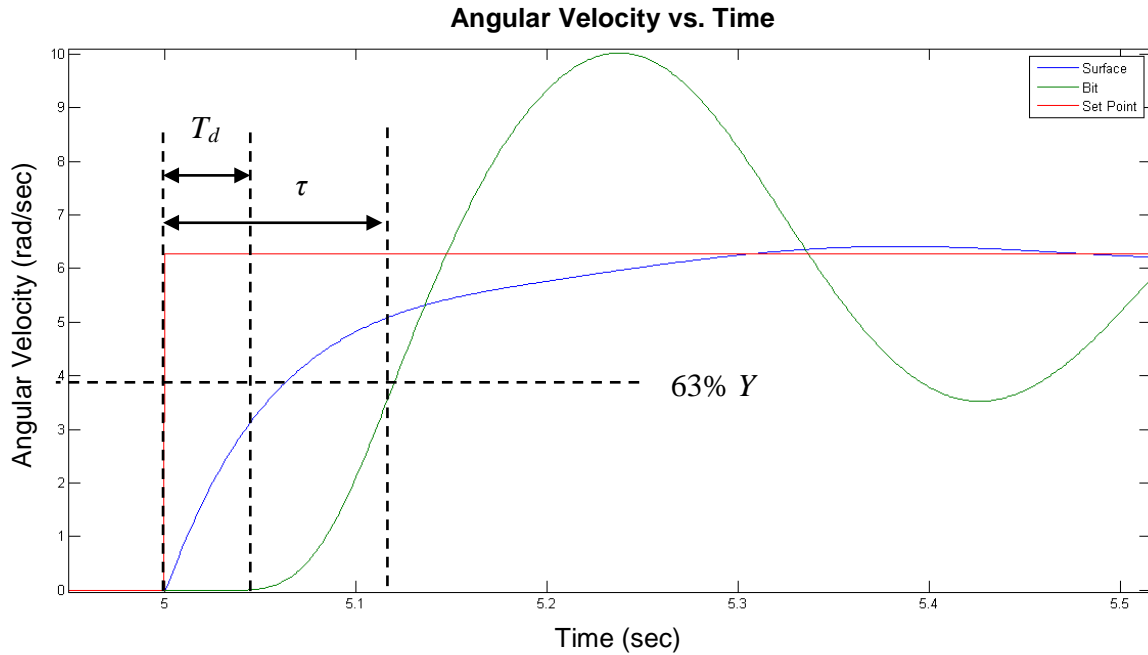


Figure 1.4: System dead time ( $T_d$ ) and time constant ( $\tau$ ), are calculated through analysis of system response to a step change in system input ( $Y$ ).

Figure 1.5 shows how the torsional time constant increases throughout the lateral section of a wellbore. This trend is a result of increased friction forces along the wellbore, due to interaction between the drill string and the formation. For reference, the time constant in an intermediate, vertical well section is generally 2-3 seconds. [Shell, 2014]

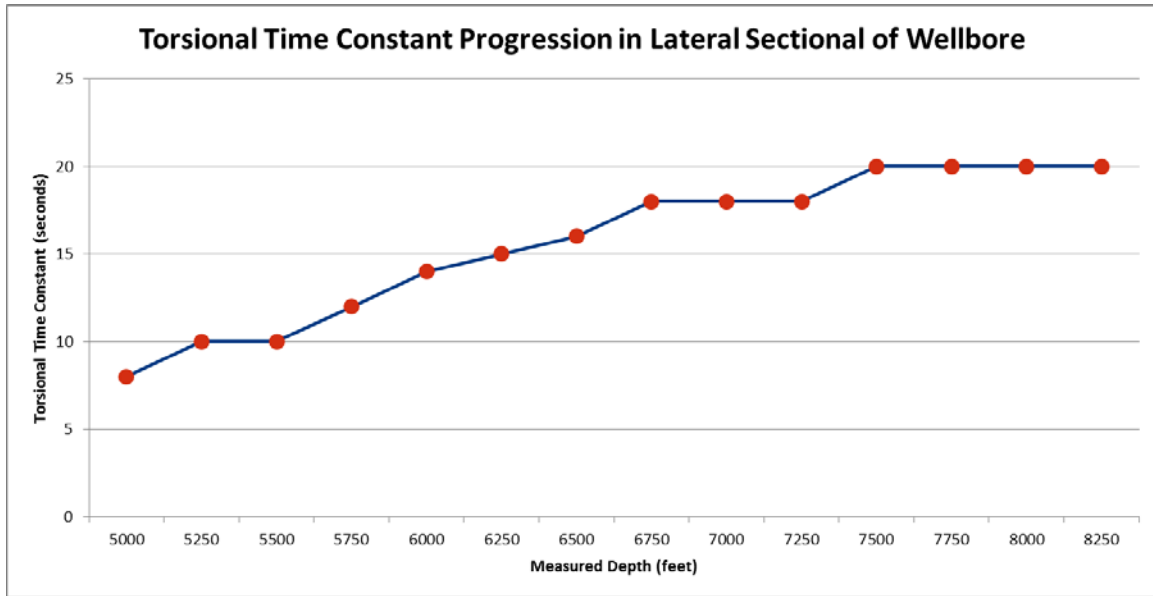


Figure 1.5: Data shows that the torsional time constant increases with measured depth, especially in lateral sections of the wellbore. This chart presents data collected on Shell Rig-1 while drilling in the Marcellus. [Shell, 2013]

### 1.1.3 Conventional Drilling vs. Automated Drilling

Human drillers and auto-drillers both use the following parameters to maximize ROP while drilling:

1. Axial force, i.e. hook load and WOB
2. Torque
3. Differential Pressure

State-of-the-art auto-drillers are capable of out-performing a human driller using multi-parameter, supervisory control algorithms [Shell, 2014]. Current computing and sensor technology makes it possible for SCADA systems to process thousands of data points – streamed from surface and down-hole tools on the order of 250 milliseconds – which far exceeds the human capacity to respond to the same signals. However, modern

auto-drillers are actually only semi-autonomous control systems. System operators are required to tune SCADA controllers in real-time by inputting time constant values that enable the system to maintain tool face and achieve ROP set points. Operators collect system tares corresponding to force, torque, and pressure and correlate how tool face response changes with respect to drilling conditions and operational set points. In some cases, this process requires completion of several tare sequences to determine how long it takes for a tool face control set point to translate to the bit. Figure 1.6 shows a side-by-side comparison of tool face control performance using an analytical, SCADA-calculated torsional time constant vs. a manually-tuned torsional time constant; manual entries consistently deliver superior tool face control results. [Shell, 2014]

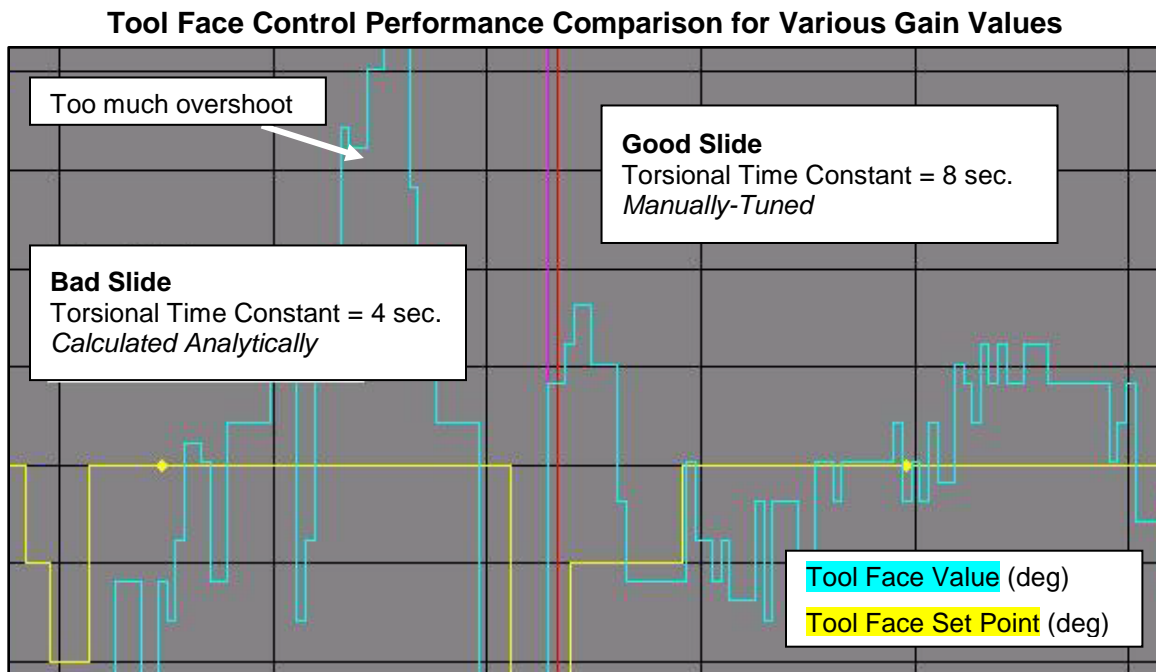


Figure 1.6: Real-time drilling data trends compare tool face controller performance while using an analytically-determined time constant (bad slide) vs. the manually-tuned time constant (good slide). The magenta and red lines mark the time at which the dead time and time constant are altered within the system – noting the transition from bad to good control performance.

Key Performance Indicators (KPI's) that relate to tool face control performance include:

1. Number of slides required to reach target
2. Average and total slide time and length
3. Hole tortuosity

Aldred et al. [2012] present a three-tiered path to automation (Figure 1.7). The physical model presented in this thesis is a stepping stone between Tier 2 and Tier 3, and it is a critical enabling technology necessary to achieve the long-term goal of fully-automated drilling. This simulator delivers the capability to accurately predict and automatically update system time constants in real time, eliminating the requirement that an experienced directional driller constantly monitor and manipulate control variables. This achievement enables SCADA systems to act autonomously by auto-tuning control parameters while drilling ahead – achieving Tier 3.

<b>Tier 3</b>	10. Decides everything and acts autonomously.
	9. Executes an action automatically and informs the driller only if it takes action.
	8. Executes an action and informs the driller only if asked.
<b>Tier 2</b>	7. Executes an action automatically, then necessarily informs the driller.
	6. Allows the driller a restricted time to veto an action before automatic execution.
	5. Secects and executes a suggestion if the driller approves.
<b>Tier 1</b>	4. Suggest a single course of action.
	3. Offers a set of alternatives and narrows the selection.
	2. Offers a complete set of decision and action alternatives.
	1. Offers no assistance; driller must make all decisions and take action.

Figure 1.7: A three-tiered path to drilling automation was presented by Aldred et al. in 2012. This demonstrates the potential for advancement in the field of drilling automation, where Tier 3 is the ultimate industry goal.

## **1.2 RESEARCH OBJECTIVES**

The goal of this thesis is to deliver a physically-meaningful drill string dynamics model and simulation platform that may be used to develop and test fully-automated directional drilling control algorithms. Key objectives leading to this goal are as follows:

1. Develop and validate a physics-based drilling system model that includes key parameters affecting drill string dynamics within a three-dimensional wellbore during rotary and slide drilling operations.
2. Create a simulation platform that makes use of realistic system inputs, capturing transient system dynamics.
3. Carry out a sensitivity analysis to develop an understanding of how key parameters affect system response.
4. Quantitatively compare the torsional time constant to prediction analytics vs. manually-tuned values entered by SCADA operators while drilling.
5. Provide recommendations for future work – citing specific observations made over the course of the project.

## **1.3 APPROACH**

This drilling system model is established using a re-formulation of first-principles classical mechanics. The physical model is supported by theoretical formulation of equations of motion that capture both rotary and slide drilling operations by coupling axial and torsional dynamics. The wellbore trajectory is interpolated between survey points using the Minimum Curvature Method (MCM), and a pseudo-soft-string model was used to describe drill string dynamics. Equations of motion are derived using energy methods capture in both Hamiltonian and Lagrangian mechanics and solved using the finite-element method. Transient dynamic solutions are obtained using Newmark integration methods.

The simulation routine resides in MATLAB – using programming constructs that translate directly to Programmable Logic Controller (PLC) language for future control

system design. Model inputs and outputs are designed to interface with an existing SCADA architecture in order to correlate various parameters and ensure a fair comparison of simulation results against field data.

The torsional time constant calculated using this drilling simulator is compared to existing prediction analytics and those calculated by the SCADA operators in real-time. The validation criteria are as follows:

1. Tool face control performance is quantified using percent-variance and standard deviation analyses to evaluate KPI's and establish acceptable control response standards. Normalized data is used to compare performance for various wells.
2. The torsional time constant calculated using the drilling simulator yields superior tool face control performance compared to that generated using the two-degree-of-freedom model within the existing SCADA architecture.
3. The torsional time constant calculated using the drilling simulator improves tool face control performance to the extent that SCADA slide drilling ROP exceeds the average driller slide drilling ROP.

#### **1.4 DELIVERABLES**

This presentation delivers a first-principles directional drilling simulator that lends itself to control design by characterizing how changes in ROP, top drive RPM, and pump speed affect transient drill string dynamics in a three-dimensional wellbore. The following considerations characterize this directional drilling model:

- Wellbore orientation
- Lithology
- Drilling fluid properties
- Friction effects
- Drill string composition
- Down-hole motor characteristics

- Bit aggressiveness
- Operational parameters

The simulator produces the following results at each time step:

- Position, velocity, and acceleration of each node
- Tension and torsion in each element
- Torque, drag, and normal force at each node
- Hook load and surface torque (control parameters)
- WOB and TOB

This information is used to characterize the nature of the torsional time constant as the wellbore orientation changes with increasing measured depth. The final product of this analysis is a proven method that can be used to estimate the torsional time constant in real-time as a well is being drilled.

## **1.5 THESIS OUTLINE**

This thesis is separated into 6 chapters. Chapter 1 provided an introduction to the problem, as well as relevant background information required to understand the remainder of this presentation. In Chapter 2, a comprehensive literature review of pertinent material is presented in order to outline the current state of the art and opportunities for advancement of the science of drilling automation, specifically in the realm of improved tool face control algorithms. Chapter 3 introduces the theoretical concepts that support the physical model. Underlying mathematical and physical principles are discussed in detail, leading up to the presentation of the equations of motion that describe this first-principles model. The numerical methods and simulation processes used to solve these equations of motion are presented in Chapter 4. Experimental results and analyses covering a range of operational scenarios are presented and discussed in Chapter 5. The final chapter offers conclusions drawn from this study, as well as recommendations for future work that build upon the work presented herein.

## **2 Literature Review**

The following sections summarize publications relating to physical principles, engineering techniques, and technological developments in the fields of directional drilling and drilling automation.

The first section presents investigations into underlying physical principles of directional drilling operations. This section outlines how researchers worked to verify physical drilling system behavior using analytical and experimental methods.

The second section outlines the evolution of engineering best practices in the field of directional drilling and describes methods used to automate drilling processes. This section covers the evolution of operational applications, goals, and objectives.

The third section highlights the state of the art of drilling automation, with an emphasis on technologies that advanced directional drilling automation over the years.

The final section of this chapter provides context for this research contribution in the field of drilling automation and outlines how results advance the state of the art.

### **2.1 PHYSICAL PRINCIPLES**

#### **2.1.1 Drill String Loads**

Traditional drill string models are framed by classical differential equations that support Timoshenko beam theory. [Timoshenko, 1936] Many drill string models adopt the simplified, linear theory of elasticity by modeling the drill string as an Euler-Bernoulli beam – neglecting shear deformation and rotational inertial effects. [Love, 1944] Figure 2.1 provides a schematic comparison of the forces that govern Euler-Bernoulli and Timoshenko Beam Theory.

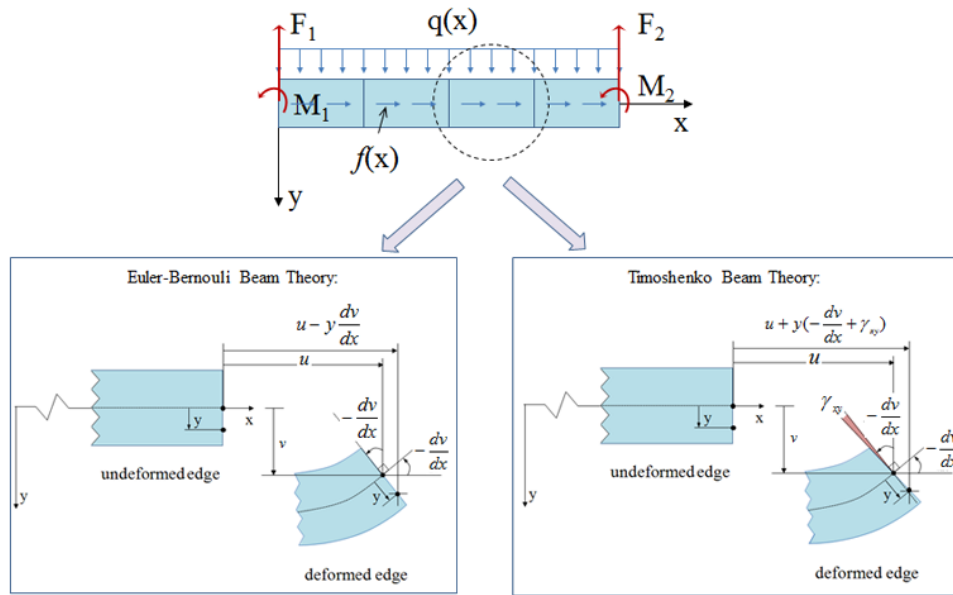


Figure 2.1: A schematic comparison between Euler-Bernoulli Beam Theory and Timoshenko Beam Theory highlights the absence of shear forces in the Euler-Bernoulli force diagram. [paulino.cee.illinois.edu]

In 1950, Lubinski published a mathematical formulation to investigate buckling of rotary drill strings using the theory of elastic stability. This study led Lubinski to perform a follow-up examination of key factors affecting directional tendencies in rotary drilling applications. Lubinski's detailed analyses of drill string forces, bending moments, and stresses laid the foundation for future drill string load analysis studies. [Lubinski, 1950; Lubinski and Woods, 1953] In 1974, Fischer published a detailed analysis of drill strings in curved boreholes, providing a tool for drilling engineers to use in drill string design and casing wear exercises. [Fischer, 1974] In 1977, Walker and Friedman presented a three-dimensional force and deflection analysis of a variable, cross-section drill string more reflective of traditional Timoshenko beam theory, considering shear deformation and rotational inertia effects. [Walker and Friedman, 1977]

Although the Timoshenko beam model may be more suitable for certain applications, it is more computationally-demanding to analyze in real-time. Nordgren

published a computational method to evaluate the motion of elastic rods, comparing traditional Timoshenko and Euler-Bernoulli formulations [Nordgren, 1973]. In 1986, Ho presented a comprehensive comparison of mathematical drill string formulations, citing the work of Lubinski, Fischer, Walker, and Friedman, among others. [Ho, 1986]

## **2.1.2 Dynamic Drill String Behavior**

### ***2.1.2.1 Axial Drill String Dynamics***

Axial vibrations occur along the longitudinal axis of the drill string. Both static and dynamic loads are placed on the drill string and measured by investigating Hook Load (HL) or WOB trends. If the axial load exceeds the critical WOB that is determined by drill string composition, buckling will occur [Lubinski, 1987] Operational guidelines are developed based on anticipated static and dynamic loads to meet certain criteria, like equipment limits or penetration rate targets. Safety factors are built into this operational envelope to account for inaccuracies that can occur as a result of model characteristics that affect load predictions. [Dunayevsky et al., 1993]

In 1985, Dareing published evidence that controlled axial vibrations can increase ROP by chipping away at the formation and breaking friction forces along the wellbore to improve weight transfer to the bit. [Dareing, 1985] This revelation set in motion the development of various tools to control axial drill string dynamics, such as down-hole agitators that break friction forces along the wellbore. For example, NOV's Drilling Agitator Tool (DAT) reduces stick slip and improves tool face by inducing low frequency, low amplitude vibrations at the BHA (Figure 2.2). [NOV, 2014]

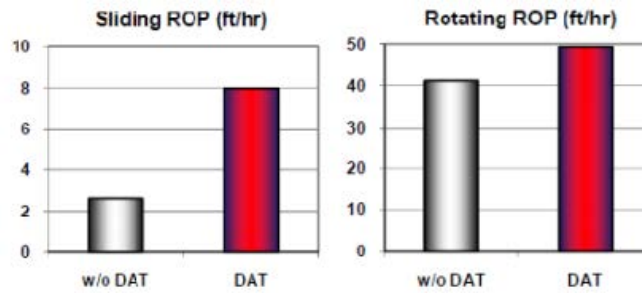


Figure 2.2: Rate of penetration improvements on the order of 200% (sliding) and 25% (rotating) were achieved using the NOV Drilling Agitator Tool (DAT). [NOV, 2014]

### 2.1.2.2 Torsional Drill String Dynamics

Due to the slender, cylindrical geometry of drill string components, frictional losses along the wellbore cause incongruences between top drive and bit rotary speed. In 1984, Daring used advanced sensors and data collection techniques to investigate key factors affecting drill string vibration and developed control guidelines based on his findings. [Daring, 1984a, 1984b]

Torsional dynamics can be transient or steady-state. Transient dynamics occur as a result of localized variations in drilling conditions, i.e. rock formation changes or hole cleaning conditions, while steady-state vibrations take place over an extended period of time. Brett delivers a thorough explanation of the origin of torsional drill string vibrations using a combination of laboratory drilling data and a lumped-parameter mass/spring system model formulation. [Brett, 1992] Smit provides a complimentary explanation on the criticality of torsional dynamics in drilling performance optimization in his dissertation on using optimal control techniques to dampen torsional drill string vibrations. [Smit, 1995]

Torsional time constant and dead time are factors not explicitly addressed in drilling automation studies to date. Although vibration mitigation studies indirectly address wave propagation characteristics, the majority of analyses are carried out in the frequency domain.

### ***2.1.2.3 Lateral Drill String Dynamics***

Lateral vibrations are the leading cause of drill string and BHA failures [Vandiver et al., 1990; Chin, 1988; Mitchell and Allen, 1985]. In comparison to torsional vibrations, lateral vibrations are more dispersive and occur at higher frequencies, causing lateral vibrations to dissipate rapidly and attenuate before reaching the surface [Payne et al., 1995]. Recent advances in down-hole sensor and MWD technology enabled researchers to design and conduct experiments that improve understanding of the severity and implications of lateral vibrations.

The primary causes of lateral vibrations are bit/formation and drillstring/borehole interactions [Aadnoy et al., 2009]. Because all vibration modes are coupled, axial and/or torsional vibrations also give rise to lateral vibrations. Additionally, mass imbalance of drill string components can be a major source of down-hole lateral vibrations [Dykstra et al., 1996].

Researchers began studying lateral drill string vibrations in the 1960's, and various models and techniques have been developed to capture and control lateral dynamics. The two most common techniques are (1) closed-form solutions and (2) finite-element discretization. Although varied degrees of success have been reached with the closed-form solution approach [Lichuan and Sen, 1993], the FEM supports a more versatile approach to this complex problem. Chen and Geradin [1995], Christoforou and Yigit [1997], and Frohrib and Plunkett [1967] studied various ways to determine natural frequencies of the drilling system. Mitchell and Allen [1985], Plunkett [1967], and Spanos et al. [1997] calculated critical bending stresses. Vaz and Patel [1995] analyzed system stability. Dykstra [1996] and Yigit and Christoforou [1998] examined ways to predict lateral displacements of drilling assemblies. Yigit and Christoforou [1998] took their analysis a bit further by identifying critical failure parameters and conditions that trigger lateral-to-torsional energy transfer that inflicts drillstring vibrations.

Although the finite-element is the widely-utilized approach to lateral vibration modeling, a continuous-lateral-vibration model can be constructed. For a continuous model, the Euler-Bernoulli beam theory is used, assuming small slopes [Aadnoy et al.,

2009]. The equations constructed using the continuous-lateral-vibration model can be solved using various numerical methods, and the finite-element technique is well-documented in publications such as Przemieniecki [1968], Reddy [1993], and Raftoyiannis and Spyarakos [1997].

#### ***2.1.2.4 Coupled Drill String Dynamics***

Drilling systems are highly nonlinear, making the analytical expression of dynamic behavior complex. Drill string vibration modes can occur individually or simultaneously, meaning it is possible to observe all three vibration modes (axial, torsional, and lateral) at the same time. Several factors play a role in the coupling between forces. For example, an initial curvature in the BHA will relate axial forces at the bit to lateral bending in the drill string. Vandiver et al. suggested the following analogy to aid in the understanding of this principle: “Linear coupling is easy to visualize by taking a thin ruler or piece of paper, giving it a slight curve, and then pressing axially on the ends. The object responds by additional bending in the plane of the initial curvature.” [Vandiver et al., 1990] While analogies like this one may help make drill string dynamics easier to visualize, it is relationships such as the one described above that increase the complexity behind modeling and simulation of drilling systems.

Some drilling problems can be addressed by considering only one vibration mode. Other studies require the consideration of coupled drill string dynamics. Traditionally, models that couple axial and torsional dynamics lend themselves to stick-slip analysis and control design. Richard et al. used a discrete drill string model with coupled axial and torsional dynamics to explore the root cause of stick-slip. Their model accounts for frictional losses resulting from drill string interaction with the wellbore, as well as and cutting behaviors at the bit/rock interface. A point mass  $M$ , a moment of inertia  $I$ , and a spring of torsional stiffness  $C$ , represent the BHA and drill pipe. Boundary conditions are characterized by the mechanical properties of the drill string and the bit-rock interaction law described in their paper. Figure 2.3 illustrates the representation of these drilling system model characteristics. [Richard et al., 2005]

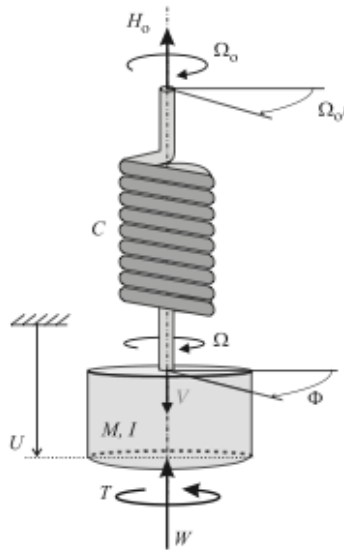


Figure 2.3: Richard et al. represent the drilling system using a discrete model characterized by the axial and torsional degrees of freedom. [Richard et al., 2005]

In 1996, Dykstra published a comprehensive characterization of drill string vibration. The theoretical analysis was based on first-principles, using energy methods to derive nonlinear relationships that govern dynamic drilling behavior. These equations were solved using the FEM. Dykstra used the Newmark- $\beta$  integration approach to evaluate transient and steady-state drill string behavior. [Dykstra, 1996]

In 1997, Yigit and Christoforou used a Lagrangian approach to investigate fully-coupled axial and transverse dynamics. Their analysis included consideration of gyroscopic moments, drill string-wellbore contact, axial excitation, and hydrodynamic damping in the presence of drilling fluid. The authors used a Rayleigh beam model with simply-supported boundary conditions at stabilizer locations. The following year, Yigit and Christoforou derived a lumped-parameter drill string model that coupled torsional and lateral dynamics to investigate the extent to which lateral motion influences stick-slip behavior. This model assumes consistent drill string contact with the wellbore and captures rolling behavior with and without drill collar slip. The authors concluded that the

lateral contribution to stick-slip behavior is significant, especially once a stick-slip cycle is initiated. Therefore, Yigit and Christoforou used this model as a basis for the development of stick-slip mitigation control algorithms in future publications. [Yigit and Christoforou, 1998, 2000, 2006]

In 2003, Christoforou and Yigit developed a fully-coupled, physics-based model that lends itself to control. This simplified, lumped-parameter model was derived using a Lagrangian approach and a continuous representation of the drill string. Stabilized sections were modeled as a simply-supported beam, and drill collars were assumed rigid in the torsional degree of freedom. [Christoforou and Yigit, 2003]

## **2.2 DRILLING ENGINEERING CONCEPTS**

### **2.2.1 Modeling Techniques**

Various drill string models were developed over the years to capture transient dynamics in both the frequency and time domains. This section contains an overview of the most prominent drill string dynamics models, including primary applications and characteristics. In general, the Society of Petroleum Engineers (SPE) publishes studies pertaining to commercial tools and performance improvement, while the Institute of Electrical and Electronics Engineers (IEEE) and American Society of Mechanical Engineers (ASME) publish studies that address underlying physics and control strategy.

#### ***2.2.1.1 Wave Equation***

The un-damped, classical wave equation provides a continuous result and allows for analysis of axial and torsional dynamics at any point along the drill string. However, it is often difficult to find a closed-form solution in the presence of nonlinearities or ambiguous forcing functions. For that reason, discretized solutions are more often utilized in the industry, in spite of their increased computational requirements. Wave equation models are generally analyzed in the frequency domain and used to address problems related to frequency-induced drill string vibrations. In 1960, Baily and Finnie used the wave equation to conduct an analytical study of drill string vibration using an

iterative method to obtain natural frequencies of the drilling system, considering axial and torsional vibrations independently. In 1968, Dareing and Livesay introduced viscous damping considerations in their model formulation developed to investigate axial drill string dynamics. An illustration of the drilling system model used for this study is shown in Figure 2.4. [Dareing & Livesay, 1968] Refer to the following publications for more examples of wave equation models and their applications: [Bradbury and Wilhoit, 1963; Dareing, 1984b; Craig, 1981]

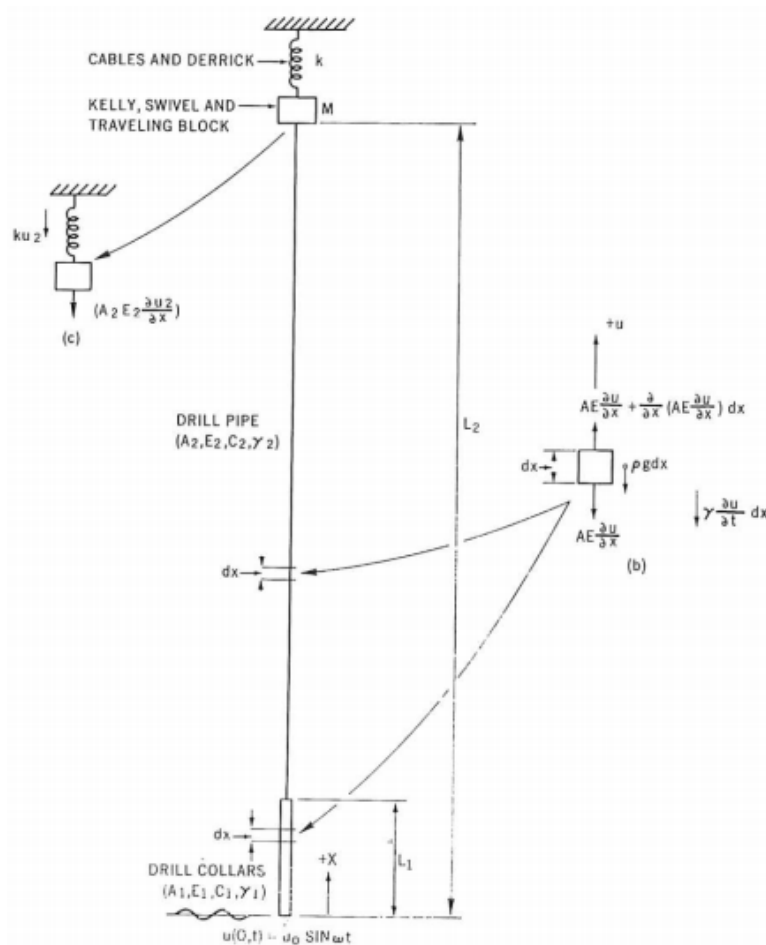


Figure 2.4: Dareing and Livesay modeled the drill string as an elastic wire cable. [Dareing and Livesay, 1968]

### ***2.2.1.2 Finite Differences***

Finite differences can be computed in three different forms: (1) forward difference, (2) backward difference, or (3) central difference. The finite difference method provides a way to approximate derivatives for the numerical solution of differential equations. Precision is lost when round-off and/or truncation errors grow to the point where the true solution is no longer sufficiently represented in the approximated solution. Bathe [1982] and Thomson and Dahleh [1997] detailed explanations of the finite difference method.

### ***2.2.1.3 Boundary Elements***

Systems of linear, partial, differential equations can be solved using the Boundary Element Method (BEM). The BEM uses boundary conditions to fit boundary values first, before formulating solutions at other points in a “post-processing” phase. This method is often more efficient than other methods, because it requires less computational effort. However, storage and computational requirements grow in proportion to the square of the problem size, whereas finite element matrices are generally banded. An assessment should be done on a somewhat case-by-case basis to deduce which method is most efficient for a specific application. The BEM is explained in greater detail by Brebbia et al. [1984], Burnett [1987], and Chen and Zhou [1992].

### ***2.2.1.4 Finite Elements***

The Finite Element Method (FEM) is recognized as the modern industry standard numerical method used to analyze dynamic drill string behavior. Most researchers agree that a reasonable level of accuracy can be achieved through using the FEM. However, the growing demand for increasingly-comprehensive analyses calls for a more computationally efficient method to execute real-time simulations. Still, most industry publications over the past several decades utilize the FEM, because this method lends itself to the geometric complexity of a drilling system and the large-scale nature of the problem. [Khulief and Al-Naser, 2005] A sensitivity analysis, such as the one

demonstrated in Figure 2.5, should be carried out in order to determine the mesh parameters required to achieve convergence for various parts of the drill string.

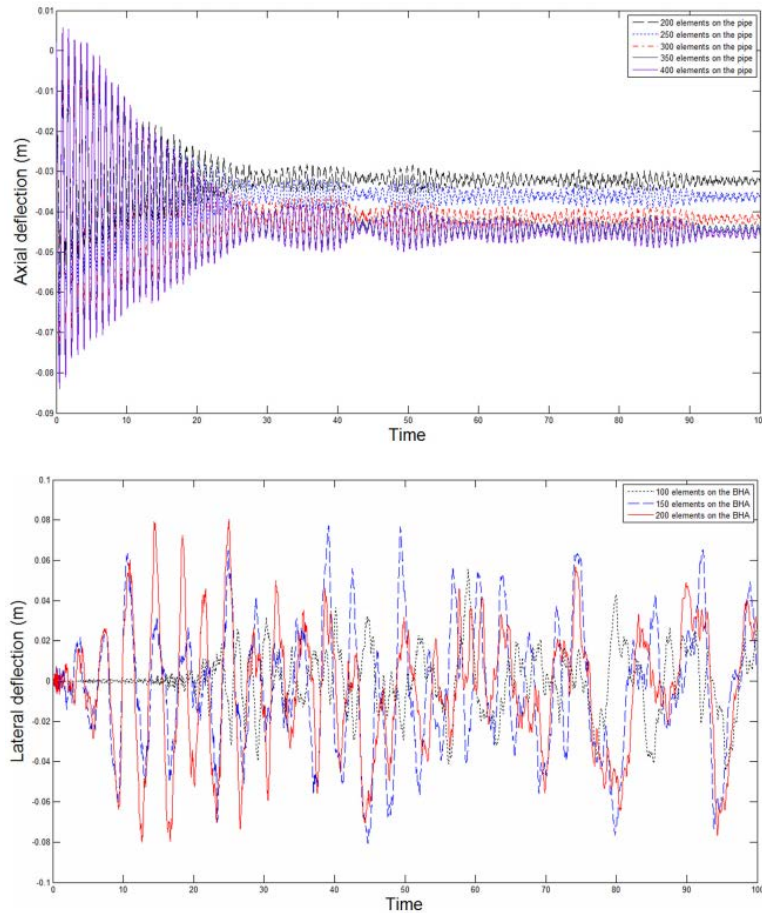


Figure 2.5: A mesh sensitivity analysis is required to achieve convergence for various drill string components. Results published by Ghasemloonia demonstrate that the pipe section requires a finer mesh to converge than the collar section, due to the geometrical characteristics of the material. [Ghasemloonia et al., 2013]

In 1978, Millheim et al. published a detailed BHA analysis using the FEM, examining stress, displacements, side forces, and dynamic response. Millheim et al. used a Lagrangian energy approach to derive equations of motion for four BHA configurations

with varying tendency to hold, build, or drop angle. Simulation results were consistent with field data, demonstrating that it is possible to characterize complex, dynamic BHA behavior using known information about the well trajectory, wellbore dimensions, drilling fluid density, and BHA dimensions. The inputs and outputs of this simulation initiative are similar to that of this presentation. [Millheim et al., 1978]

In 2005, Khulief and Al-Naser published a finite-element, dynamic analysis of drill strings, including drill pipe and drill collars. This model was formulated using a Lagrangian approach, including consideration of gyroscopic effects, coupling of torsional and bending inertia, and gravity. Each drill string component with a circular cross-section was discretized with 12 degrees-of-freedom. This publication includes a thorough literature review of historic FEM formulations. [Khulief and Al-Naser, 2005]

For more examples of this approach, refer to [Bathe and Wilson, 1976; Melakhessou et al., 2003; Przemieniecki, 1968; Reddy, 1993; Costa and Rebeiro, 1997; Apostol et al., 1990; Axisa and Antunes, 1990; Antunes et al., 1990; Dunayevsky et al., 1993; Berlioz et al., 1996; Schmalhorst et al., 2000].

### **2.2.2 Torque and Drag Analysis**

In 1971, Mason and Taylor proposed a wellbore trajectory model made up of circular arc sections, commonly referred to as the Minimum Curvature Method (MCM). Mason and Taylor proposed the use of cubic splines to describe a wellbore with continuous slope but discontinuous curvature. Zaremba followed up in 1973 by proposing the almost-identical Circular Arc Method. In 2003, Sawaryn and Thorogood published “A Compendium of Directional Calculations Based on the Minimum Curvature Method,” which presents directional algorithms in a consistent, vector form that is less computationally demanding to program and test. Although other wellbore trajectory interpolation models, such as the constant-curvature and constant-turn-rate methods, were also developed to investigate implications of discontinuities along the well path, the MCM has been recognized as an industry standard since the mid-1980’s. [Sawaryn and Thorogood, 2003]

In 1973, Johancsik et al. published the original paper on drill string torque and drag, building the foundation upon which torque and drag analysis is still performed today. Johancsik set out to develop a model capable of predicting frictional loads on the drill string along the wellbore in order to establish drill string and well design standards that minimize torque and drag. In Johancsik's torque and drag model, the drill string is represented as a lumped-parameter system. The underlying assumption is that all torque and drag is caused by sliding friction forces, due to contact between the drill string and the wellbore. Shear forces are neglected, and this model is commonly referred to as a *soft-string* model. A soft-string model implies that the drill string lies along the low-side of the wellbore, taking the shape of the well trajectory. In this case, Johancsik uses the MCM to calculate the well trajectory and assumes a linear Coulomb friction to model torque and drag forces along the drill string. [Johancsik et al. 1973]

In 1987, Sheppard et al. put the torque and drag model into standard form to perform a detailed analysis on the influence of well geometry on torque and drag. Further, Sheppard emphasized the importance of the consideration of mud pressure in torque and drag calculations, building upon Johancsik's model to include buoyancy forces acting on the drill string along the wellbore. Sheppard's model is considered the industry standard in torque and drag analysis. [Sheppard et al. 1987]

In 1988, Ho published "An Improved Modeling Program for Computing the Torque and Drag in Directional and Deep Wells", which combines a stiff-string BHA model with an improved soft-string drill pipe model to capture the effects tortuosity on torque and drag. Ho's conclusions include the recommendation that very deep vertical wells should be handled as directional wells, as a result of compounded tortuosity effects. Further, Ho confirmed that torque and drag increases exponentially with depth. [Ho, 1988]

In 1989, Lesso et al. published results in support of the soft-string torque and drag model proposed by Sheppard. Lesso used Sheppard's torque and drag model in combination with field friction data published by Lesage et al. [1988], Johancsik et al. [1973], and Falconer et al. [1989] to predict total torque losses for a collection of

directional wells in the Beaufort Sea. Lesso's work demonstrated the feasibility of using a single platform to develop an entire field, when excessive drill string torque historically limited platform design. [Lesso et al. 1989]

In 1997, Payne and Abbassian published a series of field case studies that they used to calibrate torque and drag models in the presence of fluctuating drilling parameters and operating conditions. Their results provide insight into key torque and drag factors affecting extended-reach drilling operations, including torque and drag projection and management, friction factor variability, and well trajectory design. [Payne and Abbassian, 1997]

In 2007, Mitchell published a comprehensive torque and drag model that includes the consideration of shear forces. Unlike the soft-string model, this *stiff-string* model formulation allows all drill string moment equations to be satisfied. The following year, Mitchell challenged the assumption that the Minimum Curvature Method is a valid assumption for wellbore shape. Instead, Mitchell proposed a wellbore trajectory model in which spline functions are derived from stiff-string drill string dynamics. Mitchell claims that this method is more appropriate for torque and drag analysis, because the bending moment is not smooth at survey points. Mitchell's model was shown to predict higher contact loads and produce more accurate results for demanding wellbores with high build rates. However, this method is more computationally expensive than the traditional MCM. [Mitchell, 2007; Mitchell, 2008]

In 2013, Tikhonov et al. published a dynamic model for stiff string torque and drag, including simulation results supporting their formulation. The authors reported major differences in the location and magnitude of contact forces produced using the stiff string model vs. the soft string model. Although these results are noteworthy, the complexity of the numerical algorithm makes this model too computationally-expensive for widespread implementation. [Tikhonov, 2013]

Bradbury and Wilhoit [1963] conducted a study on the effect of tool joints on passages of plane longitudinal and torsional waves along a drill pipe. This frequency-based analysis produced results supporting the hypothesis that tool joints have negligible

effect for exciting frequencies on the same order as common rotary speeds during drilling operations. However, this study did not include an analysis of the effect of tool joints on torque and drag calculations. In 2013, Mitchell et al. published a drill string analysis with a discrete torque and drag model, using tool joints to define the points that relate drill string position with a minimum-curvature well trajectory. [Mitchell et al., 2013] The results published by Mitchell et al. support the drill string model formulation used to develop the directional drilling simulator for this thesis.

### **2.2.3 Engineering Tools and Methods**

Engineers and researchers leverage their understanding of drilling dynamics to develop tools and methods that optimize drilling performance. Common applications of drill string dynamics models include bit design and selection, BHA component design and configuration, and system loading and stability analysis and prediction. Applications supported by advanced dynamic models have improved drilling performance and reduced equipment failure frequency. [Dykstra et al., 2001] Drilling automation techniques can apply these lessons to identify and close key performance gaps.

Baily et al. [2010] conducted a series of field trials and published BHA design recommendations based on vibration data collected while drilling. In one case, a 60% ROP increase was achieved using a fit-for-purpose BHA design, based on their analysis.

Vibration sensors may be placed in the BHA to collect down-hole vibration data. In 2013, Hutchinson successfully trialed a self-adapting shock-sub in the Middle East, and found the tool capable of manipulating dynamic stiffness to adjust to the changing drilling environment. This tool uses a magneto-rheological damping fluid to identify drilling dysfunction and feed data into a damping control algorithm. Hutchinson stresses the importance of starting with a high-fidelity drilling system model, citing recent model publications that relate to his research objectives. [Hutchinson, 2013]

In the 1990's automated rotary steerable systems were developed to deliver in extended-reach applications.

### 2.3 DRILLING AUTOMATION: THE STATE OF THE ART

This section focuses on drilling automation technology as it relates to increased drilling efficiency. Interested readers should refer to a report published by Albert Eustes (Colorado School of Mines) in 2007, which covers the comprehensive evolution of drilling mechanization and automation. [Eustes, 2007] Figure 2.6 shows a timeline of auto-driller development and outlines the evolution of key technologies that support the current state of the art. Although appropriate rig equipment is critical to make forward progress in control system development, the topic of particular interest for the purposes of this study is the integration of multi-parameter control systems that began in the early-2000's. [Florence et al., 2009]

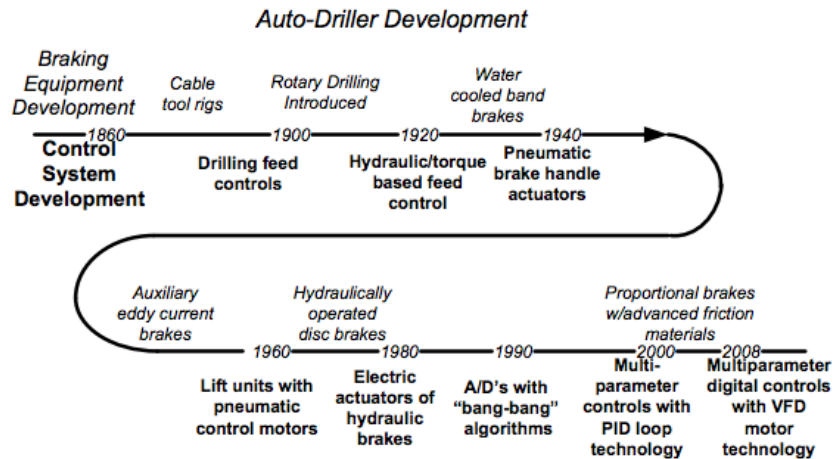


Figure 2.6: Florence et al. published a timeline of auto-driller development, which highlights the evolution of braking equipment and control system technology. [Florence et al., 2009]

### ***2.3.1.1 Research Initiatives***

In the mid-2000's, Fred Dupriest (ExxonMobil) led a performance management revolution that resulted in an 80% worldwide increase in average daily ROP for the operator. Dupriest credits the widespread success of this initiative to the collection and integration of digital data, which makes it possible to calculate and implement best practices like Mechanical Specific Energy (MSE) optimization algorithms. [Dupriest et al, 2005 (IPTC 10706); 2012]

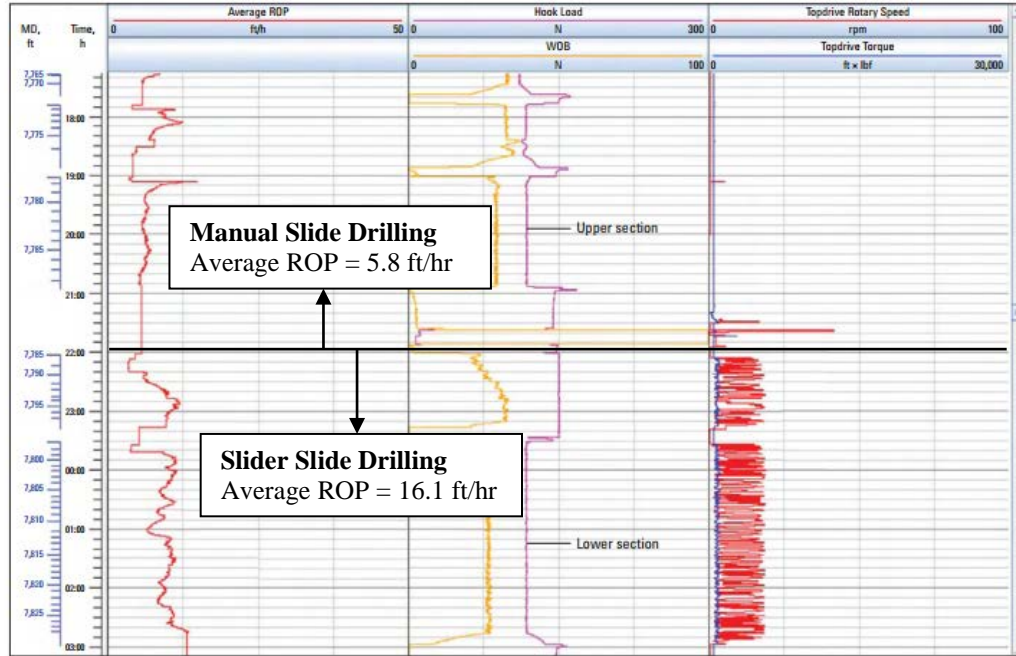
Although axial, torsional and lateral dynamics are all present and coupled in a drilling system, nonlinear dependencies and system uncertainties prevent implementation of a comprehensive drilling system model. Therefore, dynamic models and control strategies are developed to address a particular class of drilling dysfunctions or solve a specific problem. Some rigs possess an active control system to reduce torque fluctuations and torsional drill string vibrations, based on torque feedback collected by MWD tools. The top drive responds by exhibiting a decrease in RPM as torque builds and an increase in RPM as torque diminishes. This type of system is known as a soft-torque system or an impedance-control system [van den Steen, 1997; Jansen and van den Steen, 1995; Smit, 1995; de Vries, 1994; Dekkers, 1992; Javanmardi and Gaspard, 1992]. Other control systems have been implemented with some success. Serrarens et al. [1998] used an  $H_{\infty}$  controller to suppress stick-slip. In 1999, Yigit and Christoforou used a linear quadratic regulator controller to control stick-slip oscillations using a drill string model that couples torsional and lateral vibration modes. [Yigit and Christoforou, 1999, 2000]. Puebla and Alvarez-Ramirez based their work on modeling-error compensation to improve controller robustness in the presence of friction-related uncertainties. This study produced two control schemes:

1. Cascade control – favorable choice of virtual input control variables
2. De-centralized control – two control inputs are manipulated

The physical model includes two damped inertias that represent the rotary table and BHA. The drill pipe is modeled as a spring-damper system. The simplicity of this model restricts potential controller applications to a certain class of stick-slip models. [Puebla and Alvarez-Ramirez, 2008] In 2004, Navarro-Lopez and Suarez began work to implement sliding mode control schemes in stick-slip mitigation algorithms. [Navarro-Lopez and Suarez, 2004] In 2013, Li published a time-varying sliding mode adaptive controller for rotary drilling systems that tracked an ideal bit position signal. [Li, 2013]

### ***2.3.1.2 Service Company Technologies***

Service companies like Schlumberger, CANRIG, and NOV, developed proprietary commercial tools and algorithms that improve tool face control. Schlumberger's Slider system automatically maintains tool face within pre-determined limits using torque-rocking technology to reduce drag along the drill string. The top drive oscillates the drill string from surface, based on reactive torque feedback data. Figure 2.7 illustrates how torque-based top drive controllers can be used to increase ROP. [Schlumberger, 2014]



^ Marked ROP improvements. An operator used slide drilling in two sections of a well drilled in the Marcellus Shale. In the upper section, the well was drilled manually and had an average ROP of 5.8 ft/h. In the lower section, using the Slider system, ROP was raised to 16.1 ft/h (Track 1). WOB (gold) and hook load (purple) were essentially equal through both sections (Track 2). The Slider system kept topdrive torque (blue) low by adjusting rotary speed (red) through the lower sections (Track 3).

Figure 2.7: Schlumberger’s Slider is a torque rocking technology that increases sliding rate of penetration by breaking friction forces along the drill string. This graphic demonstrates the difference between sliding ROP while drilling manually (5.8 ft/hr) vs. while drilling with Slider (16.1 ft/hr). [Schlumberger, 2014]

CANRIG uses a patented, position-based control algorithm to achieve a similar result. This method is less-susceptible to measurement noise that is common in torque sensors. Figure 2.8 demonstrates ROP improvements in the Barnett Shale made possible using the ROCKIT system to reduce axial drag along the drill string-wellbore interface.

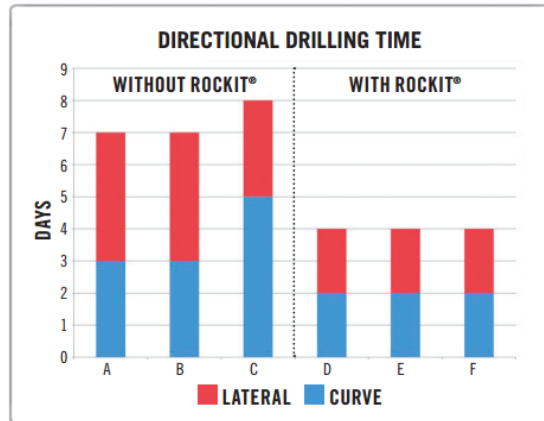


Figure 2.8: CANRIG's ROCKIT technology uses a position-based top drive control algorithm to oscillate the drill string and deliver more weight to the bit, which facilitates faster drilling rates. [CANRIG, 2014]

NOV combines high-speed telemetry technology with drilling automation initiatives to deliver a comprehensive solution called IntelliServ. The NOV solution delivers performance improvement results made possible through increased data fidelity, which reduces the need for highly-complex drilling system models. This approach, while effective, is cost-prohibitive in many cases. Figure 2.9 shows the performance improvement achieved using IntelliServ in comparison to an offset well, demonstrating that comprehensive drill string dynamics data accelerates learning curves and decreases the time required to reach target depth. [NOV, 2014]

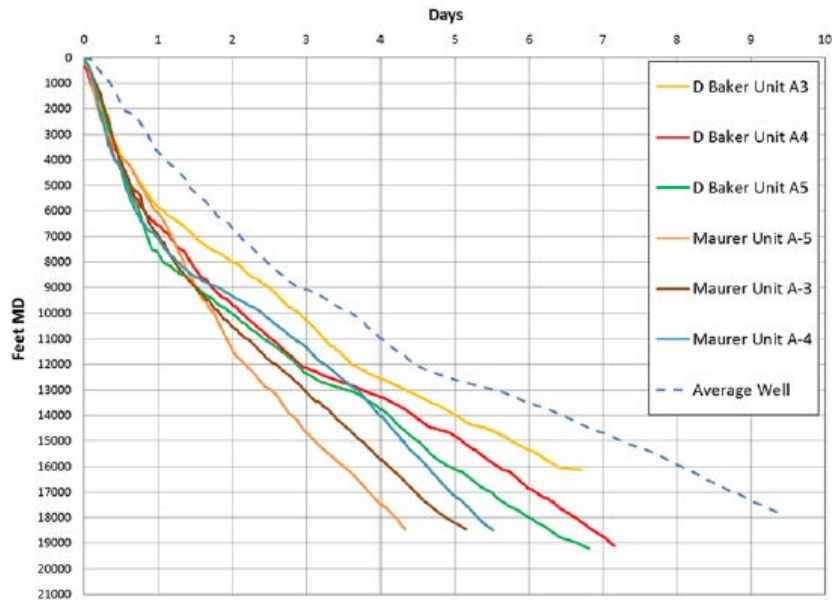


Figure 2.9: NOV’s IntelliServ technology delivers increased rate of penetration through integration of rig instrumentation systems and high-speed telemetry. [NOV, 2014]

### 2.3.1.3 Operator Technologies

In 2009, Shell set out to build the next-generation auto-driller in order to gain more control over operations. Today, Shell’s SCADAdrill system is estimated to be 2 years ahead of other systems of its kind [SPE DDC, 2014] and is operational on 10+ Shell-operated rigs in 5 countries. The system controls axial block speed, top drive rotational speed, and mud pumps (on/off and pump stroke rate) to achieve a specified maximum ROP set point – subject to WOB, differential pressure, and differential torque constraints. A SCADAdrill Operator sets up a series of drilling “batches” before beginning to drill a well – similar to the proposed drilling parameters generated by a traditional directional driller. SCADAdrill batches include system set points based on formation characteristics, well plans, and other offset well data. SCADAdrill is capable of operating in both rotary and slide drilling modes, and the system includes many auto-tuned control routines. Figure 2.10 compares ROP achieved by a manual

driller/directional driller against SCADAdrill ROP over a series of consecutive wells – highlighting the progression of this technology over time.

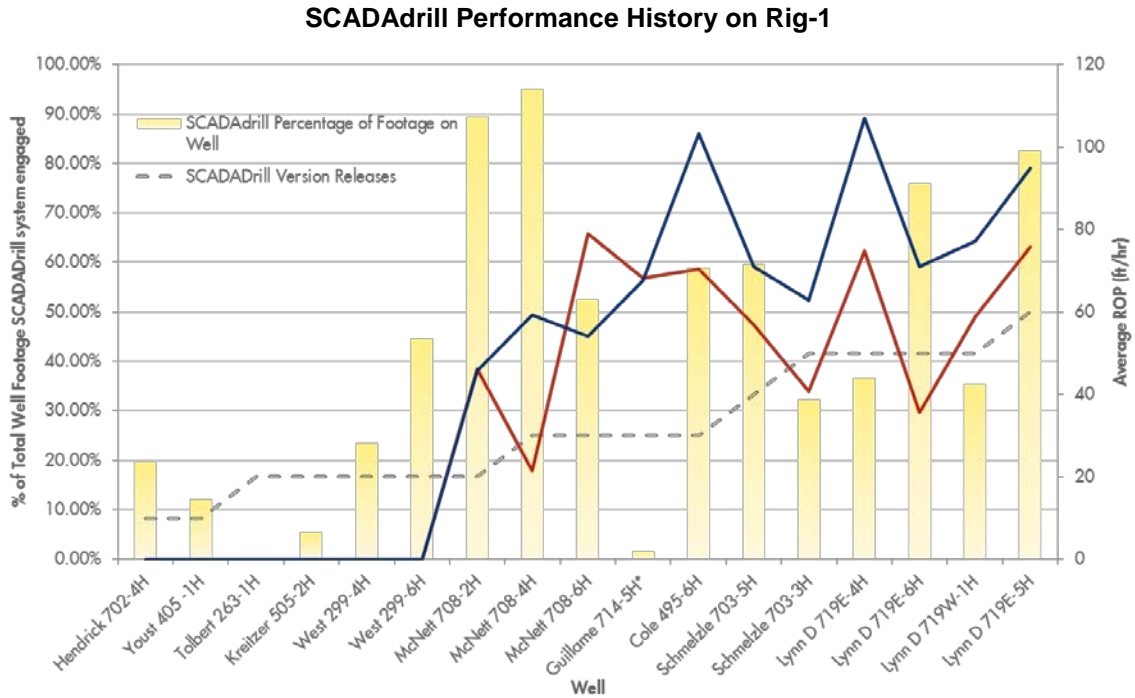


Figure 2.10: Shell’s SCADAdrill system (Blue) has evolved to the point at which it is capable of drilling faster than a manual driller/directional driller (Red).

Although capable of out-performing a manual driller, SCADAdrill is still not a fully-autonomous system. The system still requires some parameters be tuned in real-time, as controllers struggle to adapt to rapidly-changing drilling environments. In order to achieve the next tier of performance, SCADAdrill requires a more sophisticated, robust method for controlling tool face while slide drilling.

The drilling system model that SCADAdrill currently uses to calculate system time constants has 4 degrees of freedom and does not capture drill string or rig control dynamics. This rotary drilling system model uses two damped, lumped masses to represent the top drive and BHA, which are connected by a single spring to represent drill

string compliance. Figure 2.11 shows the torsional drilling system model, to which the axial drilling system model is analogous. Top drive and BHA inertias are represented by  $J_r$  and  $J_b$ , respectively, and the correlating damping terms are expressed as  $c_r$  and  $c_b$ . Drill string compliance is modeled as a torsional spring with compliance  $k$ . Torque input to the system ( $T_r$ ) governs top drive angular position ( $\theta_r$ ) and speed ( $\dot{\theta}_r$ ), and torque is transmitted along the drill string to the bit. Angular bit position ( $\theta_b$ ) is also affected by the TOB ( $T_b$ ) model, which is a function of bit speed ( $\dot{\theta}_b$ ).

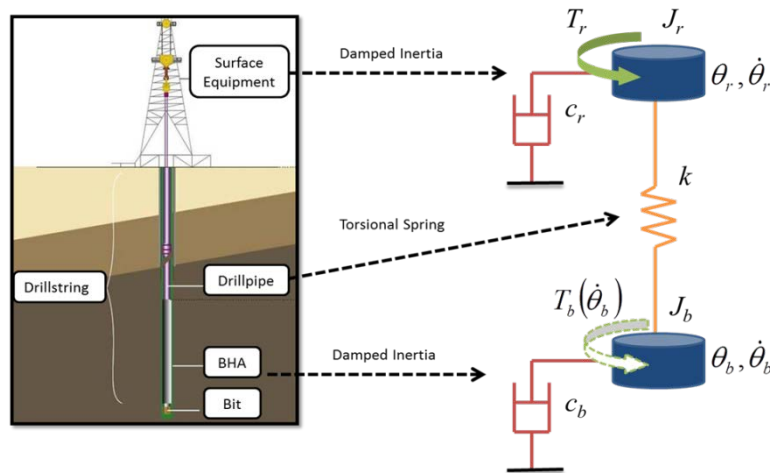


Figure 2.11: Shell’s SCADArdill system uses a 4 degree-of-freedom rotary drilling system model, where the top drive and bottom-hole assembly are represented using damped, lumped masses that are connected via a spring with axial and torsional compliance.

A three-dimensional look-up table is used to interpolate ROP from current WOB and RPM values (Figure 2.12).

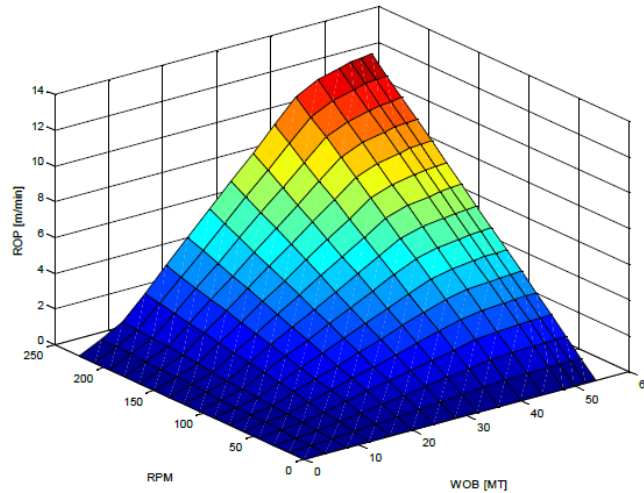


Figure 2.12: The Shell SCADAdrill drilling system simulator uses a 3D lookup table to interpolate rate of penetration using bit speed (RPM) and axial load (WOB) values.

An improved drill string model could enable SCADAdrill to accurately tune the torsional time constant in real-time. This achievement would eliminate the need for an operator to calculate this value manually in order to align and maintain tool face set points while slide drilling.

## 2.4 SUMMARY

There is an opportunity to advance the state of the art of drilling automation by developing a fit-for-purpose simulator that accurately emulates field operations and works cohesively with SCADA routines. There is a disconnect between advanced drill string dynamics models and advanced directional drilling control routines in that most advanced drill string dynamics models are too complex to run in real time, and most advanced control routines were developed using overly-simplistic physical models. The

directional drilling simulator developed for this study is unique in that it offers a physics-based, time-domain model, formulated exclusively for implementation into a SCADA-based system. This simulator balances model complexity with the capability to execute simulation routines in real-time. This program is modular and expandable – capable of serving as a platform for advanced control design using a variety of process and control variables.

### 3 Theoretical Development

This chapter describes the theoretical principles that support the drilling system model used to develop simulation routines. This presentation follows the sequential order of execution within the MATLAB-based simulator.

The first section provides an overview of the model input parameters and an explanation of how each parameter affects system response. The following section explains survey data and well trajectory interpolation methodology, and the equations supporting the Minimum Curvature Method (MCM) are described in detail. The third section provides an explanation of how the Finite Element Method (FEM) is used to discretize the drill string and form system mass, stiffness, and damping matrices. Finally, the equations of motion are presented. Solution techniques are addressed in Chapter 4.

This chapter outlines key formulations gathered from various texts – assembled in an order conducive to the explanation of this drilling system model. The interested reader should refer to the following publications for more detailed explanations of the concepts highlighted herein:

- Fundamentals of Drilling Engineering [Mitchell and Miska, 2009]
- Advanced Drilling and Well Technology [Aadony, 2011]
- Downhole Drilling Tools [Samuel, 2007]
- Nonlinear Drill String Dynamics [Dykstra, 1996]
- Finite Element Procedures in Engineering Analysis [Bathe, 1982]
- Torque and Drag in Directional Wells – Prediction and Measurement [Johancsik et al., 1984]

### 3.1 MODEL INPUT PARAMETERS

This drilling system model requires input parameters that characterize the sub-systems outlined in Figure 3.1:

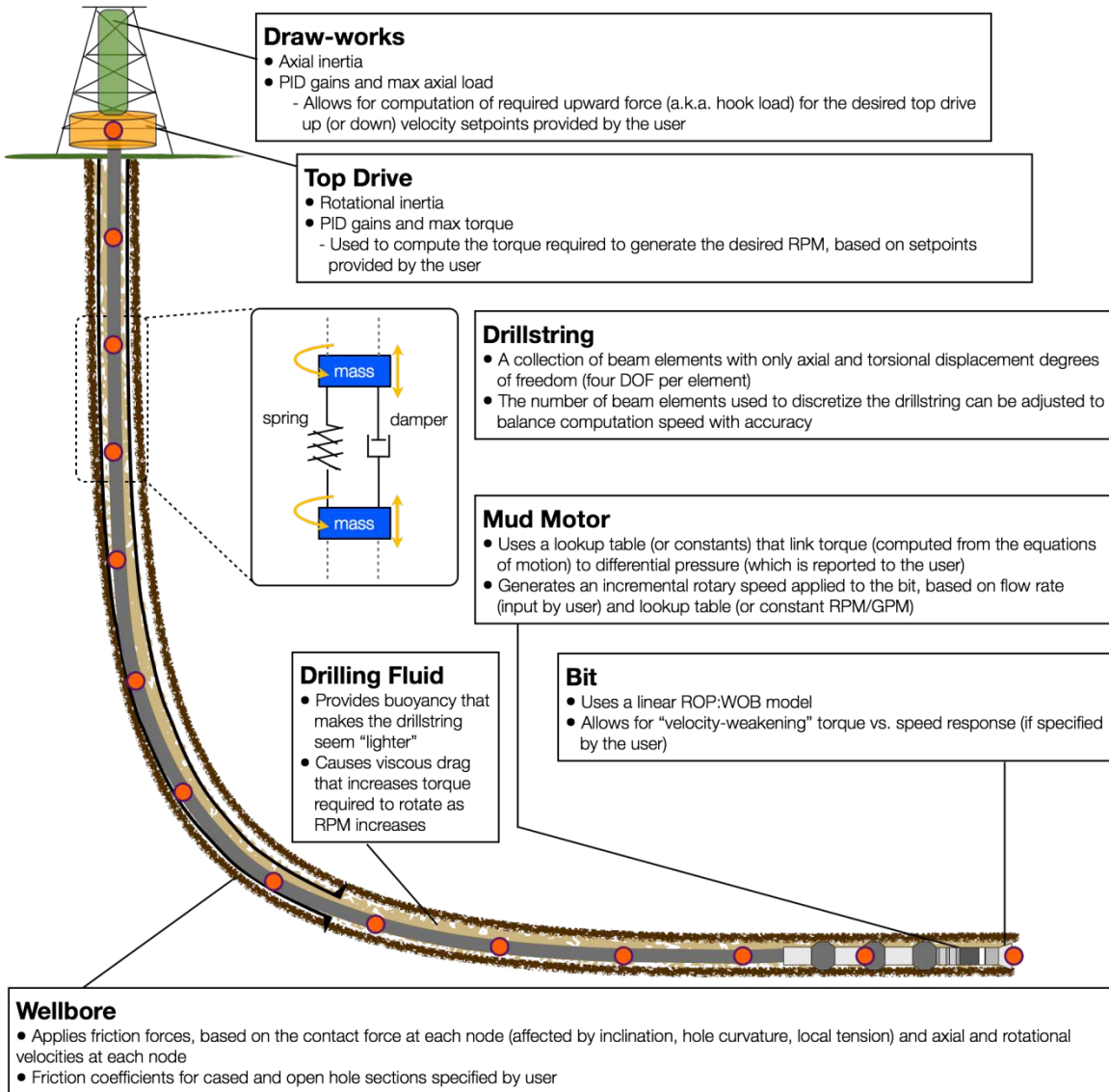


Figure 3.1: The drilling system model developed for this study incorporates various sub-systems.

### 3.1.1 Surface Equipment

This drilling system model includes parameters that describe draw-works and top drive dynamics. Controller gain values are particularly sensitive to the friction model(s) used to characterize dynamic drill string response – considering drill string/wellbore and bit/rock interaction. The PI controllers for the hoisting and rotary equipment were tuned using equations that relate the closed loop controller gain and integral time to the open loop process model gain, dead time, and time constant. Circulating system dynamics are not considered.

#### 3.1.1.1 Hoisting Equipment

The rig hoisting system raises and lowers the drill string into and out of the hole. The main components of a rig hoisting system are the crown block, traveling block, hook, drilling line, and draw-works. The hoisting system is supported by the rig derrick or mast (Figure 3.2).

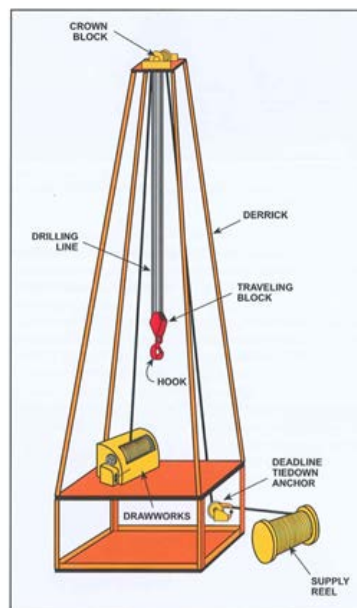


Figure 3.2: The draw-works model used in this study is a simplified representation of a drilling rig hoisting system. [Bommer, 2008]

The controlled hoisting parameter is *block speed*, which is the rate at which the traveling block moves up or down within the derrick or mast. Manipulation of this set point affects torque and drag calculations and is manifested by varying hook load and WOB values.

Draw-works response is modeled using a Proportional-Integral (PI) controller to mimic the delayed response of block speed command and compliance (Figure 3.3). The weight of the block and hook is considered as a point mass and implemented into the feedback control loop – manipulating hook load to achieve ROP set points.

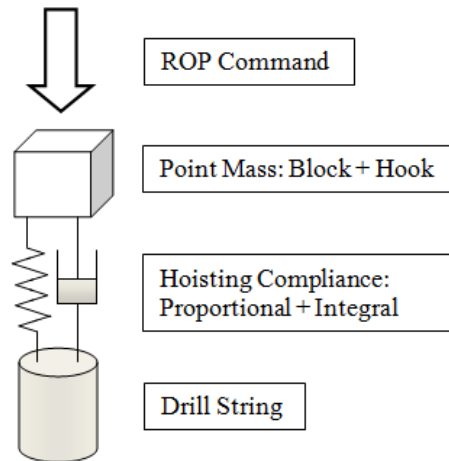


Figure 3.3: An axial velocity (ROP) command is issued to the draw-works. The block and hook is modeled as a point mass, and a proportional-integral controller characterizes hoisting response.

### 3.1.1.2 Rotary Equipment

The rig rotary system rotates the drill pipe from surface. On modern drilling rigs, a top drive transfers clockwise torque to the drill string<sup>1</sup> (Figure 3.4).



Figure 3.4: The top drive is suspended from the traveling block, and axial position is set through manipulation of the block speed. [Bommer, 2008]

The controlled rotary parameter is *rotary speed*, which is the angular velocity (RPM) at which the top drive rotates. Top drive response is also modeled using a PI controller, which captures the delayed response of RPM command and compliance, due to equipment inertia. The top drive is modeled as a uniform, steel cylinder with dimensions reflecting modern top drive design (Figure 3.5). Appendix A contains specifications for the top drive used to conduct this field study.

---

<sup>1</sup> Top drives replaced traditional rotary table / kelly systems on drilling rigs. Interested readers should refer to Chapter 9 of *A Primer of Oilwell Drilling* [Bommer, 2008] for more information on rig components.

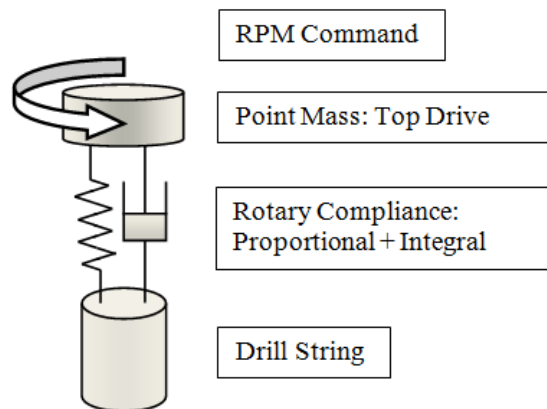


Figure 3.5: A rotary speed (RPM) command is issued to the top drive. The top drive is modeled as a point mass, and a proportional-integral controller characterizes rotary compliance.

### 3.1.1.3 Circulating Equipment

Transient drilling fluid dynamics and pressure effects are not considered in this model. Changes in drilling fluid pump rate immediately affect motor and bit speed. It follows that this drilling system model does not tackle hole cleaning, borehole stability, or equivalent circulating density analyses.

### 3.1.2 The Drill String

The drill string transmits force, torque, and drilling fluid from surface to the drill bit in order to drill along a planned well trajectory. Major drill string components are tubular elements that are classified according to their geometry and purpose. Table 3.1 describes the parameters required to characterize drill string elements.

Table 3.1: Drill string elements are defined using a standard set of parameters.

Parameter	Symbol	Units	General Description
<b>Length</b>	<i>L</i>	<i>ft</i>	Defines total length of tubular class contained in the drill string. Designates length of drill pipe, HWDP, and drill collars separately.
<b>Outer Diameter</b>	<i>OD</i>	<i>in.</i>	Measures outer diameter of each tubular class. Designates OD of drill pipe, HWDP, and drill collars separately.
<b>Inner Diameter</b>	<i>ID</i>	<i>in.</i>	Measures inner diameter of each tubular class. Designates ID of drill pipe, HWDP, and drill collars separately.
<b>Contact Diameter</b>	<i>CD</i>	<i>in.</i>	Defines maximum diameter of each tubular element, i.e. the tool joint diameter. In the case of stabilizers, this parameter is analogous to the blade diameter.
<b>Modulus of Elasticity</b>	<i>E</i>	<i>psi</i>	Ratio of unit stress to unit strain. Also known as 'Young's Modulus'.
<b>Modulus of Rigidity</b>	<i>G</i>	<i>psi</i>	Ratio of shear stress to shear strain. Also known as the 'shear modulus'.
<b>Material Density</b>	<i>ρ</i>	$\frac{lb}{ft^3}$	Mass per unit volume of material.

Table 3.2 lists calculated parameters derived from the drill string element model parameters described in Table 3.1.

Table 3.2: Drill string dynamics are influenced by a set of parameters that are calculated using parameters found in Table 3.1.

Parameter	Symbol	Formula	Units
Cross-Sectional Area	$A$	$A = \frac{\pi}{4}(D_o^2 - D_i^2)$	$in^2$
Pipe Weight in Air	$W$	$W = A \cdot \rho$	$lbf$
Outer Area	$A_o$	$A_o = \frac{\pi}{4} \cdot D_o^2$	$in^2$
Inner Area	$A_i$	$A_i = \frac{\pi}{4} \cdot D_i^2$	$in^2$
Area Moment of Inertia	$J$	$J = \frac{\pi}{32} \cdot (D_o^4 - D_i^4)$	$in^4$
Mass Moment of Inertia	$I$	$I = \left(\frac{\rho}{g}\right) \cdot \left(\frac{L}{12^4}\right) \cdot J$	$lbm \cdot ft^2$
Flexural Rigidity	$w_A$	$w_A = E \cdot I$	$\frac{lbf}{in^2} \times lbm \cdot ft^2$
Torsional Rigidity	$w_T$	$w_T = J \cdot G$	$lbf \cdot in^2$

### 3.1.3 Down-Hole Motor

Positive displacement motors (PDM) are driven by the reverse-Moineau principle, which means torque is directly proportional to motor differential pressure, and rotary speed is directly proportional to flow rate. It is a common drilling practice to place a bent sub directly above the PDM to create a deflection assembly. A typical bend-angle is 1-3 degrees from the sub body axis. This combination of tools is commonly referred to as a *bent-housing mud motor*. The bent sub creates sideways forces at the bit that guides the assembly along a curved path (Figure 3.6).

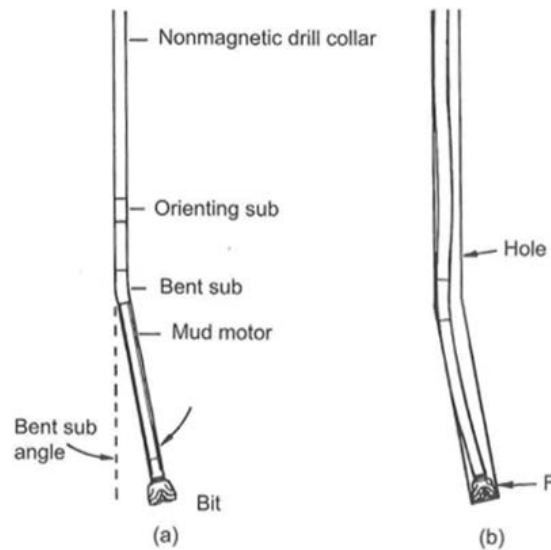


Figure 3.6: A bent sub is placed above the down-hole motor to create a deflection assembly by applying a side-force at the bit. Unconstrained and constrained drill string configurations are shown in (a) and (b), respectively. [Mitchell and Miska, 2009]

Although this system model considers motor geometry as it relates to bit speed as a function of pressure and pump rate, it does not model deflection tendencies as a result of side forces at the BHA and bit. It follows that this simulator drills along a prescribed well trajectory and does not calculate deviations from the well plan.

Bit RPM is a function of down-hole motor properties and drilling fluid flow rate. Relevant down-hole motor properties are illustrated in Figure 3.7.

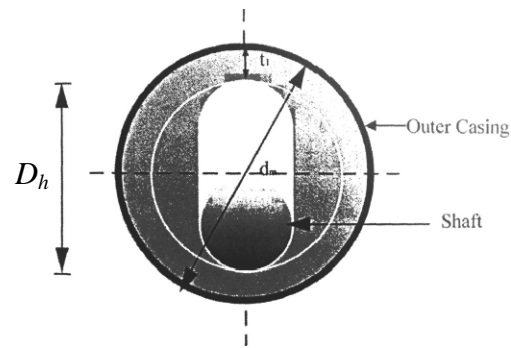


Figure 3.7: This cross-section of down-hole motor highlights dimensions that affect motor torque and speed.

Motor torque is a function of pressure drop across the motor, motor configuration, housing diameter, motor pitch, and motor efficiency:

$$\text{Equation 1: } T_m = 0.01 \cdot \Delta P \cdot K_i \cdot D_h^2 \cdot p_h \cdot \eta$$

$T_m$  = motor torque (ft-lbf)

$\Delta P$  = pressure drop across the motor

$K_i$  = a representation of motor configuration (Equation 2)

$D_h$  = housing diameter (in.)

$p_h$  = motor pitch (in.)

$\eta$  = motor efficiency

The  $K_i$  term simplifies the consideration of the rotor/stator motor configuration ratio,  $i_m$ :

$$\text{Equation 2: } K_i = i_m \cdot \left[ \frac{(1 + i_m)}{(2 - i_m)^2} \right]$$

Motor speed RPM is a function of motor configuration, housing diameter, motor pitch, and flow rate. (Equation 3a, 3b)

$$\text{Equation 3a: } N_m \left( \frac{\text{rev}}{\text{min}} \right) = \frac{230.98 \cdot Q}{0.79 \cdot K_i \cdot p_h \cdot D_h^2}$$

$$\text{Equation 3b: } N_m \left( \frac{\text{rad}}{\text{sec}} \right) = N_m \cdot \frac{2 \cdot \pi}{60}$$

$N_m$  = angular motor speed

$Q$  = flow rate (gpm)

These physical relationships can be used to build motor power curves that are used to select operating parameters during drilling operations (Figure 3.8).

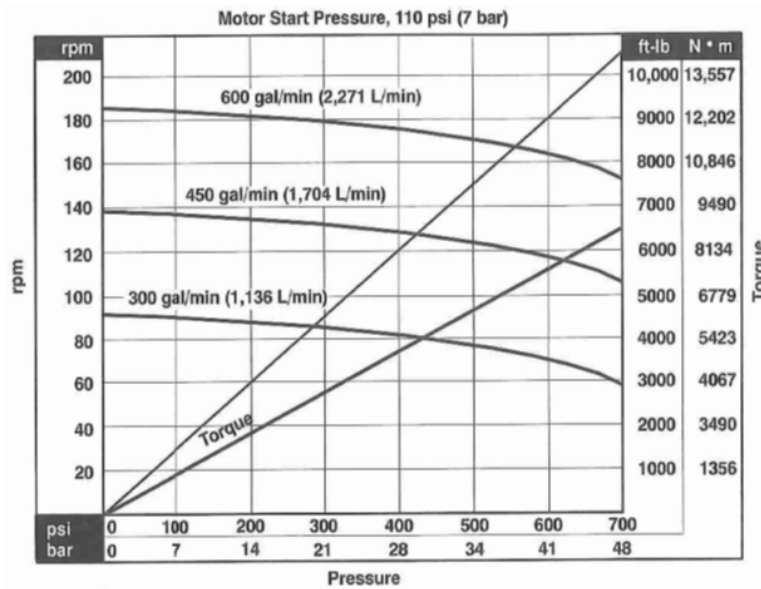


Figure 3.8: Physical motor characteristics can be used to build power curves that are referenced during drilling operations. [Mitchell and Miska, 2009]

Motor characteristics affect reactive torque calculations that may feed into tool face control algorithms. Therefore, an accurate down-hole motor representation was included in this study, despite the fact that deflection tendencies are not captured.

### 3.1.4 Bit

Bit-rock interaction can be characterized by a bit coefficient of friction, which is commonly referred to as *bit aggressiveness*. Bit aggressiveness is defined as the slope of the TOB vs. WOB curve. (Figure 3.9)

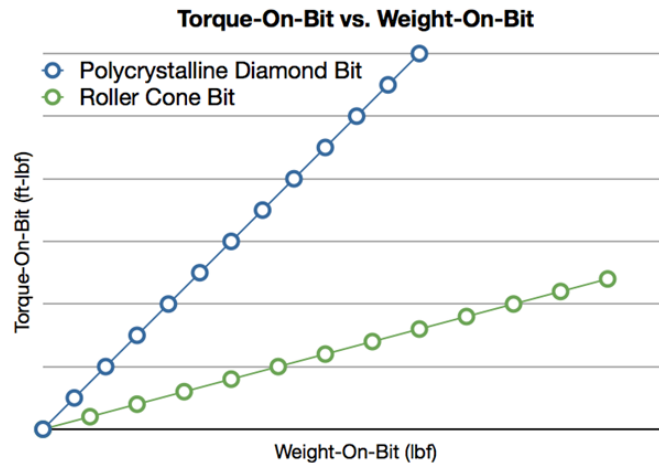


Figure 3.9: This comparison illustrates how bit aggressiveness varies by bit type.

Assuming a constant coefficient of friction at the bit-rock interface, it is possible to derive a bit-specific coefficient of friction using analytical methods. [Pessier and Fear, 1992] Consider an idealized scenario, where the bit-rock interaction is modeled as a cylinder pressing against a flat plate. (Figure 3.10)

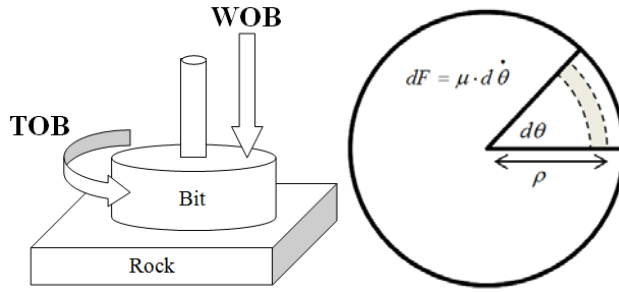


Figure 3.10: Bit-rock interaction is modeled as a cylinder pressing against a flat plate.

Angular bit speed is a function of *WOB* and bit diameter:

$$\text{Equation 4: } \dot{\theta} = \frac{WOB}{\frac{\pi}{4} \cdot D^2}$$

$\dot{\theta}$  = angular bit speed (rpm)

*WOB* = weight-on-bit (lbf)

*D* = bit diameter (in.)

Assuming constant bit coefficient of friction, *Torque On Bit (TOB)* can be determined analytically:

Equation 5a:

$$TOB = \int_0^{\frac{D}{2}} \int_0^{2\pi} \rho^2 \frac{4 \cdot \mu \cdot WOB}{\pi \cdot D^2} \cdot d\rho \cdot d\theta = \int_0^{\frac{D}{2}} \frac{8 \cdot \mu \cdot WOB}{D^2} \cdot \rho^2 \cdot d\rho = \frac{8 \cdot \mu \cdot WOB}{D^2} \left( \frac{\rho^3}{3} \right)_0^{\frac{D}{2}}$$

$$\therefore TOB = \frac{\mu \cdot WOB \cdot D}{3}$$

Note: In Equation 5a, bit diameter is expressed in feet.

Equation 5b shows TOB as a function of bit diameter expressed in inches - the field standard.

$$\text{Equation 5b: } TOB = \frac{\mu \cdot WOB \cdot D}{36}$$

Equation 5b can be re-written to form an expression for bit aggressiveness (Equation 6).

$$\text{Equation 6: } \mu = \frac{36 \cdot TOB}{WOB \cdot D}$$

Bit coefficient of friction is a parameter of particular interest for the model parameter sensitivity analysis. Bit aggressiveness will vary based on bit type and drilling fluid properties. Table 3.3 provides suggestions for bit aggressiveness for various bit types while drilling in different formations.

Table 3.3: Bit aggressiveness varies according to bit type and formation characteristics. [SIEP, 2009]

Bit Type	Formation Type*, **	Aggressiveness
Aggressive PDC	Limestone (15 kpsi)	0.80
	Shale (10 kpsi)	1.20
	Shale (5 kpsi)	1.70
Standard PDC	Limestone (15 kpsi)	0.60
	Shale (10 kpsi)	0.80
	Shale (5 kpsi)	1.20
Diamond Impregnated Matrix	Limestone (15 kpsi)	0.30
IADC 517 Roller Cone	Shale (10 kpsi)	0.20
IADC 116 Roller Cone	Shale (10 kpsi)	0.25
* Compressive strength of formation shown in parentheses.		
** Note: All values represent drilling with 2 kpsi bottom-hole pressure.		

### 3.1.5 Drilling Fluid

Drilling fluid (a.k.a. mud) is circulated through a drilling system to remove cuttings, clean and cool the bit, maintain borehole stability, and power the down-hole

motor. Drilling fluid density and viscosity affect dynamic behavior at various pump speeds. Mud density controls bottom-hole pressures and hole stability. These considerations must be balanced with drilling performance requirements, due to the fact that high-density muds increase friction losses and decrease rate of penetration. Mud viscosity characterizes drilling fluid rheology.

This drilling system model assumes constant drilling fluid density and viscosity, representative of a Newtonian fluid. Drilling fluid density defines the buoyancy factor (Equation 7), which is used to calculate the buoyant weight of the drill string in the wellbore (Equation 8).

$$\text{Equation 7: } BF = 1 - \left( \frac{\rho_{mud}}{\rho_{pipe}} \right)$$

$$\text{Equation 8: } W_b = W \cdot BF$$

$BF$  = buoyancy factor

$\rho_{mud}$  = mud density (ppg, psi/ft, kPa/m, etc.)

$\rho_{pipe}$  = steel density (units consistent with  $\rho_{mud}$ )

$W_b$  = buoyant pipe weight (lbf, kdaN, etc.)

$W$  = dry pipe weight (units consistent with  $W_b$ )

Mud viscosity affects system pressure calculations and friction considerations. This drilling system model does not explicitly quantify these effects. Instead, the drilling fluid viscosity and weighting material listed in the mud program is used to estimate an appropriate friction factor coefficient range for use in a sensitivity analysis (Table 3.4).

Table 3.4: Experimentally-determined friction coefficients characterize casing-tool joint interaction for various drilling fluid compositions. [Bol, “Effect of mud composition on wear and friction...” 1986]

Mud Type	Density (kg/m <sup>3</sup> )	Weighting Material	Additives	Friction Coefficient (dimensionless)
IOEM*	900	—	—	0.15
IOEM	900 to 1400	Barite	—	0.15
Water-based**	1000 to 1050	—	—	0.40 to 0.50
Water-based	1000 to 1050	—	Polymers, lignosulfonate, lignite, salts, sand (2 to 4%)	0.35 to 0.50
Water based	1000 to 1050	—	diesel (10%) and glass beads	0.40 to 0.50
Water-based	1050 to 2300	Barite	—	0.25 to 0.35
Water-based	1050 to 2300	Barite	Polymers, lignosulfonate, lignite, glass beads, sand, and salts	0.25 to 0.35
Water-based	1200	Iron oxide	—	0.35
Water-based	1150	Chalk	—	0.35
Water-based	2300	Iron oxide/ barite (1:1)	Polymers, salts, and lignosulfonate	0.25
Water-based	1200	Drilled solids (mainly clays)	—	0.35

\*IOEM is a standard, commercially available oil-based mud.

\*\*Freshwater-based mud with 60 kg/m<sup>3</sup> bentonite.

The control parameter in the circulating system is mud pump speed. Changes in this set point affect how quickly drilling fluid is circulated through the system. For the purposes of this study, the primary relationship of interest is how changes in pump speed affect down-hole motor performance (See Equation 3a, 3b). Frictional pressure losses along the drill string are neglected in this model.

### 3.1.6 Casing and Formation Characteristics

In addition to drilling fluid viscosity considerations, this model assigns friction factor coefficients according to nodal position within the wellbore. Therefore, each drill string node correlates to either a cased- or open-hole friction factor. (Figure 3.11)

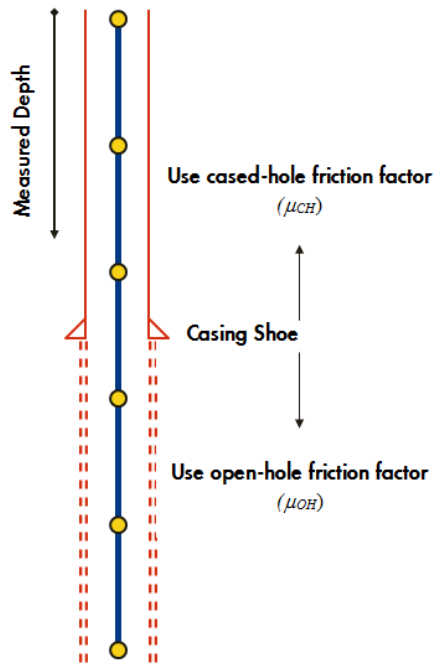


Figure 3.11: Cased- and open-hole friction factors are assigned based on the measured depth of each drill string node.

## 3.2 WELL TRAJECTORY

Well trajectory and tortuosity are critical factors that affect drill string dynamics, due to their influence on static and dynamic loads on the drill string. Three-dimensional wells can be designed to minimize torque and drag loads if there is sufficient understanding of how the wellbore interacts with the drill string at various orientations and depths.

### 3.2.1 Survey Data Inputs

Well trajectories are interpolated, based on the following survey data inputs:

- Measured Depth – the distance between the surface and survey locations, measured along the wellbore
- Inclination – the angular deviation of the wellbore from vertical, measured with respect to a true vertical line

- Azimuth – the projected angle of the wellbore onto a horizontal plane, measured with respect to true North

Note: Total Vertical Depth (TVD) is often included in directional surveys. However, TVD can be calculated using the survey data inputs described above.

Figure 3.12 shows how measured depth, inclination, and azimuth affect the overall well trajectory and dogleg severity along the wellbore.

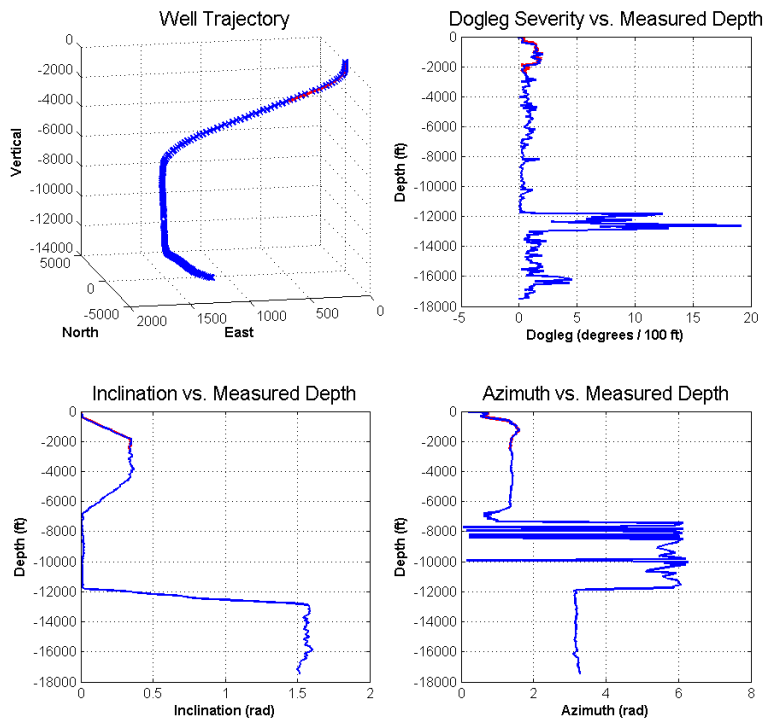


Figure 3.12: Measured depth, inclination, and azimuth values characterize a three-dimensional well trajectory and dogleg severity values along the wellbore.

### 3.2.2 Wellbore Interpolation via Minimum Curvature Method

The Minimum Curvature Method (MCM) is recognized as the industry standard for calculation of well trajectory based on directional survey data. Although this method is not ideal for every scenario, it is used for this study in order to remain consistent with the methodology employed by directional service providers. An overview of MCM theory and the equations that support the well trajectory model used in this directional drilling simulator is presented below. For a comprehensive presentation of the MCM, refer to [Sawaryn and Thorogood, 2005].

The MCM uses a collection of circular arcs and linear segments to represent a well path. The underlying concept is that two adjacent survey points are considered to lie on a circular arc which is located in a plane whose orientation is governed by inclination and azimuth values at each point (Figure 3.13).

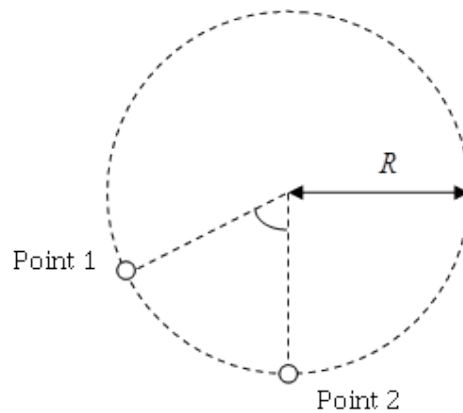


Figure 3.13: The Minimum Curvature Method uses adjacent survey points to interpolate the well trajectory using a circular arc formulation.

The coordinate reference frame traditionally used in directional drilling applications is comprised of a right-handed set of North, East, and Vertical coordinates. Equations 9, 10, and 11 refer to Figure 3.14.

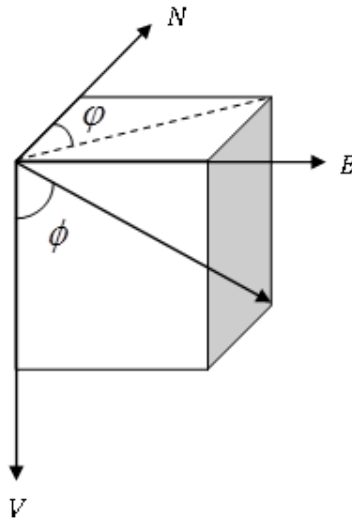


Figure 3.14: The Minimum Curvature Method uses a coordinate reference frame based on North, East, and Vertical coordinates.

It follows that the position ( $p$ ) of any point along the well path can be represented by a vector containing its North, East, and Vertical coordinates:

$$\text{Equation 9: } \underline{p} = \begin{bmatrix} N \\ E \\ V \end{bmatrix}$$

A unit direction vector incorporates local inclination and azimuth values to describe changes in North, East, and Vertical coordinates between two points (Equation 10).

$$\text{Equation 10: } \underline{t} = \begin{bmatrix} \Delta N \\ \Delta E \\ \Delta V \end{bmatrix} = \begin{bmatrix} \sin(\phi) \cdot \cos(\varphi) \\ \sin(\phi) \cdot \sin(\varphi) \\ \cos(\phi) \end{bmatrix}$$

Inclination is a function of North, East, and Vertical changes between two survey points:

$$\text{Equation 11: } \phi = \tan^{-1} \left( \frac{\sqrt{\Delta N^2 + \Delta E^2}}{\Delta V} \right)$$

Azimuth is a function of North and East changes between two survey points:

$$\text{Equation 12: } \phi = \tan^{-1} \left( \frac{\Delta E}{\Delta N} \right)$$

Dogleg Severity (DLS) is the term used to describe the aggressiveness of build/turn rates along the well path; it is a function of the changes in inclination and azimuth between two points at known depths (Figure 3.15).

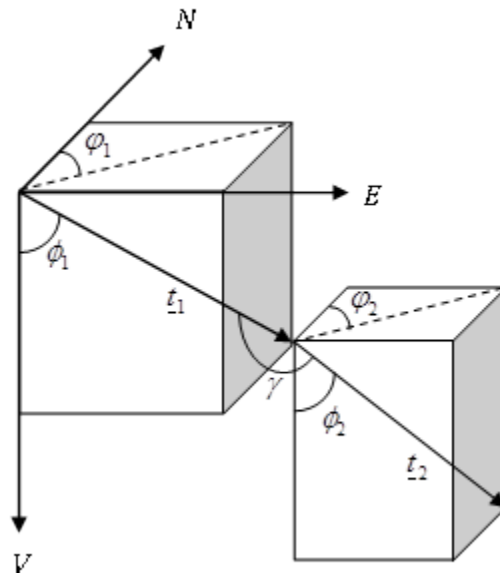


Figure 3.15: Dogleg severity is a function of the changes in inclination and azimuth between two points at known depths.

The relative angle ( $\gamma$ ) between unit direction vectors  $t_1$  and  $t_2$  is a trigonometric function of inclination and azimuth measurements at each survey point:

$$\text{Equation 13: } \gamma = 2 \cdot \sin^{-1} \left[ \sqrt{\sin^2 \left( \frac{\phi_2 - \phi_1}{2} \right) + \sin(\phi_1) \cdot \sin(\phi_2) \cdot \sin^2 \left( \frac{\varphi_2 - \varphi_1}{2} \right)} \right]$$

The DLS between two survey points is expressed in oilfield units using Equation 14:

$$\text{Equation 14: } DLS = \frac{\left( \frac{18,000 \cdot \gamma}{\pi} \right)}{D_2 - D_1}$$

The position vector of a subsequent survey point can be analytically determined using the wellbore geometry shown in Figure 3.16.

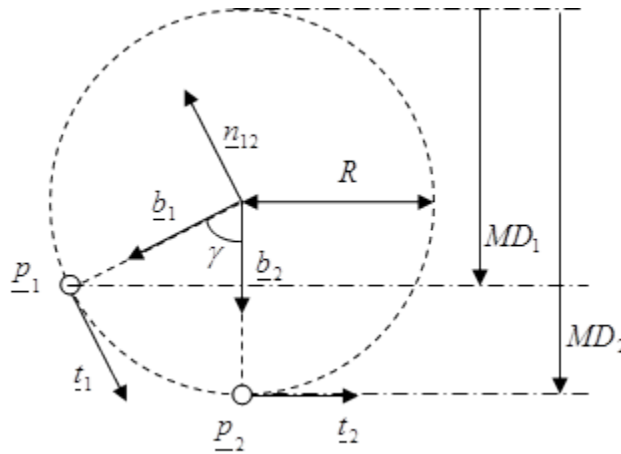


Figure 3.16: The position vector of a subsequent survey point is a function of the measured depth and unit tangent vectors that characterize those points.

The position vector ( $p_2$ ) is calculated using Equation 15:

$$\text{Equation 15: } \underline{p}_{(i)} = \underline{p}_{(i-1)} + \frac{(MD_{(i)} - MD_{(i-1)})}{2} \cdot \left( \frac{\tan\left(\frac{\gamma}{2}\right)}{\left(\frac{\gamma}{2}\right)} \right) \cdot (\underline{t}_{(i)} - \underline{t}_{(i-1)})$$

### 3.3 FINITE ELEMENT DISCRETIZATION

#### 3.3.1 Physical Explanation

This model considers only the axial and torsional degrees of freedom, and it is an adaptation of a complete non-linear drill string dynamics analysis that includes the derivation of equations of motion that capture axial, torsional, and lateral dynamics. [Dykstra, 1996; Khulief and Al-Naser, 2005] The underlying drill string dynamics model used in this study is supported by Hamilton's Principle, which states that system dynamics are dependent upon all physical characteristics of the system and the forces acting upon it.

$$\text{Equation 16: } \delta \int_{\Delta t} (T - V) + \int_{\Delta t} \delta W = 0$$

In Equation 16,  $T$  represents kinetic energy,  $V$  represents potential energy, and  $W$  represents work done by forces that cannot be derived from a potential. For a continuous system, these terms can be derived in terms of displacement ( $u_x$ ) and rotation ( $\theta_x$ ) variables that describe drill string dynamics in a rectangular, Cartesian coordinate system. The  $(T-V)$  term in Equation 16 represents the Lagrangian function, which can be expanded into Equation 17:

$$\text{Equation 17: } \frac{d}{dt} \left[ \frac{\partial T}{\partial \dot{U}_i} \right] - \frac{d}{dt} \left[ \frac{\partial V}{\partial \dot{U}_i} \right] - \frac{\partial T}{\partial U} + \frac{\partial V}{\partial U} = F_i$$

The kinetic energy of the system is expressed using Equation 19, where the first term represents translational kinetic energy, and the second term represents rotational kinetic energy:

$$\text{Equation 18: } T = \int_0^L \frac{\rho \cdot A}{L} \cdot \left( \dot{u}_x \right)^2 \cdot dx + \int_0^L \frac{J_t}{2} \cdot \left( \dot{\theta}_x \right)^2 \cdot dx$$

Assuming shear deflections are negligible and Equation 19 holds true, the elastic potential energy of the system is expressed using Equation 20. [Dykstra, 1996]

$$\text{Equation 19: } L \geq 7\sqrt{d_o^2 - d_i^2}$$

$$\begin{aligned} \text{Equation 20: } V = & \frac{E \cdot A}{2} \cdot \int_0^L \left( \frac{\partial u_x}{\partial x} \right)^2 \cdot dx + \frac{G \cdot I_x}{2} \cdot \int_0^L \left( \frac{\partial \theta_x}{\partial x} \right)^2 \cdot dx + \dots \\ & \frac{E \cdot A}{2} \cdot \int_0^L \left( \frac{\partial u_x}{\partial x} \right)^3 \cdot dx + \frac{E \cdot I_x}{2} \cdot \int_0^L \frac{\partial u_x}{\partial x} \cdot \left( \frac{\partial \theta_x}{\partial x} \right)^2 \cdot dx \end{aligned}$$

In Equation 19,  $L$  represents the element length, and  $d_o$  and  $d_i$  represent the element outer and inner diameters, respectively. In Equation 20, the first and second terms are linear contributions due to tension and torsion, and the third term is a non-linear axial load term. The last term represents coupled tension and torsion effects.

The work terms considered in this model result from gravitational and viscous drag forces acting upon each drill string element. A drill string element can be modeled as a distributed mass, giving rise to distributed axial and transverse gravitational loads as shown in Figure 3.17.

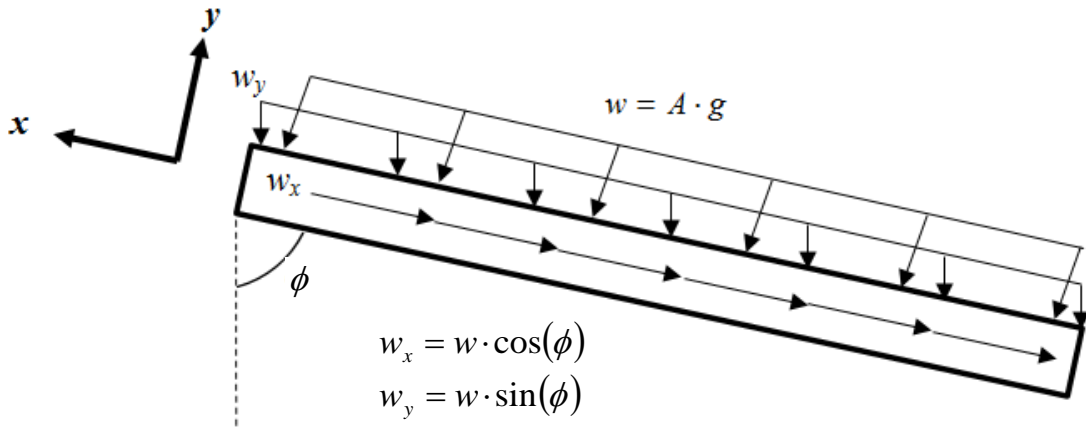


Figure 3.17: Distributed gravitational forces act upon a drill string element in an inclined wellbore.

The gravitational forces shown in Figure 3.17 contribute to the overall work done on the system.

$$\text{Equation 21: } \delta W_G = \int_0^L \left( \vec{F}_G \cdot \delta \vec{\phi} \right) \cdot dx = \int_0^L \left[ \left( -w_x \cdot \vec{i} - w_y \cdot \vec{j} \right) \cdot \delta \vec{\phi} \right] \cdot dx$$

The Finite Element Method (FEM) is based upon the fundamental assumption that if continuous longitudinal displacements  $u(x,t)$  and rotations  $\theta(x,t)$  at some nodes are known, it is possible to interpolate displacement and rotation values at all other points in between. This drill string model uses 2 nodes to define each tubular element (Figure 3.18). Each node has 2 Degrees Of Freedom (DOF) – an axial displacement ( $u_x$ ) and an angular rotation ( $\theta_x$ ). It follows that each element has 4 DOF.

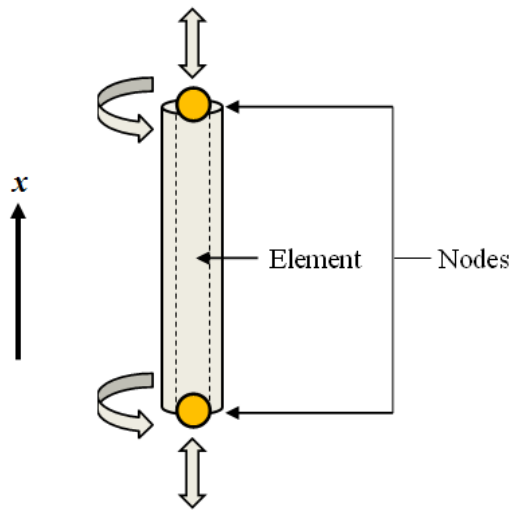


Figure 3.18: A drill string element is defined by 2 nodes, and each node has 2 degrees-of-freedom.

Axial and torsional DOF are independent and can be interpolated using Equation 22 - Equation 23.

$$\text{Equation 22: } u_x = a_1 + a_2 x$$

$$\text{Equation 23: } \theta_x = a_3 + a_4 x$$

Coefficients  $a_{1-4}$  are defined in terms of nodal displacements  $U_{1-4}$ , as shown in Figure 3.19.

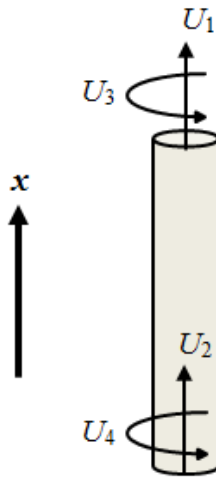


Figure 3.19: Generalized displacements define coefficients that are used to interpolate degrees-of-freedom between nodes.

Boundary conditions  $u_x(0) = U_1$ ,  $u_x(L) = U_2$ ,  $\theta_x(0) = U_3$ , and  $\theta_x(L) = U_4$  can be expressed using Equation 24, which can also be expressed in matrix form (Equation 25).

$$\text{Equation 24: } u_x = \left(1 - \frac{x}{L}\right) \cdot U_1 + \frac{x}{L} \cdot U_2$$

$$\text{Equation 25: } \{u\} = [A]\{U\}$$

Equation 24 can be substituted into Equations 18 - 21. The discrete system of equations is derived through integration of those energy and work equations, and the Lagrangian (Equation 17) is applied to that discrete system to produce a system of 4 equations for each element – representative of each DOF. The discrete system of equations can be written in matrix form:

$$\text{Equation 26: } [M]\{\ddot{U}\} + [C]\{\dot{U}\} + [K]\{U\} = \{F\}$$

In Equation 26,  $\{\ddot{U}\}$ ,  $\{\dot{U}\}$ ,  $\{U\}$ , and  $\{F\}$  represent the generalized acceleration, velocity, position, and force vectors, respectively.  $[M]$ ,  $[C]$ , and  $[K]$  represent the mass damping, and stiffness matrices, respectively.

### 3.3.2 Mass Matrix

The mass matrix  $M$  includes both axial and torsional inertia contributions, represented by  $M_A$  and  $M_T$ , respectively.

$$\text{Equation 27: } M = \begin{bmatrix} \frac{M_A}{3} & 0 & \frac{M_A}{6} & 0 \\ 0 & \frac{M_T}{3} & 0 & \frac{M_T}{6} \\ \frac{M_A}{6} & 0 & \frac{M_A}{3} & 0 \\ 0 & \frac{M_T}{6} & 0 & \frac{M_T}{3} \end{bmatrix}$$

$$\text{Equation 28: } M_A = \frac{W_b}{g}$$

$$\text{Equation 29: } M_T = I$$

### 3.3.3 Stiffness Matrix

The stiffness matrix  $K$  includes both linear and nonlinear inertia contributions. Axial and torsional stiffness terms are represented by  $K_A$  and  $K_T$ , respectively.

$$\text{Equation 30: } K = \begin{bmatrix} K_A & 0 & -K_A & 0 \\ 0 & K_T & 0 & -K_T \\ -K_A & 0 & K_A & 0 \\ 0 & -K_T & 0 & K_T \end{bmatrix}$$

$$\text{Equation 31: } K_A = \frac{E \cdot A}{L}$$

$$\text{Equation 32: } K_T = \frac{G \cdot J}{L}$$

### 3.3.4 Damping Matrix

The damping matrix  $C$  includes dissipative components and does not consider gyroscopic effects. The Rayleigh damping model is used, incorporating linear contributions of the mass and stiffness matrices.

$$\text{Equation 33: } C = \alpha_c \cdot M + \beta_c \cdot K$$

Coefficients  $\alpha_c$  and  $\beta_c$  are tuning parameters that can be adjusted to more accurately describe system dynamics. Recommended values provided in the original publication are:

$$\alpha_c = 0.01$$

$$\beta_c = 0.01$$

### 3.3.5 External Force Vector

The external force vector considers gravity effects, incorporating generalized nodal forces illustrated in Figure 3.17.

$$\text{Equation 34: } F_g = \frac{1}{2} \cdot W_b \cdot \cos(\phi_{avg})$$

## 3.4 SUMMARY

Use of the FEM approach for transient drill string dynamic analysis historically produces simulation routines that are not executable in real-time. The number of elements required

to achieve numerical convergence for a dynamic analysis is dependent upon material properties and geometrical configuration of the drill string. For example, Khulief and Al-Nasar achieved numerical convergence for the drill string configuration shown in Table 3.5 using 24 equal, finite-shaft elements<sup>2</sup>. While this assessment might be useful as a general rule of thumb, it is not applicable to all simulation scenarios.

Table 3.5: Khulief and Al-Naser used simplified drill string configuration specifications to conduct modal and dynamic response analysis using the finite-element method. [Khulief and Al-Naser, 2005]

Drillstring configuration data	
<i>Drillpipe specification</i>	
Drillpipe length ( $L_p$ )	1000 m
Drillpipe outer diameter ( $D_o$ )	0.127 m
Drillpipe inside diameter ( $D_i$ )	0.095 m
<i>Drillcollar specification</i>	
Drillcollar length ( $L_c$ )	200 m
Drillcollar outer diameter ( $D_o$ )	0.2286 m
Drillcollar inside diameter ( $D_i$ )	0.0762 m
<i>Material specification</i>	
Drillstring density ( $\rho$ )	7850 kg/m <sup>3</sup>
Modulus of elasticity ( $E$ )	$210 \times 10^9$ N/m <sup>2</sup>
Shear modulus ( $G$ )	$7.6923 \times 10^{10}$ N/m <sup>2</sup>

Merits of the approach established in this thesis are as follows:

1. Only parameters necessary for the analysis of directional drilling control routines are included in this model.

---

<sup>2</sup> This consistent-mass FEM formulation includes 25 nodes, each with 6 degrees of freedom, for a total of 140 degrees of freedom.

2. FEM mesh size for the drill string is standardized as the length of one joint of drill pipe, which supports the semi-soft string model used for torque and drag analysis.
3. Drill string dynamics can be evaluated in a three-dimensional wellbore.
4. Basic simulation routines are executable in real-time.
  - a. See Chapter 4 for an example of how a 30-second drilling simulation was executed by MATLAB in 29.18 seconds.
5. The simulation structure is established in MATLAB and readily-translatable to PLC language for real-time interaction and comparison with existing SCADA system.

## 4 Numerical Analysis

This chapter presents numerical solution techniques used to solve the equations of motion. Described herein are circumstantial boundary conditions, drill string/wellbore interaction concepts, dynamic torque and drag loading, and the Newmark- $\beta$  integration technique used to solve the equations of motion. Basic model validation results are presented, along with a parameter sensitivity analysis.

### 4.1 BOUNDARY CONDITIONS

Boundary conditions on surface, along the drill string, and at the bit govern system dynamics. At the surface, draw-works and top drive equipment characteristics define longitudinal and rotational loads acting on the uppermost drill string node. Along the drill string, wellbore constraints govern system dynamics. At the bit, the axial position and rotational velocity affect boundary conditions.

#### 4.1.1 Surface Contributions

The draw-works and top drive are each represented as lumped masses, and *ROP* and RPM set points pass through a PI controller to before manifesting themselves as hook load and surface torque acting upon the surface node, respectively. (Figure 4.1)

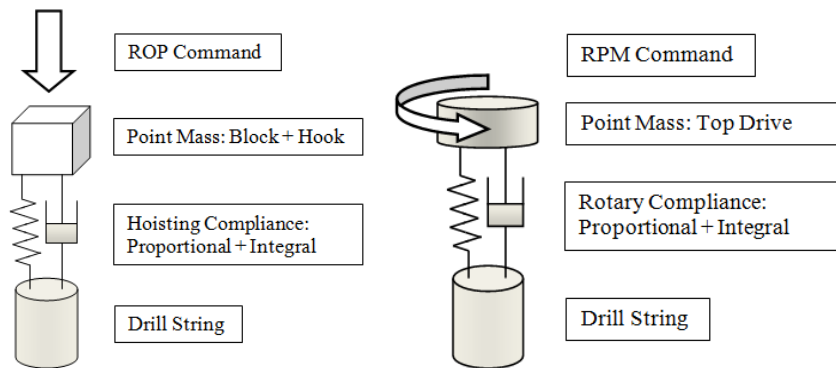


Figure 4.1: ROP and RPM set points are system inputs that govern hook load and surface torque inputs, respectively, based on PI controller characteristics.

Draw-works and top drive PI controller gain values were derived using traditional Ziegler-Nichols step response methods. A detailed description of this process can be found in most introductory control systems textbooks. [Astrom and Murray, 2008]

#### 4.1.2 Wellbore Constraints

This system model considers a semi-soft-string drill string model, which means that the drill string lies on the low side of the wellbore, and tool joints represent the points of contact between the drill string and the wellbore. Therefore, wellbore position governs the drill string position, and torque and drag loads applied at each node affect dynamic behavior along the drill string. The semi-soft string model is considered a good model for straight wellbore sections, i.e. vertical, slant, and lateral portions of the well. However, the model neglects buckling and tortuosity effects, which makes it less accurate in build sections or in other cases where these effects are magnified. [Mitchell and Miska, 2009] Figure 4.2 illustrates how wellbore constraints govern boundary conditions in the semi-soft-string model:

## Semi-Soft-String Model

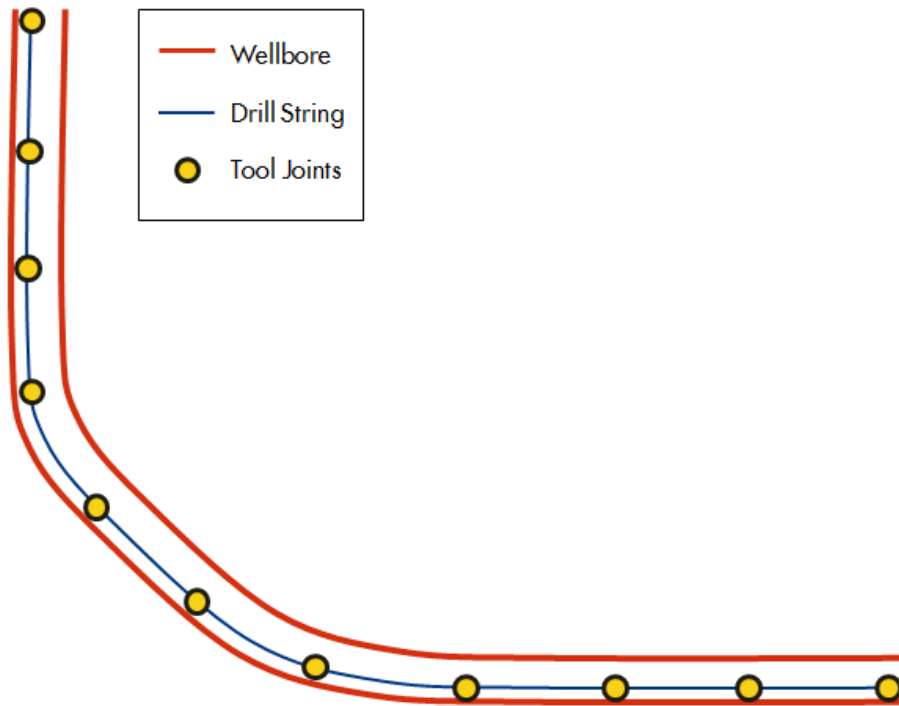


Figure 4.2: In the semi-soft-string drill string model, the drill string lies on the low side of the wellbore, where tool joints mark points of contact.

### 4.1.3 Bit Boundary Conditions - Off-Bottom

When the lowermost node position ( $U_{bit}$ ) is less than the current measured depth, the bit is off-bottom (Figure 4.3).

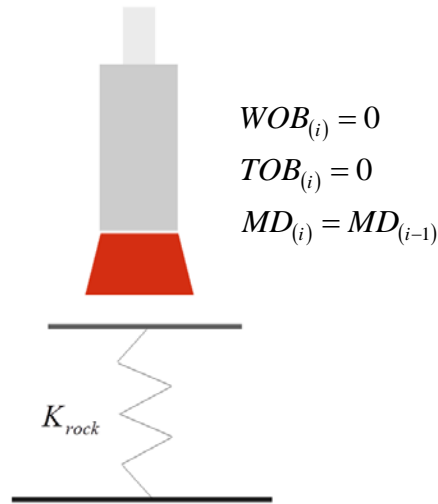


Figure 4.3: An illustration of the off-bottom scenario demonstrates how bit boundary conditions are defined.

In an off-bottom scenario,  $WOB$  and  $TOB$  at this time step ( $i$ ) are zero, and the  $MD$  remains the same as calculated at the previous time step ( $i-1$ ).

### 4.1.4 Bit Boundary Conditions - On-Bottom

Equations governing bit boundary conditions while on-bottom may also be considered as the ROP model used in this simulator. When the lowermost node position ( $U_{bit}$ ) is greater than the current measured depth, the bit is on-bottom (Figure 4.4). Either of the following conditions may apply:

- a) Bit RPM is less-than the threshold RPM required to drill ahead
- b) Bit RPM is sufficient to drill ahead

This bit speed threshold must be adjusted based on controller gains set using the process described in Section 4.1.1. Inclusion of such criteria prevents controller wind up. For the purposes of this explanation, assume the bit speed threshold is 1 rad/sec.

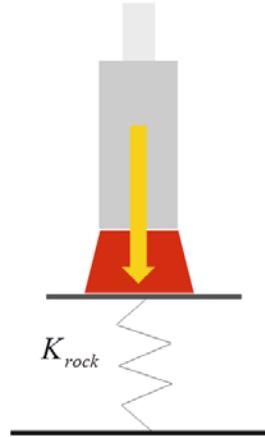


Figure 4.4: An illustration of the on-bottom scenario demonstrates how bit boundary conditions are defined.

Condition a)  $\dot{\theta}_{bit} < 1 \frac{rad}{sec}$

WOB is a function of bit position, drill string length, measured depth, and rock stiffness – effectively modeling the formation as an axial spring.

Equation 35:  $WOB_{(i)} = U_{bit(i)} + L_{tot} - MD_{(i-1)} \cdot K_{rock}$

TOB is calculated using the model described in Chapter 3 and is dependent upon the direction of bit rotation.

Equation 36:  $TOB_{(i)} = \frac{\mu_{bit(i)} \cdot WOB_{(i)} \cdot D_{bit}}{36} \cdot \left( -sign\left(\dot{\theta}_{bit(i)}\right) \right)$

Bit RPM is not sufficient to drill ahead, so the MD does not change.

$$\text{Equation 37: } MD_{(i)} = MD_{(i-1)}$$

$$\text{Condition b) } \dot{\theta}_{bit} \geq 1 \frac{rad}{sec}$$

If bit RPM is above the pre-determined threshold required to drill ahead, *WOB* is a function of Compressive Strength of the Formation (*CSF*), axial bit velocity ( $\dot{U}_{bit}$ ), bit diameter ( $D_b$ ), rotational bit velocity ( $\dot{\theta}_{bit}$ ), and bit aggressiveness ( $\mu_{bit}$ ).

$$\text{Equation 38: } WOB_{(i)} = \frac{CSF \cdot 36 \cdot \dot{U}_{bit(i)}}{D_{bit} \cdot \dot{\theta}_{bit(i)} \cdot \mu_{bit}}$$

*TOB* is calculated using Equation 36.

The new *MD* is calculated using the current bit position,  $U_{bit(i)}$ .

$$\text{Equation 39: } MD_{(i)} = MD_{(i-1)} + U_{bit(i)} - U_{bit(i-1)}$$

## 4.2 DRILL STRING DISCRETIZATION

The drill string is discretized using a pre-defined element length – breaking up each component length into evenly-distributed element lengths, if possible. (Figure 4.5)

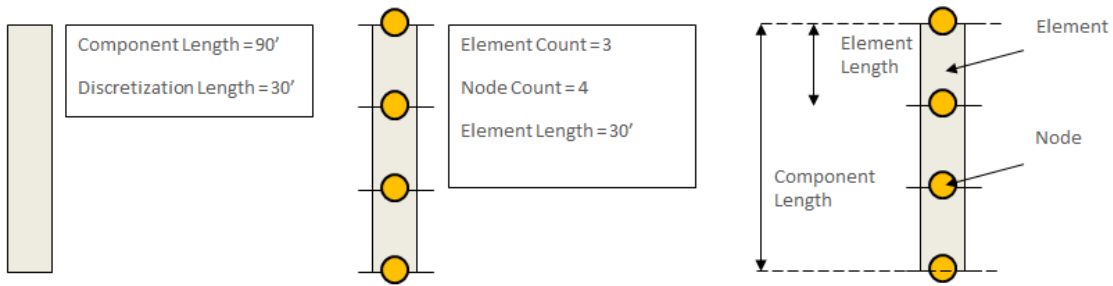


Figure 4.5: This illustration of the drill string discretization process shows how component length, discretization length, element count, node count, and element length are defined.

In the case where a component length is not a multiple of the discretization length, the uppermost element of that component will be the shortest element. Figure 4.6 provides an example of this scenario:

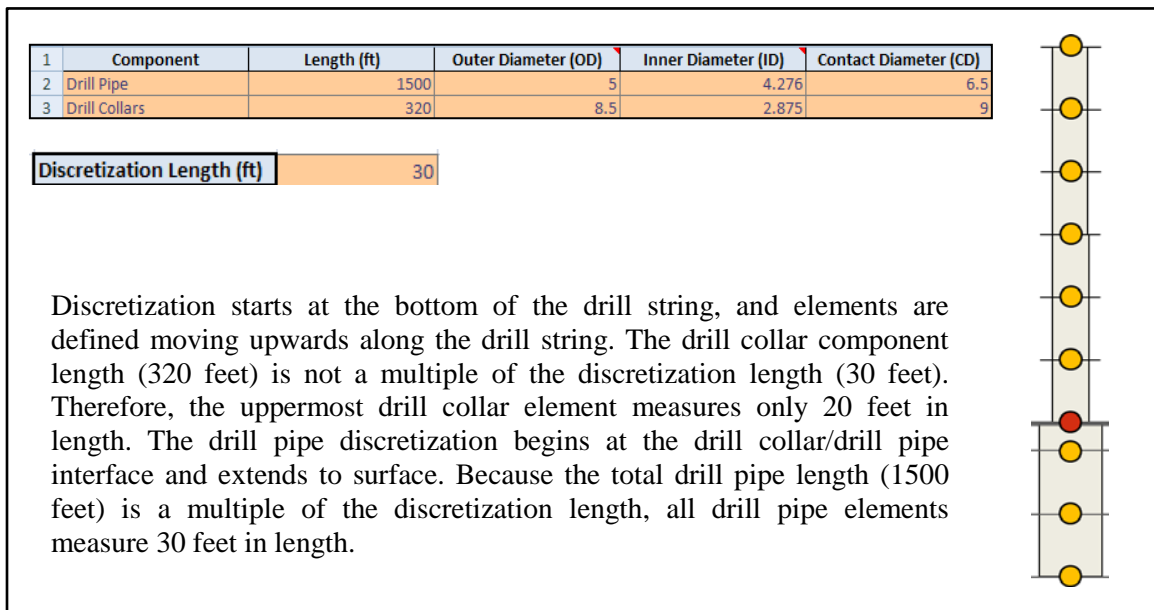


Figure 4.6: Example of a scenario in which a drill string component length is not a multiple of the discretization length.

Relatively short discretization lengths will increase computational requirements, while relatively long discretization lengths may speed up the simulation. A practical assumption is that drill string elements are the length of a typical joint of drill pipe, i.e. approximately 30 feet. This assumption places nodes at each tool joint location, which improves the accuracy of the drill string/wellbore interaction model.

### 4.3 DRILL STRING /WELLBORE INTERACTION

The following geometrical characteristics define each drill string component (Figure 4.7):

1. Length ( $L$ ) - total, continuous length of component
2. Outer diameter ( $OD$ ) of pipe body
3. Inner diameter ( $ID$ ) of pipe body
4. Contact diameter ( $CD$ ) – “tool joint” diameter

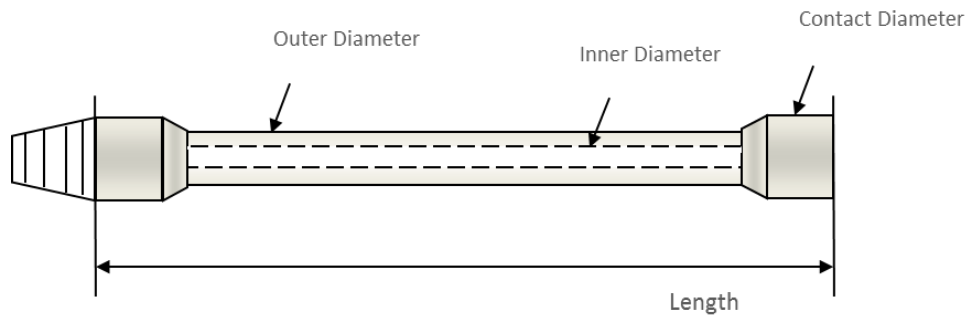


Figure 4.7: Geometrical characteristics of a tubular drill string component.

The outer and inner diameters are used to calculate component areas and inertias, which factor into mass, stiffness, and damping matrices. The contact diameter effectively represents the tool joint diameter, which is assumed to be the portion of the drill string that comes into contact with the wellbore.

Tool joints are modeled through consideration of a contact diameter, which is assigned to each drill string component type and assigned to corresponding nodes.

Therefore, inertial effects of tool joints are ignored. Instead, tool joint effects describe parameters used in torque and drag calculations - covered in Section 4.5. The effective angular velocity at each point of contact is a function of tool joint diameter and nodal angular velocities:

$$\text{Equation 40: } \dot{\theta}_{CD} = \frac{CD}{2} \cdot \frac{1}{12} \cdot \dot{\theta}$$

Note: The units of  $\dot{\theta}_{CD}$  must match the units of ROP.

The resultant speed used for torque and drag calculations is a function of axial and effective angular velocities at each point of contact.

$$\text{Equation 41: } VEL = \sqrt{U^2 + W^2}$$

#### 4.4 INTERNAL FORCES

Internal forces acting on a drill string element can be computed using the pre-calculated stiffness matrices and the relative displacement of two nodes, as illustrated in Figure 4.8.

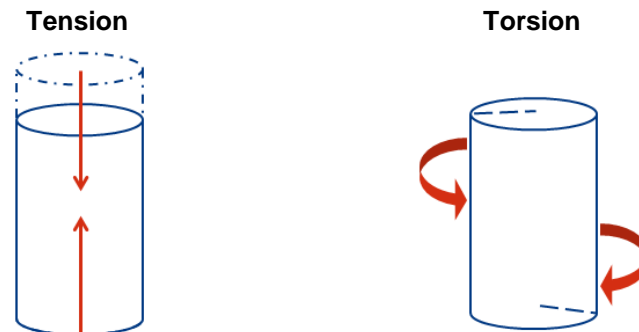


Figure 4.8: Internal tension and torsion forces acting on drill string elements.

Tension and torsion may be calculated separately using Equation 42 and Equation 43, respectively.

$$\text{Equation 42: } T_p = K_A \cdot (U_n - U_{n-1})$$

$$\text{Equation 43: } T_\varphi = K_T \cdot (\theta_n - \theta_{n-1})$$

In Equations 42 - 43,  $K_A$  and  $K_T$  represent axial and torsional stiffness terms, respectively. The subscripts  $n$  and  $n-1$  distinguish neighboring nodes – beginning at the bottom of the drill string and working towards surface. To simplify this calculation, all internal forces can be determined in one step using Equation 44.

$$\text{Equation 44: } \Phi = [K] \cdot \Delta U$$

#### 4.5 TORQUE AND DRAG LOADS

Torque and drag loads are applied to each node exhibiting transient dynamics. Torque and drag loads are dependent upon the normal force acting upon each drill string node in contact with the wellbore. [Johancsik et al., 1984] Figure 4.9 shows loads acting upon a drill string component in an inclined wellbore.

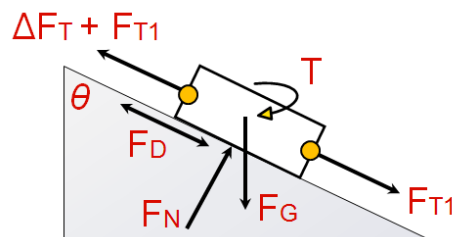


Figure 4.9: Gravitational ( $F_G$ ), normal ( $F_N$ ), torque ( $T$ ), and drag ( $F_D$ ) loads act on a drill string component in an inclined wellbore while internal tension forces ( $F_T$ ) affect normal force contributions.

Normal force is a function of gravitational force, internal tension contributions, and wellbore inclination. (Equation 45)

$$\text{Equation 45: } F_N = \sqrt{\left[F_T \cdot \Delta\phi \cdot \sin(\theta_{avg})\right]^2 + \left[F_T \cdot \Delta\theta + F_G \cdot \sin(\theta_{avg})\right]^2}$$

$$\text{Equation 46: } \Delta F_T = F_G \cdot \cos(\theta) \pm \mu_{rock} \cdot F_N$$

Drag force is a function of formation friction characteristics ( $\mu_{rock}$ ), normal force, axial velocity ( $\dot{U}$ ), and resultant speed at each node ( $VEL$ ). (Equation 47)

$$\text{Equation 47: } F_D = -\frac{\mu_{rock} \cdot F_N \cdot \dot{U}}{VEL}$$

Torque at each node is calculating using formation friction characteristics, normal force, radius of angular rotation ( $R$ ), angular velocity ( $W$ ), and resultant speed. (Equation 48)

$$\text{Equation 48: } T = -\frac{\mu_{rock} \cdot F_N \cdot R \cdot W}{VEL}$$

	Well No. 1	Well No. 2	Well No. 3
Depth, ft	9,790	15,573	12,200
Percent of hole cased, %	70	83	99
Drillstring	124 ft of 7¾-in. DC 990 ft of 4½-in. HW 8,676 ft of 4½-in. DP	458 ft of 6¾-in. DC 15,115 ft of 5-in. DP	372 ft of 6½-in. DC 840 ft of 5-in. HW 10,988 ft of 5-in. DP
Well profile	build and hold	build and hold	build and hold
Kick-off point, ft	1,000	3,000	2,400
Average angle, degrees	32	24	44
Maximum angle, degrees	37	27	49
Mud weight, lbm/gal	11.6	12.5	9.8
Rotating string weight, lbf	153,000	290,000	218,000
Pickup weight, lbf	202,000	377,000	376,000
Slack-off weight, lbf	122,000	232,000	141,000
Rotating torque, ft-lbf	15,900	18,300	24,500
Pickup	0.28	0.31	0.40
Slack-off	-0.27	-0.31	-0.40
Rotating	0.27	0.29	0.39

Figure 4.10: Johancsik et al. calculated friction coefficients from surface torque and drag data for several wells. [Johancsik et al., 1984]

#### 4.6 NEWMARK BETA INTEGRATION

The Newmark- $\beta$  integration method lends itself to evaluation of the transient response of structures and solids, due to its ability to tackle complex, dynamic systems using a one-step, implicit approach. [Bathe, 1982] Dykstra demonstrated the versatility of this integration scheme during his study of non-linear drill string dynamics [1996], and the Newmark- $\beta$  is now widely used for related studies – especially those involving the analysis of lateral drill string dynamics.

The effective stiffness matrix is a one-time calculation performed before initiating the integration routine:

$$\text{Equation 49: } K_{eff} = K + a_0 \cdot M + a_1 \cdot C$$

The effective force vector is calculated at each time step:

$$\text{Equation 50: } F_{eff} = F_c + F_0 + F_{dyn} + \dots$$

$$..M \cdot \left( a_0 \cdot U + a_2 \cdot \dot{U} + a_3 \cdot \ddot{U} \right) + C \cdot \left( a_1 \cdot U + a_4 \cdot \dot{U} + a_5 \cdot \ddot{U} \right)$$

The terms in Equation 50 are defined as follows:

- $F_c$  represents controller inputs, i.e. hook load and surface torque.
- $F_0$  represents the contribution of gravitational force.
- $F_{dyn}$  represents external forces generated by torque and drag forces acting on the tubular elements along the wellbore.
- $M$  represents the mass matrix
- $C$  represents the damping matrix

Note: Coefficients  $a_{0-7}$  are integration constants unique to the Newmark Beta Method, based on a Taylor-series expansion, and they are defined as:

$$a_0 = \frac{1}{\alpha \cdot dt^2}; \quad a_1 = \frac{\delta}{\alpha \cdot dt}; \quad a_2 = \frac{1}{\alpha \cdot dt}; \quad a_3 = \frac{1}{2 \cdot \alpha} - 1; \quad a_4 = \frac{\delta}{\alpha} - 1; \quad a_5 = \frac{dt}{2} \cdot \left( \frac{\delta}{\alpha} - 2 \right);$$

$$a_6 = dt \cdot (1 - \delta); \quad a_7 = \delta \cdot dt$$

Where  $\alpha$  and  $\delta$  are tuning constants that are set according to the nature of the approach (trapezoidal rule, linear acceleration, purely explicit, etc.). In this case,  $\alpha$  and  $\delta$  are set to 0.25 and 0.5, respectively.

The initial-value problem is solved using pre-defined initial conditions at a discrete time, using the set of equations shown in Equation 51:

$$\text{Equation 51: } \left\{ \begin{array}{l} [M] \ddot{U}_i + [C] \dot{U}_i + [K] U + F_{eff} = F_g \\ U_{i=0} = U_0 \\ \dot{U}_{i=0} = \dot{U}_0 \end{array} \right\}$$

The equations of motion are solved at each subsequent time step using Equations 52- 54:

$$\text{Equation 52: } U_i = \frac{F_{eff}}{K_{eff}}$$

$$\text{Equation 53: } \ddot{U}_i = a_0 \cdot (U_{(i)} - U_{(i-1)}) - a_2 \cdot \dot{U}_{(i-1)} - a_3 \cdot \ddot{U}_{(i-1)}$$

$$\text{Equation 54: } \dot{U}_i = \dot{U}_{(i-1)} + a_6 \cdot \ddot{U}_{(i-1)} + a_7 \cdot \ddot{U}_{(i)}$$

Figure 4.11 presents flow chart to illustrate the iterative simulation routine:

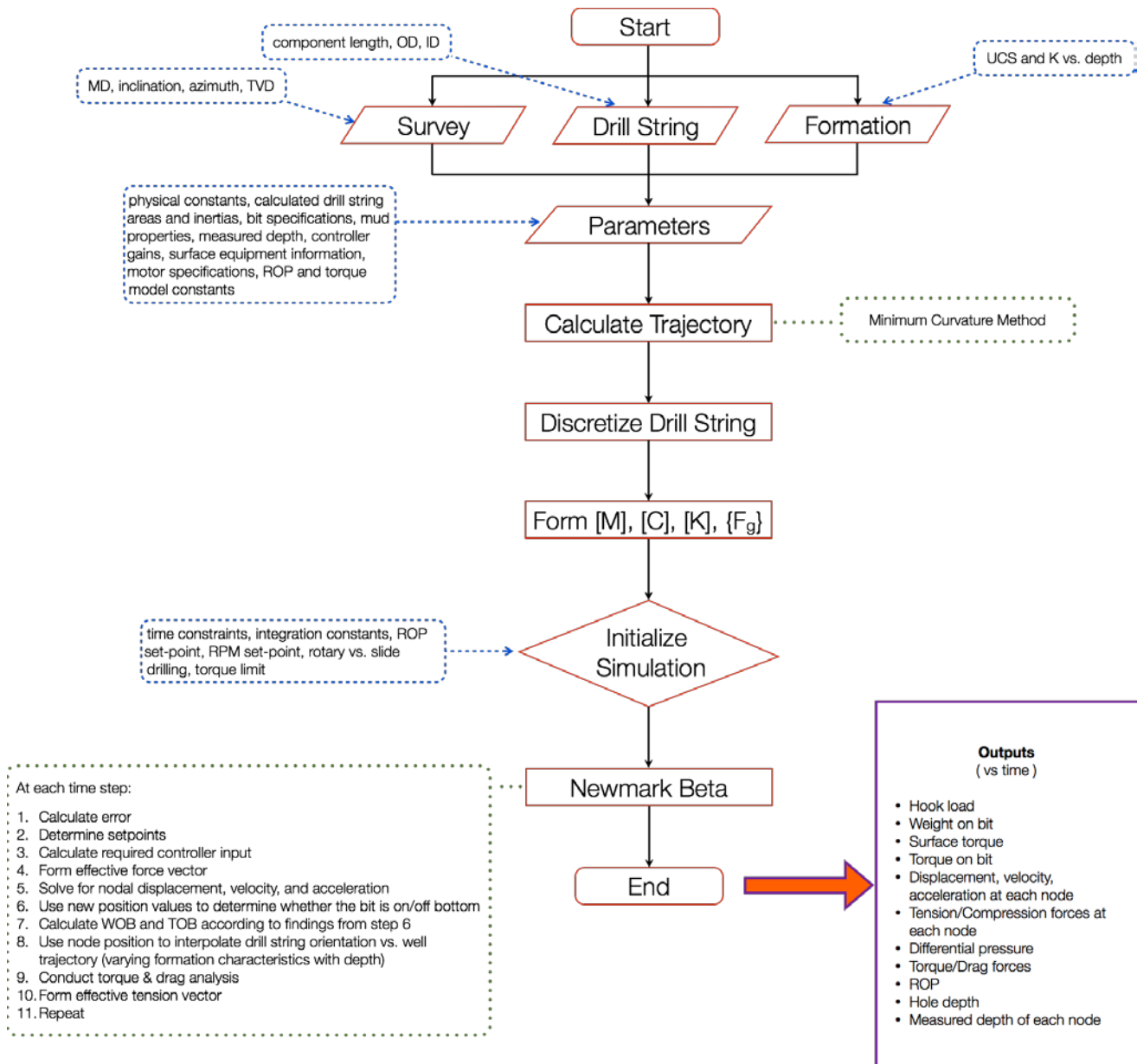


Figure 4.11: The simulation routine uses survey data, drill string composition, formation characteristics, and auxiliary system parameters to calculate well trajectory and analyze system loads and dynamic behavior at each time step.

## 4.7 MODEL CHARACTERISTICS AND SENSITIVITIES

### 4.7.1 Static Analysis

Static model validation was performed using a uniform drill string of a known length in a vertical hole, where known material properties allow for exact determination of system response using mechanics of materials principles. Expected axial stretch can be determined using Equations 55 and 56, and those calculations are validated using the results shown in Figure 4.12.

$$\text{Equation 55: } U_{Surface} = \frac{P}{K_i}$$

$$\text{Equation 56: } U_{Bit} = \frac{P \cdot L}{A \cdot E}$$

$P$  = axial load (lbf)

$K_i$  = axial, integral controller gain (ft)

$L$  = section length (ft)

$A$  = cross-sectional area (in<sup>2</sup>)

$E$  = Young's modulus (psi)

Table 4.1: Uniform drill pipe and motor assembly – 1,000' total in length.

Component	Length (ft)	Outer Diameter (OD)	Inner Diameter (ID)	Contact Diameter (CD)
Drill Pipe	900	5	4.276	6.5
HWDP	0	5	3	6.5
Drill Collars	0	7	3	8
Motor	100	5	4.276	9
Bit	0	9.88	0	9.88
<b>Total Length</b>	1000			

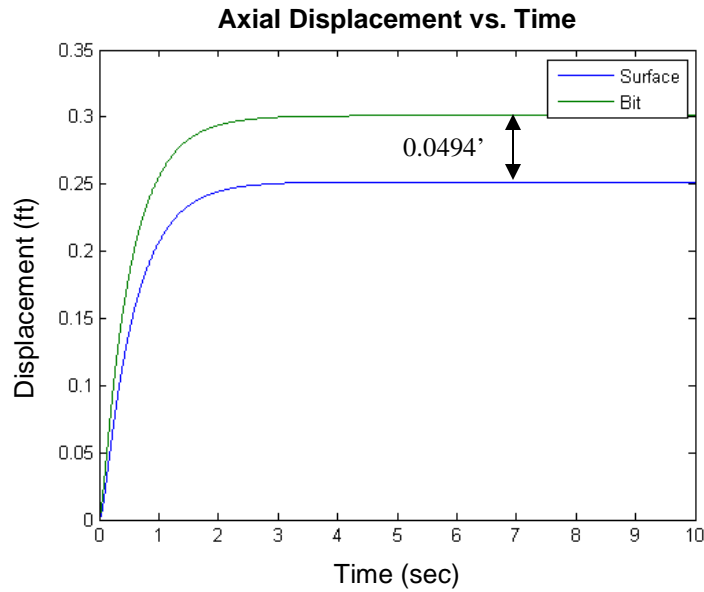


Figure 4.12: Drill pipe stretch at various locations is verified analytically in a vertical wellbore. This graph shows the displacement between surface and bit nodes for the drill string configuration described in Table 4.1.

Transient velocity and acceleration calculations support first-principles analytical solutions for the described scenario:

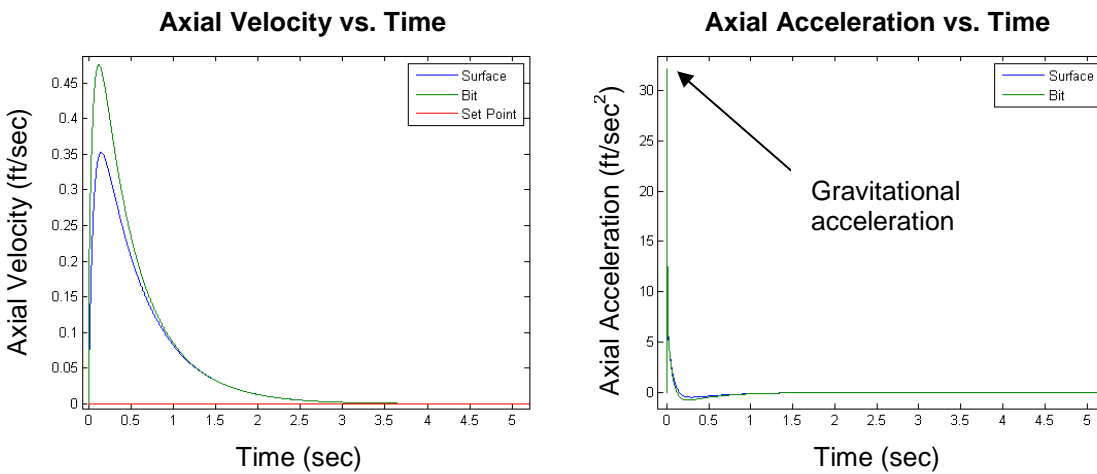


Figure 4.13: Drill pipe velocity and accelerations match first-principles analytical solutions at various points along the drill string.

## 4.7.2 Step Change Analyses

Step changes analyses were used to tune surface equipment controllers and validate the finite-element drill string model. These tests are performed for the axial and torsional degrees-of-freedom to tune the hoisting and rotary controller gains, respectively.

### 4.7.2.1 Block Speed

Draw-works controller gains were tuned by performing a step test in the axial domain. A step change in block speed (axial velocity) produces a transient response along the drill string. Figure 4.14 illustrates how bit velocity is slower to respond at first, but it ultimately overshoots the set point to a greater extent than does the surface set point. This is a result of the relationship between drill string material properties and draw-works controller gains.

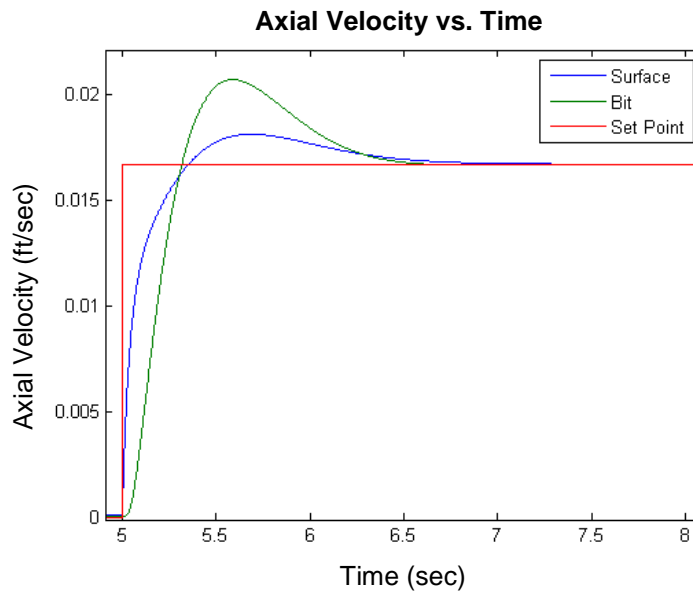


Figure 4.14: A block speed step test was performed to tune hoisting equipment controllers and validate the finite-element drill string model in the axial domain.

#### 4.7.2.2 Top Drive RPM

Top drive controller gains were tuned using the same procedure outlined in Section 1.4.7.2.1. A step change in top drive RPM (angular velocity) initiates a torque transmission wave along the drill string. The contribution of material damping is a function of vibration frequency, drilling fluid properties, drill string composition, and wellbore characteristics. The magnitude of initial overshoot of bit angular velocity over surface angular velocity may be used to tune Rayleigh damping coefficients used to build the damping matrix. [Brakel, 1986] (Figures 4.15 and 4.16)

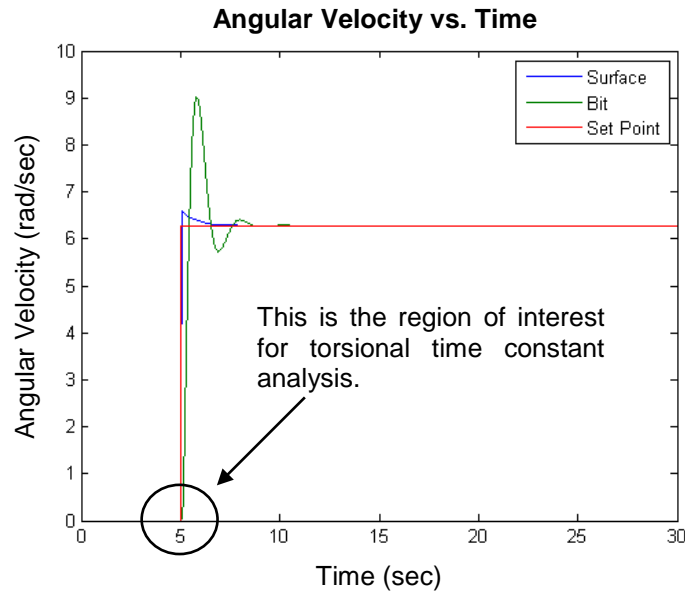


Figure 4.15: A top drive RPM step test was performed to tune rotary equipment controllers and validate the finite-element drill string model in the torsional domain. Figure 4.16 shows the region of interest in greater detail.

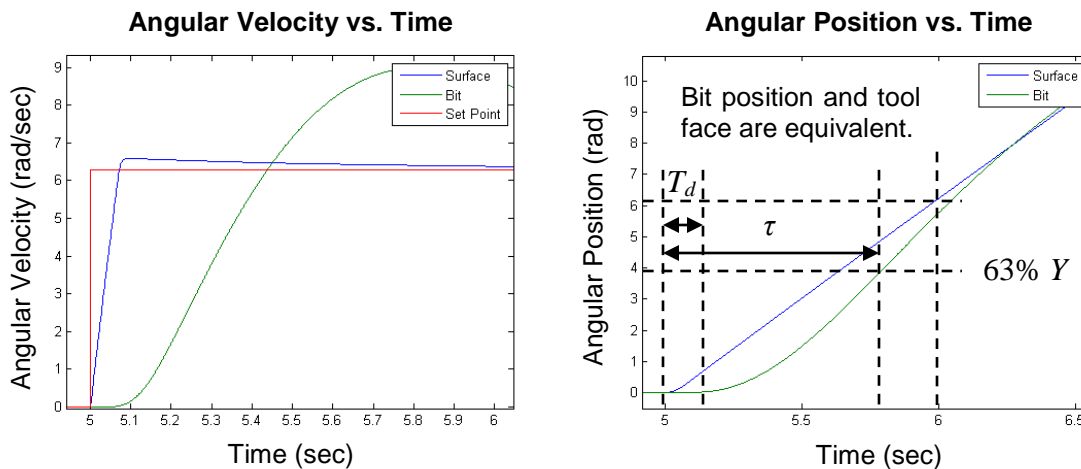


Figure 4.16: The region of interest for transient torsional response is located at the time at which the step change is introduced.

Although the rotary set-point is top drive angular velocity, the process variable of interest is bit angular position. Therefore, the torsional dead time and time constant are determined through analysis of angular position vs. time, based on a positional set-point defined through manipulation of the top drive angular velocity, as shown in Figure 4.16. This is a critical point – defining the basis for analysis for the remainder of this presentation.

#### 4.7.2.3 Pump Rate

Recall that bit RPM is a function of top drive RPM, pump rate, and motor characteristics. Figure 4.17 shows how bit RPM tracks surface RPM until pumps are switched on – triggering an immediate response at the bit.

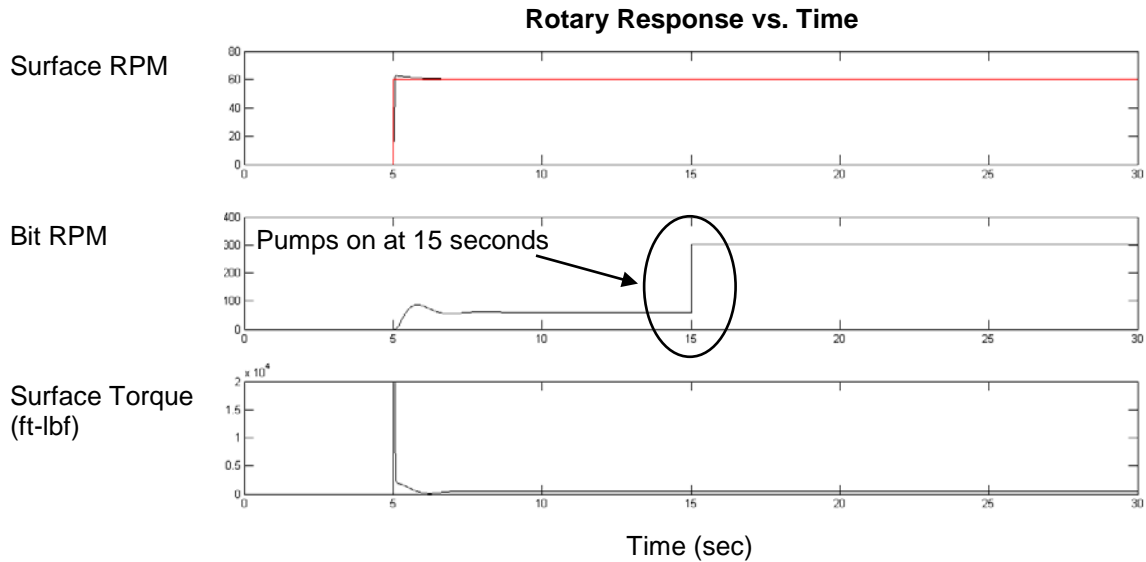


Figure 4.17: This model does not capture transient behavior for fluid dynamics initiated at the mud pumps. Instead, changes in flow rate immediately manifest pressure effects at the down-hole motor, which affects bit RPM.

Implications of excluding transient pressure effects from this model are discussed in Section 4.7.3.3.

### 4.7.3 Model Sensitivities

This section outlines key model parameters that influence dynamic simulation results. A brief explanation of how manipulations in model parameters affect the torsional time constant is presented with each result.

#### 4.7.3.1 Drill String Composition

Elongation of the drill string due to an applied tensile load is dependent upon mechanics of materials that compose the drill string. Total elongation of the drill string may be obtained through the summation of the individual elongations of each drill string element. Drill string composition also affects torque transmission vs time, as wave behavior is a function of material properties and geometry. Tables 4.2 - 4.4 describe the

drill string configurations used to generate the results shown in Figure 4.18-Figure 4.20, respectively. In each case, the drill string is allowed to relax for 10 seconds before the top drive RPM is changed from 0 to 60. These plots compare axial stretch and torque transmission vs. time for each drill string configuration.

Table 4.2: Drill String #1: Uniform Drill Pipe and Motor Assembly

Component	Length (ft)	Outer Diameter (OD)	Inner Diameter (ID)	Contact Diameter (CD)
Drill Pipe	4970	5	4.276	6.5
Motor	30	5	4.276	6.5
Bit	0	9.88	0	9.88
Total Length	5000			

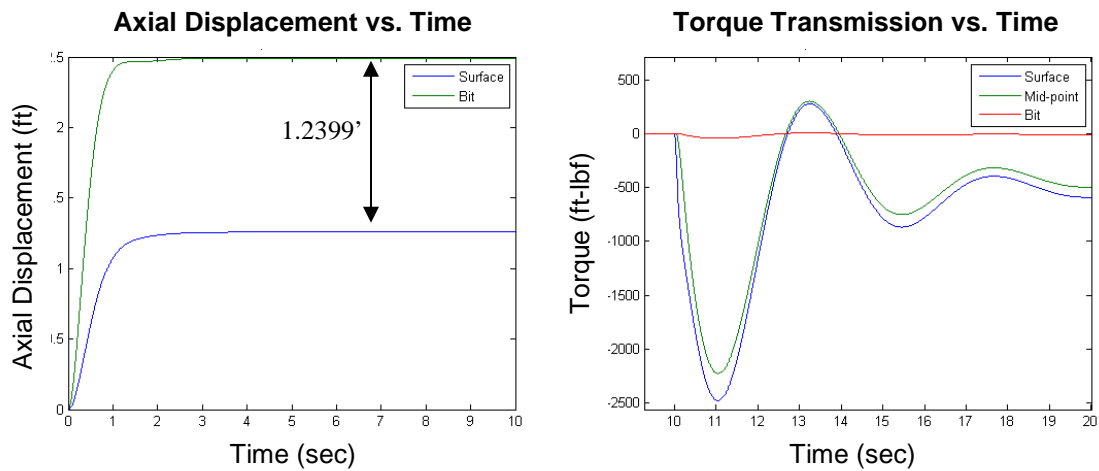


Figure 4.18: Axial displacement and torque transmission vs. time for Drill String #1- described in Table 4.2.

Table 4.3: Drill String #2: Drill Pipe, Drill Collars, and Motor Assembly

Component	Length (ft)	Outer Diameter (OD)	Inner Diameter (ID)	Contact Diameter (CD)
Drill Pipe	3470	5	4.276	6.5
Drill Collars	1500	7	3	8
Motor	30	8.5	2.875	9
Bit	0	9.88	0	9.88
<b>Total Length</b>	5000			

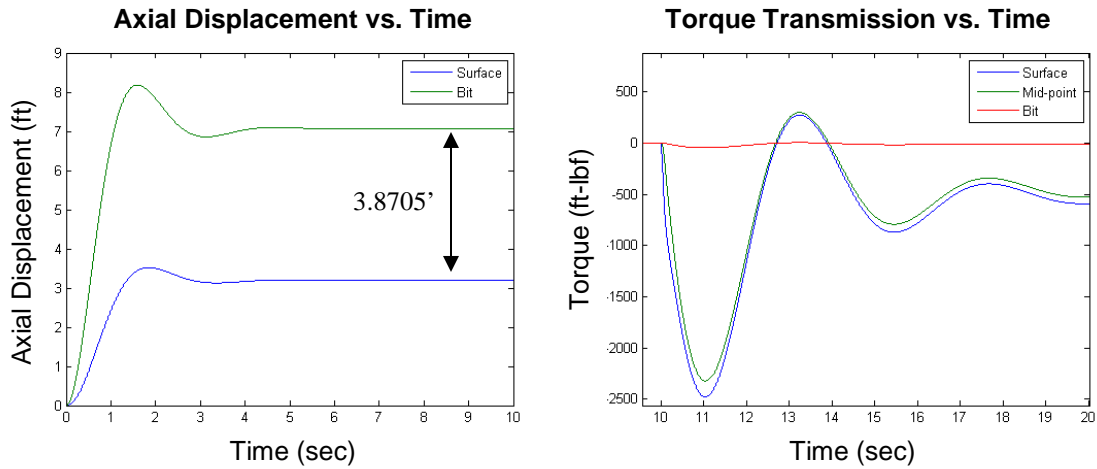


Figure 4.19: Axial displacement and torque transmission vs. time for Drill String #2- described in Table 4.3.

Table 4.4: Drill String #3: Drill Pipe, HWDP, Drill Collars, and Motor Assembly

Component	Length (ft)	Outer Diameter (OD)	Inner Diameter (ID)	Contact Diameter (CD)
Drill Pipe	2970	5	4.276	6.5
HWDP	500	5	3	6.5
Drill Collars	1500	7	3	8
Motor	30	8.5	2.875	9
Bit	0	9.88	0	9.88
<b>Total Length</b>	5000			

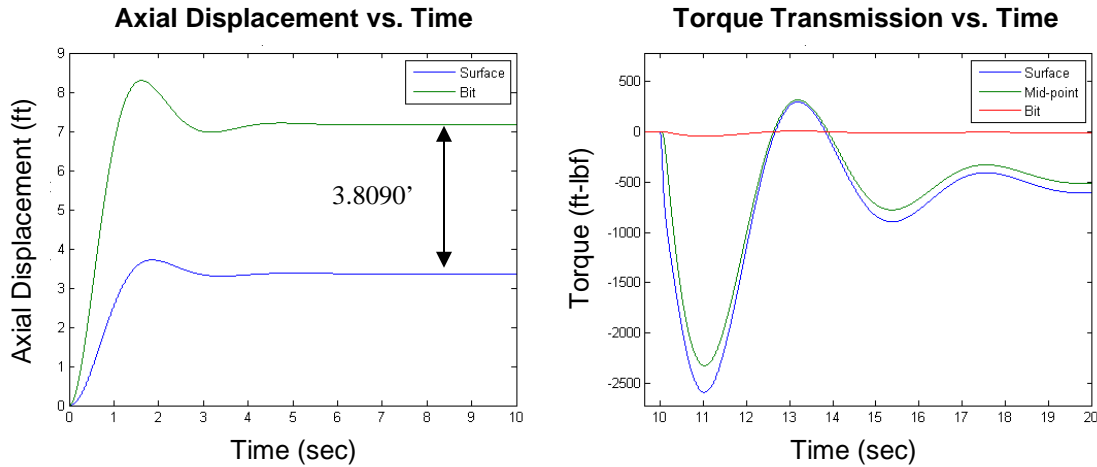


Figure 4.20: Axial displacement and torque transmission vs. time for Drill String #3- described in Table 4.4.

Using the simulation results presented in Figures 4.18 - 4.20, it is possible to demonstrate how the torsional dead time and time constant change for various drill string configurations. Note that time constant for Drill String #1 is highest in magnitude – a result of the following factors:

- Drill String #1 has the lowest cumulative torsional rigidity, i.e. drill pipe is the most flexible drill string component, compared to HWDP and drill collars.
- Material damping coefficients cause the velocity impulse to dissipate more quickly in drill pipe than in HWDP and drill collars, due to the fact that the angular velocity wave travels relatively quickly through these elements. For

reference, compare the dead time of Drill String #1 to values exhibited by other drill string configurations.

Also note that the dead time for Drill String #2 is highest in magnitude. This is due to the fact that the drill pipe is responsible for supporting the same BHA as in Drill String #3, without the additional torsional rigidity offered by the transition pipe (HWDP).

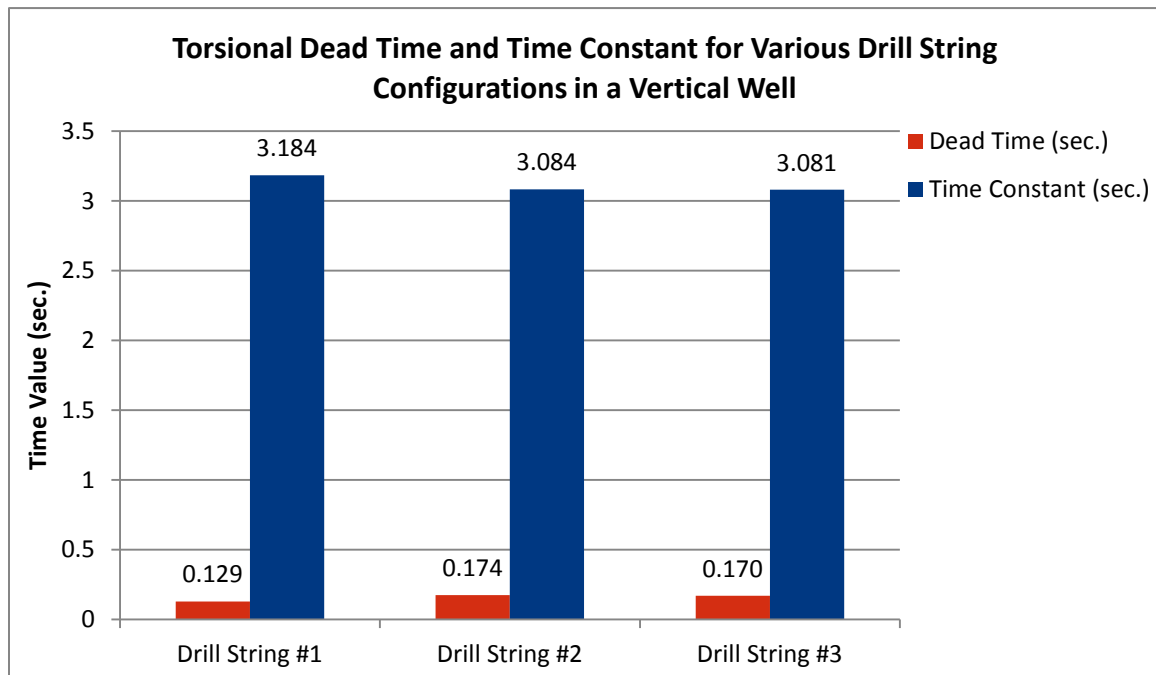


Figure 4.21: Drill string composition affects transient torsional response.

#### 4.7.3.2 Well Trajectory

The drill string configuration described in Table 4.2 (Drill String #1) was used to analyze how well trajectory affects dynamic response. Transient drill string response to a step change in top drive RPM is compared for idealized vertical, build, slant, and lateral wellbores.

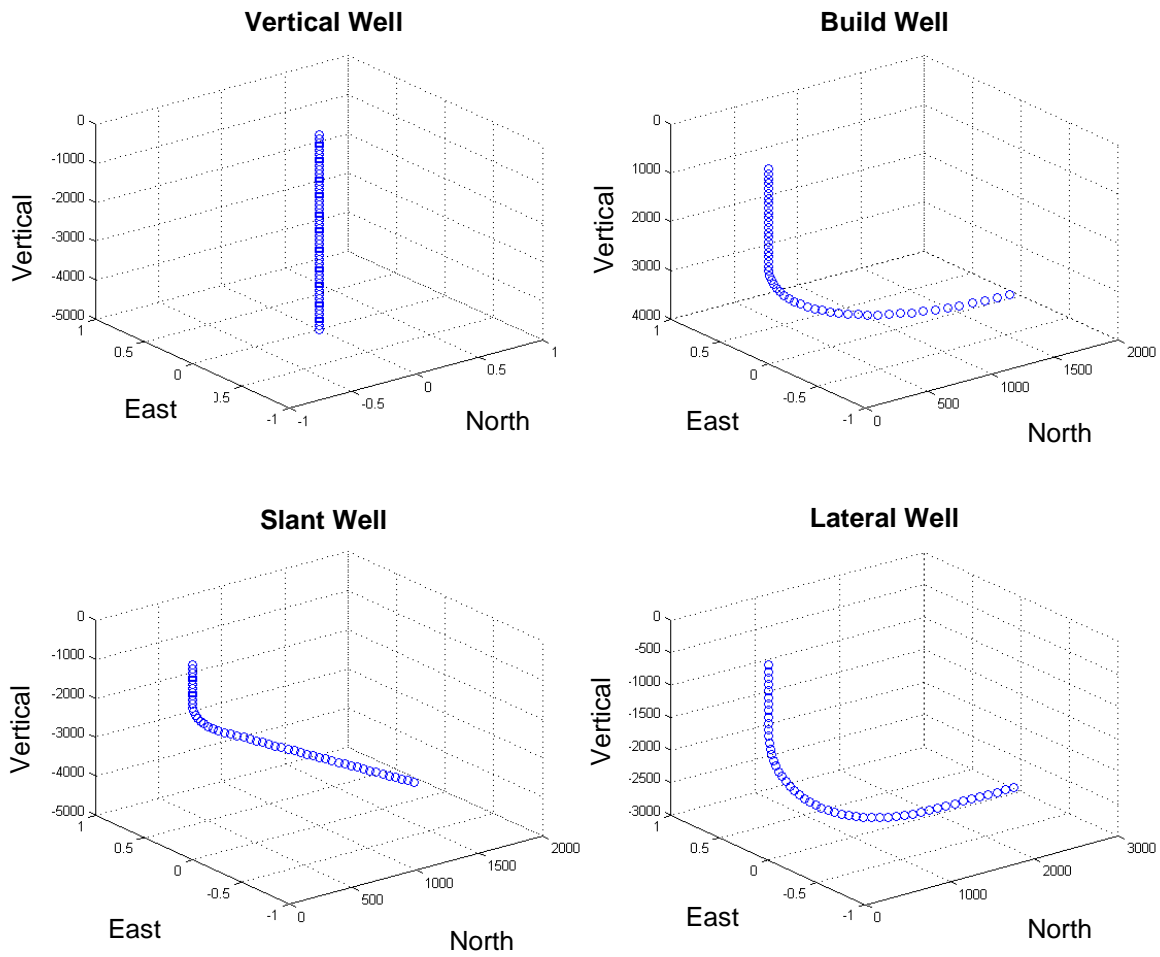


Figure 4.22: Vertical, build, slant, and lateral well plans are compared to demonstrate how well trajectory affects dynamic simulation results.

See Appendix A for survey data that defines the well trajectories shown in Figure 4.22.

Gravitational, internal, and normal drill string forces affect torque and drag calculations for various wellbore orientations (Figure 4.23).

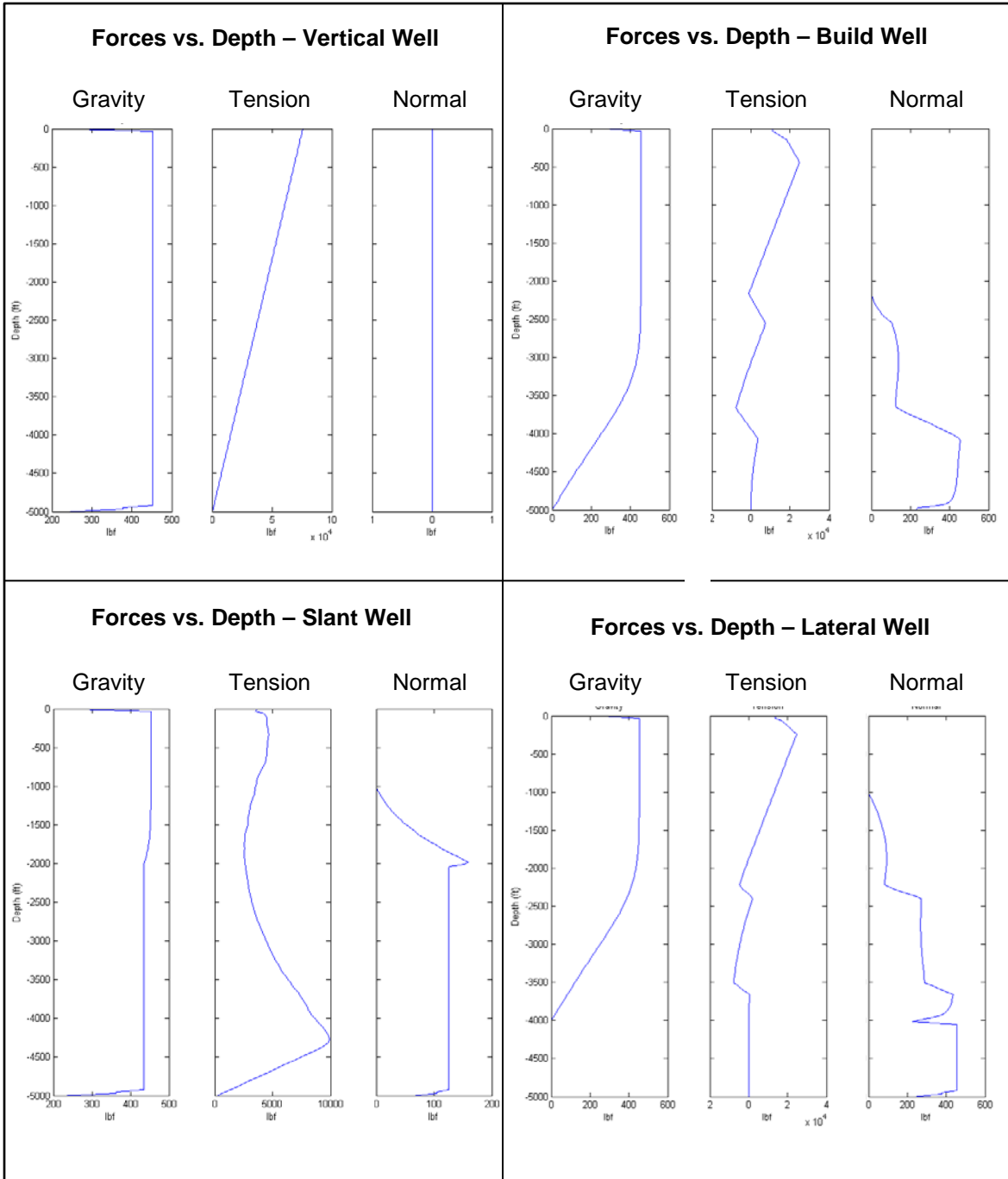


Figure 4.23: Wellbore orientation affects static drill string forces. These plots compare gravitational, tension, and normal forces for vertical, build, slant, and lateral wells.

As expected, the torsional dead time and time constant are highest for the lateral well trajectory. This behavior is a direct result of increased friction forces in the horizontal section of the wellbore. Note that this analysis was carried out with no axial weight applied to the bit, i.e. off-bottom.

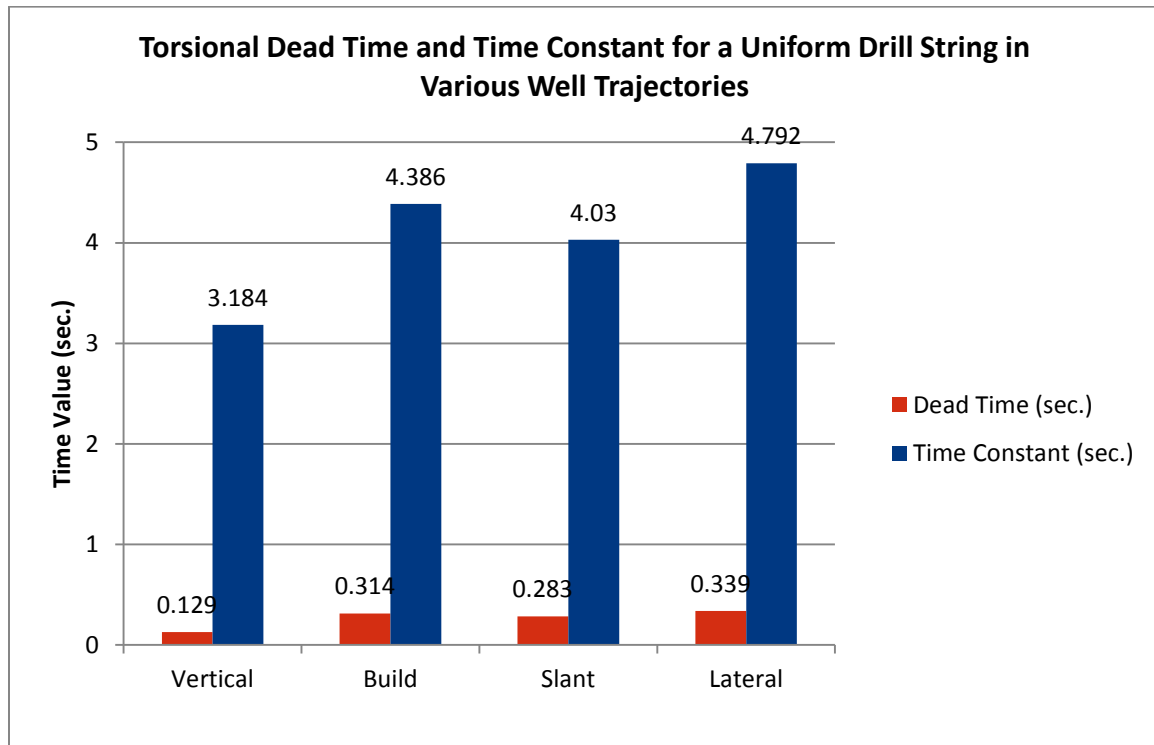


Figure 4.24: Wellbore orientation affects transient torsional response.

Use of the semi-soft string model makes build and lateral wellbore simulations most susceptible to inaccuracies, because these well paths include the greatest percentage of total length in a build section. Buckling and tortuosity effects are more likely to manifest themselves in these wellbores, especially when drilling with a down-hole motor, as it becomes more difficult to transfer weight to the bit. Model assumptions would cause the torsional dead time and time constant to be over-estimated in these cases.

### 4.7.3.3 Operating Parameters

Operating parameters affect boundary conditions, which can have a significant impact on transient drill string response. This section presents results from a 60-second simulation, during which various changes in ROP and RPM set-points were made. Table 4.5 shows the axial and angular velocity set-points that define the following progression:

1. The drill string is allowed to relax from 0-5 seconds.
2. The top drive is activated at the 5-second mark, demonstrating torsional response while off-bottom.
3. The block starts lowering at the 10-second mark, and the bit tags bottom approximately 25 seconds into the simulation.
4. At the 40-second mark, the top drive RPM is increased to demonstrate torsional response while on-bottom.
5. The ROP set-point is reduced by half at the 45-second mark to reduce WOB.
6. At the 50-second mark, the top drive RPM is reduced by half in order to compare torsional response when decreasing the rotary set-point.
7. Both the ROP and RPM set-points are doubled at the 55-second mark to demonstrate system response when both set-points are changed simultaneously.

Table 4.5: Rate of penetration and top drive RPM set-point changes were made over a 60-second time interval.

Time (seconds)	ROP (ft/hr)	RPM
0	0	0
5	0	50
10	120	50
40	120	60
45	60	60
50	60	30
55	120	60

### Transient Axial and Torsional Dynamics for Various Combinations of Axial and Angular Velocity Set-Points

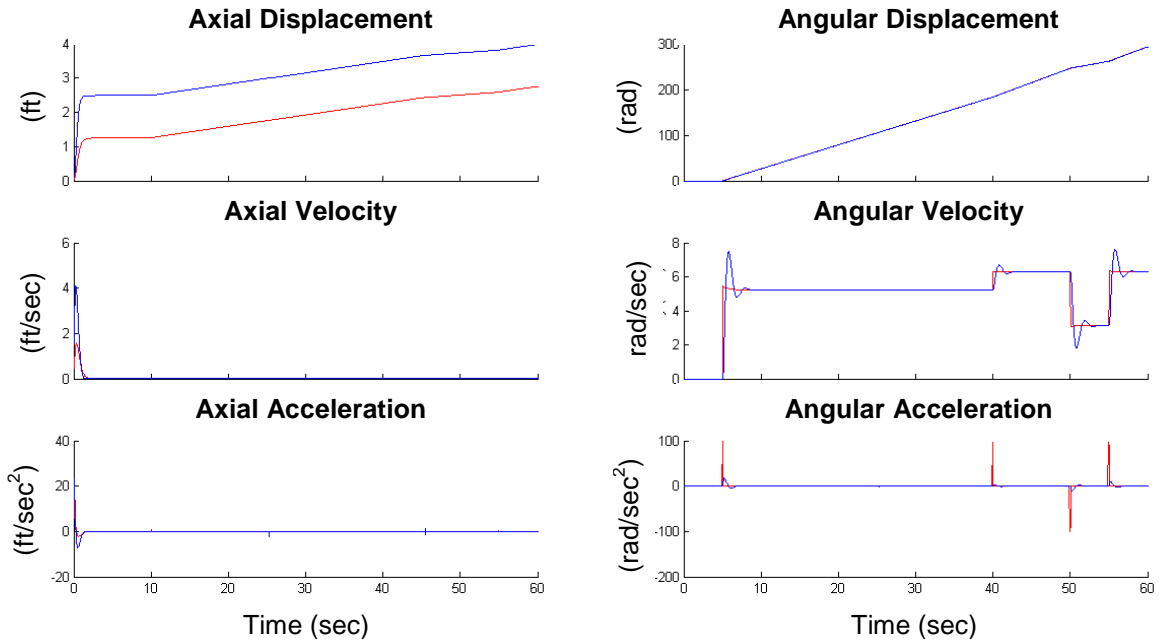


Figure 4.25: Axial and torsional dynamics are affected by changes in operating parameters and boundary conditions.

**Torque Transmission vs. Time for Various Operating Parameter Combinations – Including Both Off-Bottom and On-Bottom Conditions**

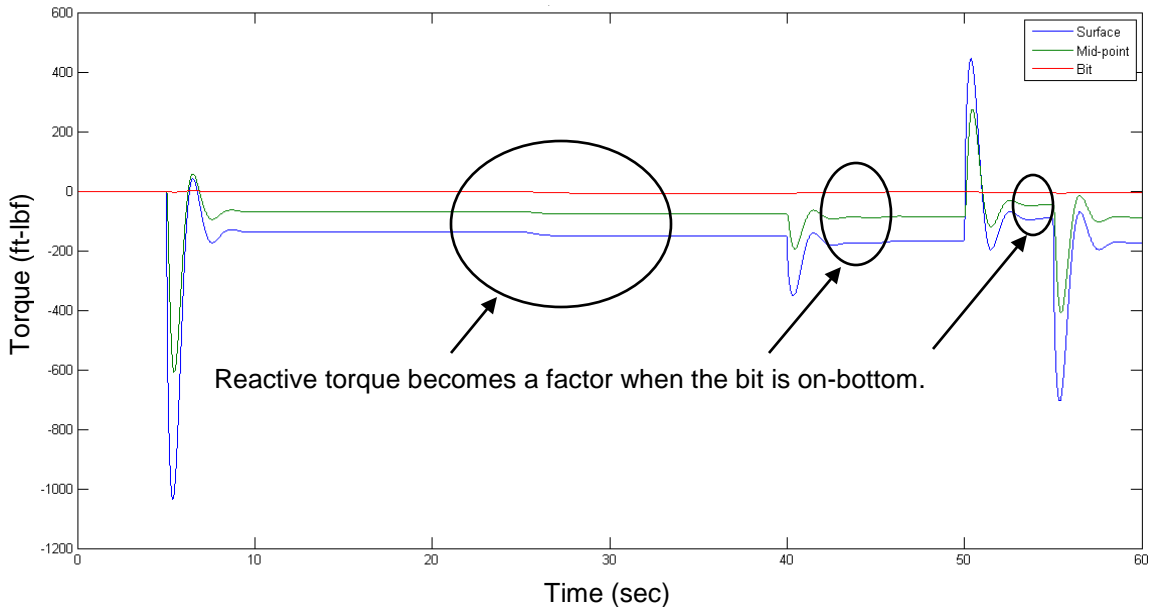


Figure 4.26: Torque transmission behavior is dependent upon the magnitude of the disturbance and boundary conditions.

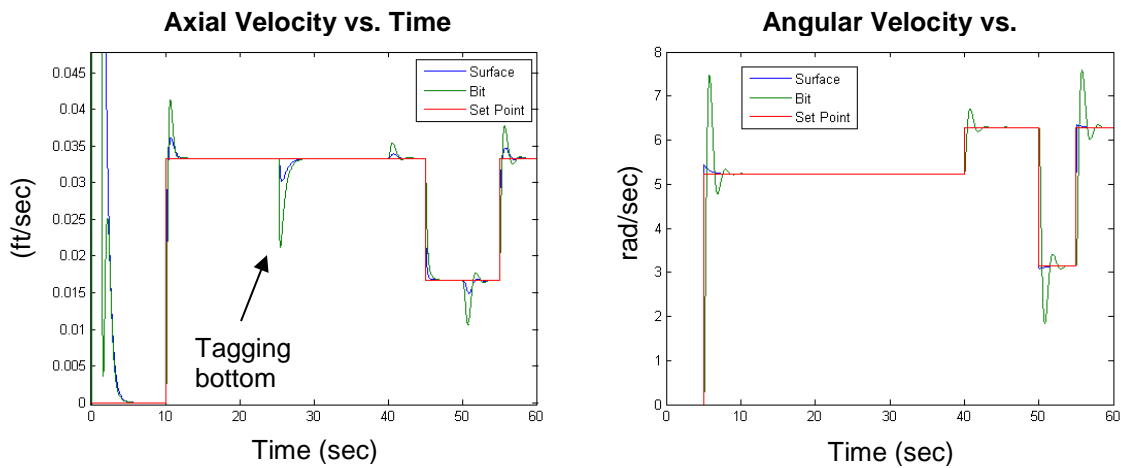


Figure 4.27: Step changes in axial and angular velocity set-points affect the system differently as boundary conditions change.

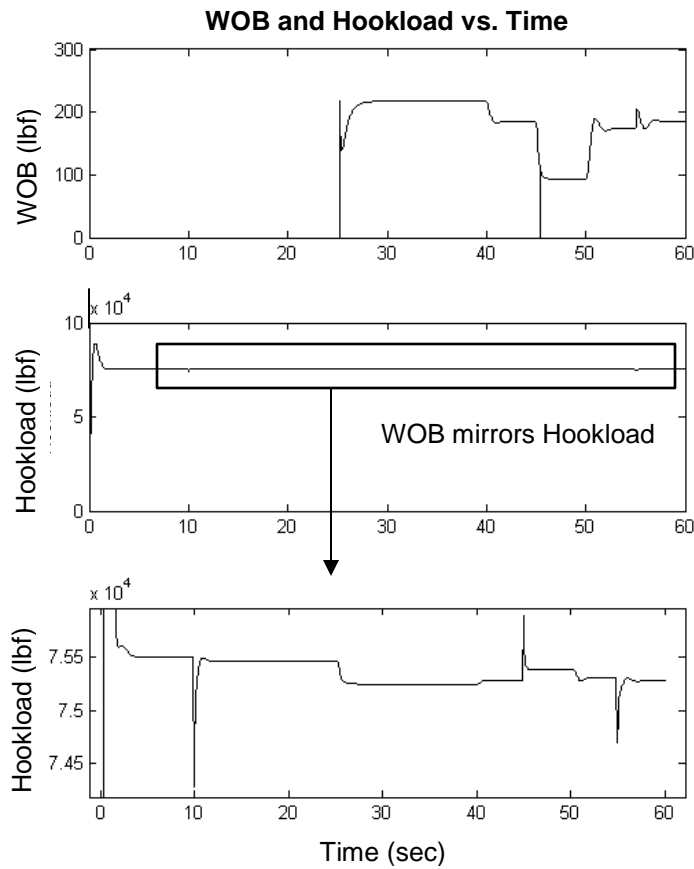


Figure 4.28: Weight-on-bit is a key factor that affects the torsional time constant. This parameter is controlled using hook load measurements. Notice that the two values mirror each other when on-bottom.

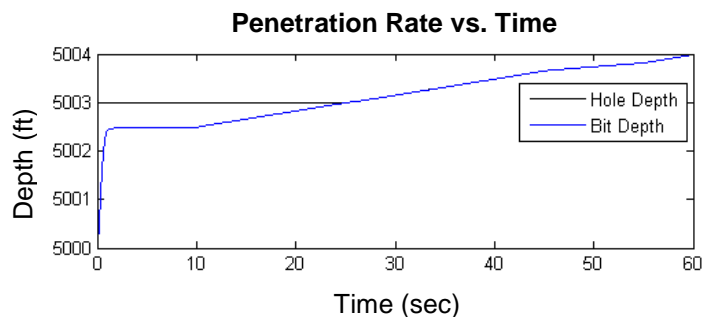


Figure 4.29: Rate of penetration is a function of weight- and torque-on-bit.

This simulation captures reactive torque effects as the bit tags bottom and continues to drill ahead. There are two ways in which reactive torque influences the torsional time constant:

1. Increased reactive torque changes the bit boundary conditions – causing WOB to increase and countering TOB applied via surface rotation and down-hole motor operations. The implications of these effects in regards to the torsional dead time and time constant are dependent upon the magnitude of reactive torque generated at the bit. Refer back to Figure 4.26 to observe how reactive torque varies under different operating conditions.
  - a. Increased WOB decreases the torsional dead time and time constant.
  - b. Counter-active torque increases the torsional dead time and time constant.
2. Reactive torque introduces a disturbance to the drill string that interrupts the angular velocity wave travelling from surface to the bit. This disturbance manifests itself in the form of drill string twist, which ultimately affects the bit angular position, i.e. tool face. Therefore, it is reasonable to expect to see higher torsional dead time and time constant values as increased reactive torque is encountered.

As transient pressure effects are excluded from this model formulation, the pump rate set-point is not considered in this simulation. If a pump rate step change were to be introduced to the system, bit speed would instantaneously increase to reflect that manipulation. It follows that WOB would immediately decrease as bit angular increases, if all else is held constant. Therefore, exclusion of the consideration of transient pressure effects would lead to an under-estimation of the torsional dead time and time constant in the period of time immediately following a step-change increase in pump rate.

### 4.7.3.4 Viscosity and Friction Effects

Friction is the main contributing factor to system stability. Excessive wellbore friction factors lead to chatter. Figure 4.30 illustrates the effects of excessive wellbore friction ( $\mu_{rock} = 0.5$ ) for the slant well trajectory. The first 5 seconds of this simulation show the effects of excessive wellbore friction as the drill string relaxes – demonstrating the consequences of axial movement in the absence of rotation. Axial chatter is instantaneously reduced when the top drive starts rotating at the 5-second mark. During the sixth second of this simulation, the top drive angular velocity set-changed from 0 rpm to 60 rpm before returning to 0 rpm for the duration of the simulation.

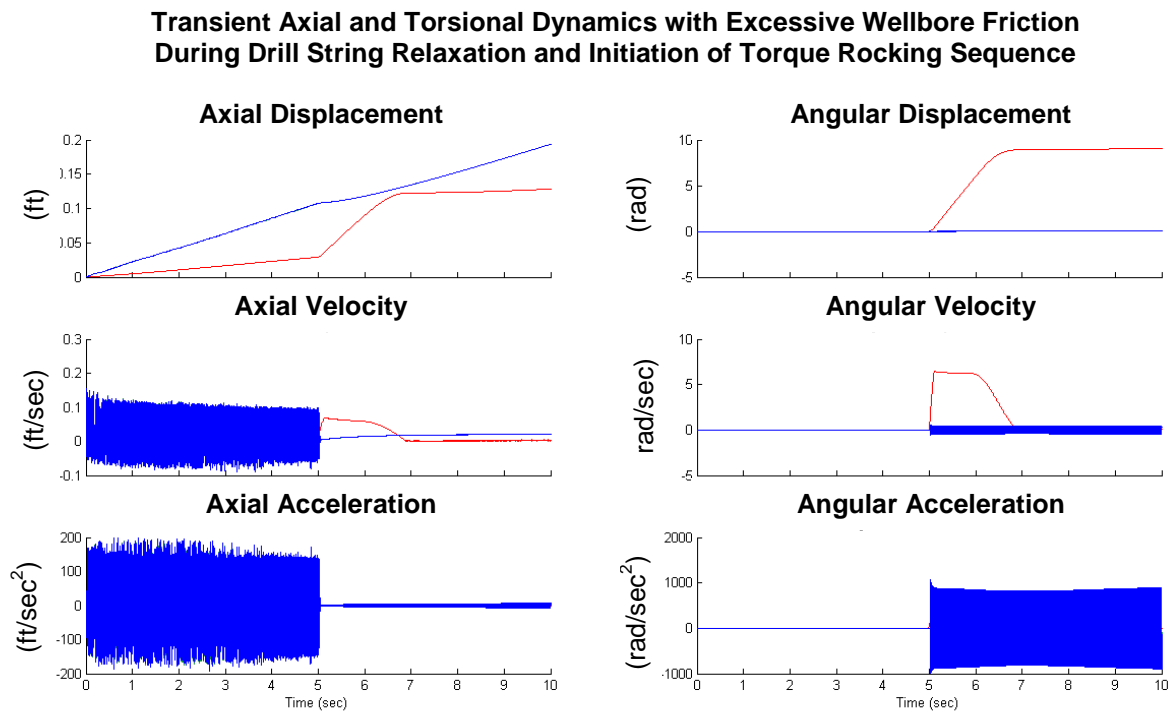


Figure 4.30: Excessive wellbore friction factors lead to system instability.

The sequence executed in this simulation mimics the process of initiating a torque rocking sequence in a single direction – without oscillating the top drive back and forth or returning to the starting position. This effectively initiates a change in tool face through initiation of a “right-hand bias”.

Drilling fluid viscosity effects are not explicitly modeled. Therefore, it is necessary to adjust the wellbore friction factors to capture the reduction in along-hole friction as a result of increased drilling fluid viscosity. Over-estimation of friction effects along the wellbore has a direct and proportional impact on torsional dead time and time constant calculations.

#### ***4.7.3.5 Formation Characteristics***

As shown in Equation 38, this model considers a linear relationship between *WOB* and *CSF*. Based on the simulation results presented in Section 4.7.3.3, the torsional dead time and time constant should decrease as *CSF* values increase (all else held constant).

## **4.8 SUMMARY**

Transient drill string dynamics analyses were conducted using the Newmark- $\beta$  integration method. Drill string boundary conditions are governed by surface contributions made by the draw-works, top drive, and mud pumps, as well as wellbore and bit constraints. Bit boundary constraints are determined according to whether the bit is on-bottom or off-bottom at each time step.

The drill string is discretized using finite-element techniques – where external loads due to drill string/wellbore interaction act on each node. Internal tension and torsion contributions are calculated for each element, based on loading at the end nodes.

Torque and drag loads are dependent upon the normal force acting upon each node – based on drill string orientation within the wellbore. The formation coefficient of friction affects the extent to which dynamic torque and drag loads impact drill string dynamics.

Both static and dynamic analyses were used to validate the model formulation. Static cases were run to verify internal drill string forces acting in response to gravitational force, while step change analyses were used to tune controller gains and inspect dynamic response due to loading along the wellbore. Key model sensitivities are drill string composition, well trajectory, operational parameters, friction effects, and formation characteristics. Of these sensitivities, the best opportunity to improve the directional drilling simulation routine lies in the ability to determine accurate coefficients of friction.

## 5 Experimental Results and Discussion

### OVERVIEW

The experimental component of this study includes a comparison of the torsional time constant calculated using simulation results against analytical and manual calculations made in real-time. The analytical torsional time constant feeds into the tool face projection algorithm, which influences controller response. This tool face projection algorithm is also a function of differential pressure effects and *positional bias*<sup>3</sup> introduced via top drive position.

The analytical torsional time constant is calculated using the principle of *String Delta Torque (SDT)*, which is defined as the difference between surface torque and down-hole motor torque. String delta torque balances friction forces present along the drill string while rotating at a constant angular velocity, and the calculation is made as operations transition from rotary to slide drilling. Analytical calculations are automatically set as default values in the SCADA system, and the operator may elect to manually override these values in order to achieve desired tool face control performance while sliding. The analytical torsional time constant is calculated using Equation 57 [Dykstra, 2012]:

$$\text{Equation 57: } \tau = \frac{\left[ \left( \frac{SDT}{\dot{\theta}_{TD}} \right) \cdot L_{DS} \right]}{(G \cdot J)}$$

---

<sup>3</sup> Positional bias is required if the operator needs to change tool face and is outside the scope of this study.

Simulation results include tool face position data at each time step, i.e. every millisecond. Simulation-based torsional dead time and time constant are determined using the criteria defined in Section 4.7.2.2.

An Appalachia-based case study of drilling in the Marcellus Shale highlights the progression of the torsional time constant in the lateral section of a wellbore. A post-well analysis provided baseline results and an opportunity to validate the first-principles directional drilling simulator against field data.

A subsequent case study of drilling in the Montney Shale was conducted in Groundbirch, and results were compared to those from Appalachia. An investigation of the effect of the torsional time constant on drilling performance was carried out by tracking tool face control performance and other KPI's for two wells drilled back-to-back on the same pad.

## **5.1 APPALACHIA CASE STUDY**

In order to improve slide drilling performance, i.e. tool face control capabilities, process automation and control engineers asked an experienced<sup>4</sup> SCADA drill operator to adjust and record the torsional time constant that led to optimal tool face control every 250 feet while drilling the lateral section with a down-hole motor.

Primary goals of this exercise include:

- Track how controller response is affected by increased torque and drag in the lateral.
- Understand what experienced operators (directional drillers) consider optimal tool face control performance.

---

<sup>4</sup> This operator had more than two years of experience drilling with the SCADA system at the time of this experiment. This operator previously worked as a directional driller in the Marcellus.

- Quantify the value of a properly-tuned tool face controller by comparing ROP to offset wells.

First-principles simulation results were compared to field data using planned well design data to describe the well trajectory (Appendix A). Figure 5.1 illustrates the well trajectory, and key characteristics are noted. This well design includes a combination of the characteristics described in Section 4.7.3.2.

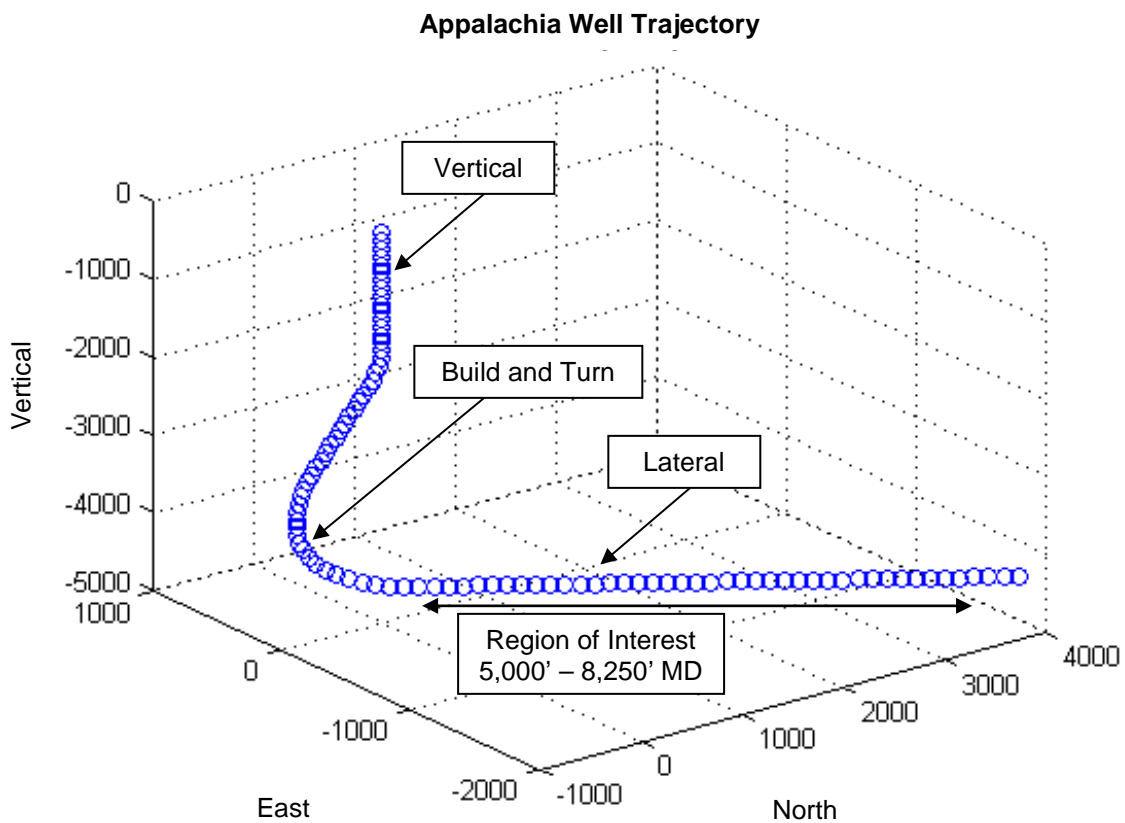


Figure 5.1: Appalachia well plans include vertical, build, hold, and lateral section.

The drill string design used for this simulation was built to reflect a generic design for lateral sections in Appalachia (Appendix B).

Table 5.1 outlines the drill string composition used for the Appalachia simulations. Note that the drill pipe length was increased to reflect the Measured Depth (MD) of each simulation.

Table 5.1: This drill string composition was used to simulate transient behavior for the Appalachia case study.

Component	Length (ft)	Outer Diameter (OD)	Inner Diameter (ID)	Contact Diameter (CD)
Drill Pipe	4800	5	4.276	5
HWDP	270	4	3	5
Drill Collars	180	6.5	2.875	5.5
Motor	30	6.625	0	6.625
Bit	0	7.875	0	0

Real-time drilling data was gathered from a database in order to determine WOB targets for each simulation. This data was also used to back-calculate the analytical time constant, which is not explicitly stored in the database. The casing shoe was set at 5,000 feet, and the casing and formation friction coefficients were set to 0.1 and 0.3, respectively.

Key assumptions for this analysis are as follows:

- Motor torque for the analytical time constant was back-calculated using bit RPM, pump rate, and motor characteristics.
- The top drive RPM value used for analytical and simulation calculations was 60 RPM – a common set-point for torque rocking systems.
- The polar moment of inertia  $J$  used to calculate the analytical time constant was calculated based only on drill pipe geometry – neglecting contributions from the HWDP and drill collars. The HWDP and drill collars are neglected for the analytical calculations, because BHA information is not updated in the system in real-time and the calculation is not iterative.
- The drill string length used to calculate the analytical time constant was set to equal bit depth.

- The analytical torsional time constant calculations were averaged over the course of a slide, while the torsional time constant calculated using simulation results was based on a point-analysis at the depth of interest.

Table 5.2: Simulation-based time constant calculations generally fall between analytically-determined and manually-entered values.

Measured Depth (ft)	Manually-Entered Time Constant (sec)	Analytically-Determined Time Constant (sec)	Simulation-Based Dead Time (sec)	Simulation-Based Time Constant (sec)
5,000	8	3.48	2.40	5.86
5,250	10	6.24	3.12	6.72
5,500	10	6.40	4.05	8.43
5,750	12	6.13	4.69	10.29
6,000	14	6.58	4.83	11.64
6,250	15	7.22	4.90	12.80
6,500	16	7.39	5.00	13.99
6,750	18	8.51	5.08	15.24
7,000	18	9.33	5.17	16.34
7,250	18	9.36	5.28	17.58
7,500	20	10.29	5.67	18.72
7,750	20	10.86	6.01	20.00
8,000	20	12.19	7.02	21.20
8,250	20	12.34	7.80	22.01

As shown in Table 5.2, analytical calculations of the torsional time constant vary from the manually-entered torsional time constant by 28.9%, on average and consistently under-estimate values when compared to the manually-entered time constant. The relative consistency of this offset indicates that a proportional multiplier might improve analytical time constant calculations. Further, inclusion of HWDP and drill collar effects would likely shift results closer to manually-entered values.

Simulation results led to torsional time constant calculations that varied from the manually-entered torsional time constant by 14.5%, on average. The simulation-based torsional time constant fell between the analytical and manually-entered time constant values in all instances except for the last two runs – when the simulation-based time constant exceeds the real-time prediction. (See Figure 5.2 for a graphical representation

of how torsional time constant calculations vary with measured depth for analytical, real-time, and simulation results.

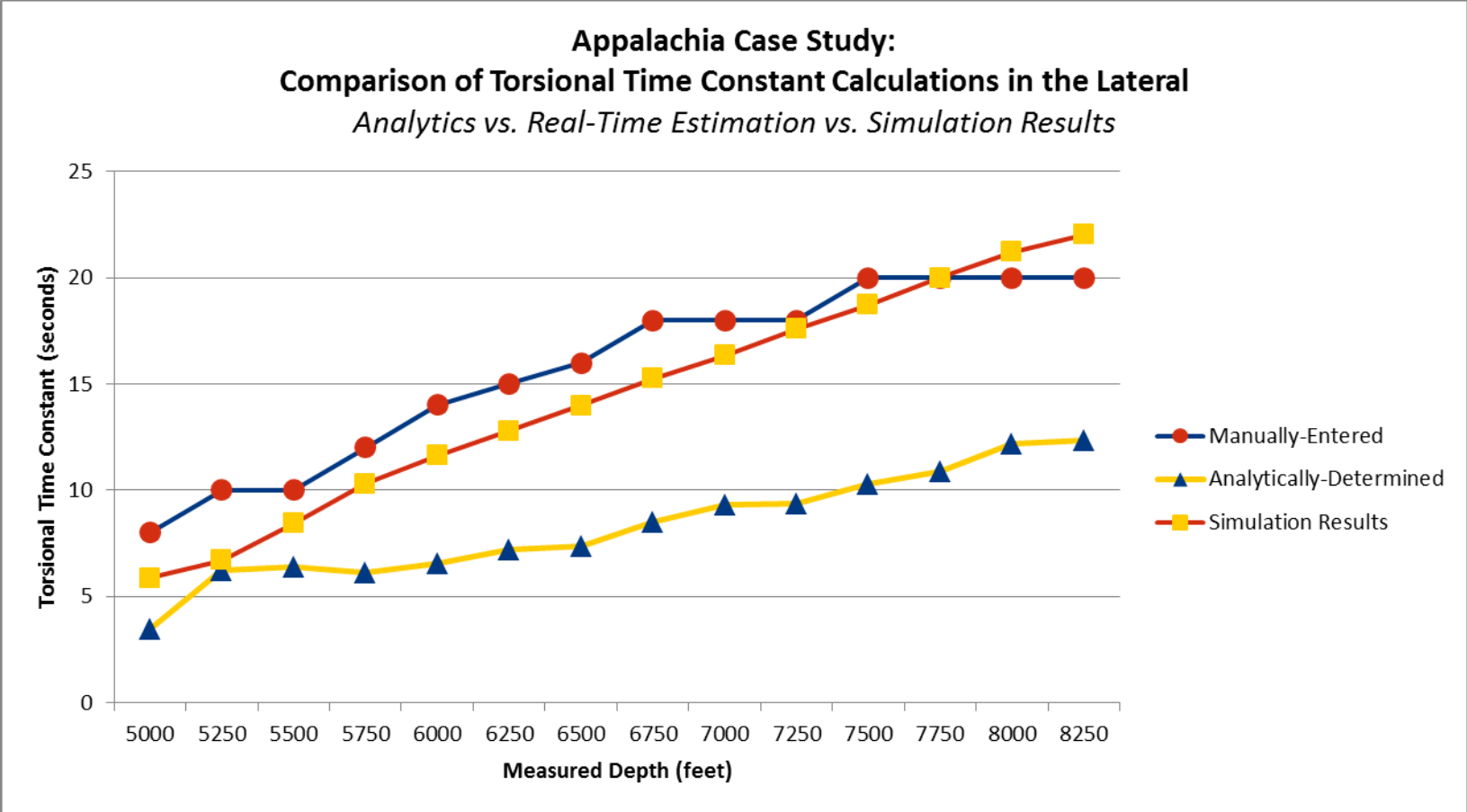


Figure 5.2: Analytical calculations generally under-estimate the torsional time constant value that produces satisfactory tool face control results in the lateral section of Appalachia wells.

Torsional time constant values calculated based on simulation results exhibit a near-linear behavior, while the analytical time constant calculations are more sensitive to sensor noise and operating parameter variance. Because data points are being collected every 250 milliseconds, outlying data points are more likely to have adverse effects on the analytical time constant calculations. Typical standard deviation in analytical time constant calculations is on the order of 50% per section. Simulation-based torsional time constants were not subjected to tortuosity effects, since idealized well plans were used.

Note in Figure 5.2 that the manually-entered time constant values remain constant between several depth intervals – a trend that defies basic physical principles. Therefore, this should serve as a demonstration that these values are subjective, as is the opinion of what is optimal tool face control performance. The near-linear trend exhibited by the simulation results is expected – as the lateral section should add resistance to additional pipe elements according to Coulomb friction principles. If this analysis would have been completed using actual survey data, these simulations would be subject to the tortuosity of the wellbore – likely affecting the linearity of this trend to increase the magnitude of the torsional time constant.

Note that the percent-variance between manually-entered and simulation-based time constant calculations is wider for smaller values (5-12 seconds) and converges as time constant values reach 16-20 seconds. The implication of this behavior could be increased tortuosity in upper-wellbore sections. However, it is not usually necessary to use torque-rocking systems in shallow hole. Therefore, it may be necessary to either adjust the first-principles model to reflect increased friction effects in upper-wellbore sections or elect to use a different control scheme in shallow hole.

In this case, the assumption is that the manually-entered time constants are best-suited for drilling in this environment. This assumption is based on the fact that the SCADA drill operator in control is experienced both in this field and in using the SCADA system. Further investigation is required to address whether the manually-entered time constant values offer superior drilling efficiency optimization results, in addition to

tackling the issue of objectivity regarding optimal tool face control performance. It is likely that the simulation-based time constant calculations offer comparable or superior tool face control performance in certain scenarios. Further the simulation routine is capable of producing predictable and repeatable results. Recall that the manually-entered time constant values in this case study were entered by a top-tier SCADA-drill operator. As the technology gains momentum, it is unlikely that all SCADA-drill operators and/or directional drillers could reproduce accurate results in real-time. Therefore, there is considerable upside-potential while operating while using simulation-based time constants – given the fact that even experienced SCADA-drill operators may use several minutes to tune slide drilling controller gains. Even if simulation-based time constants are automatically provided as a “starting point”, it is likely that this enhancement would normalize SCADA performance and prevent non-optimal control in case inexperienced operators fail to input valid controller gain values.

Because simulation results so closely match the trend of manually-entered torsional time constants, no sweeping model adjustments were required. As demonstrated in the sensitivity analysis from Section 4.7.3, formation coefficients of friction are the most important factor when seeking to scale torsional time constant calculations in the lateral section of the wellbore.

Based on results from the Appalachia case study in the lateral, it is reasonable to expect that this model will produce valid results in upper well sections. This expectation is based on the fact that lateral considerations inherently include upper well sections. In the case where actual survey data is used to run real-time or post-well analysis using the first-principles directional drilling simulator, the user should expect time constant values to be higher in the lateral – a result of hole tortuosity. The sensitivity analysis conducted in Section 4.7.3.2 indicates that the torsional time constant will also be affected by varying well trajectories.

Further testing is required to determine whether or not the current model is valid for determination of the torsional time constant in cases where the well trajectory and/or

formation characteristics vary considerably from those encountered in Appalachia. The Groundbirch case study outlined in the following section addresses these questions.

## 5.2 GROUNDBIRCH CASE STUDY

To determine whether the first-principles directional drilling simulator results are valid in diverse drilling scenarios, simulation results were compared to field data and drilling performance for two wells drilled in the Montney Shale. Groundbirch wells F4-14 and E-14 were drilled back-to-back on the same pad, and a Rotary Steerable System (RSS) was used to drill the lateral sections of these wells. Simulation result trends for the upper-well sections in Groundbirch that are comparable to those from Appalachia would signal:

- This model formulation is sufficient to estimate how the torsional time constant progresses over the duration of a well for various well designs, drill string compositions, and formation characteristics.
- There is a consensus regarding what SCADAdrill operators consider to be optimized tool face control.

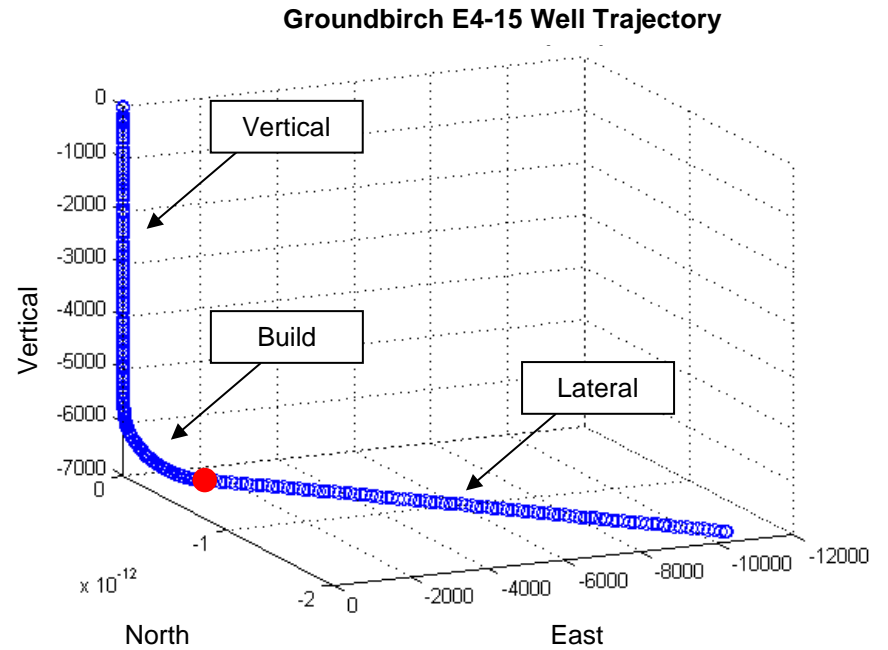
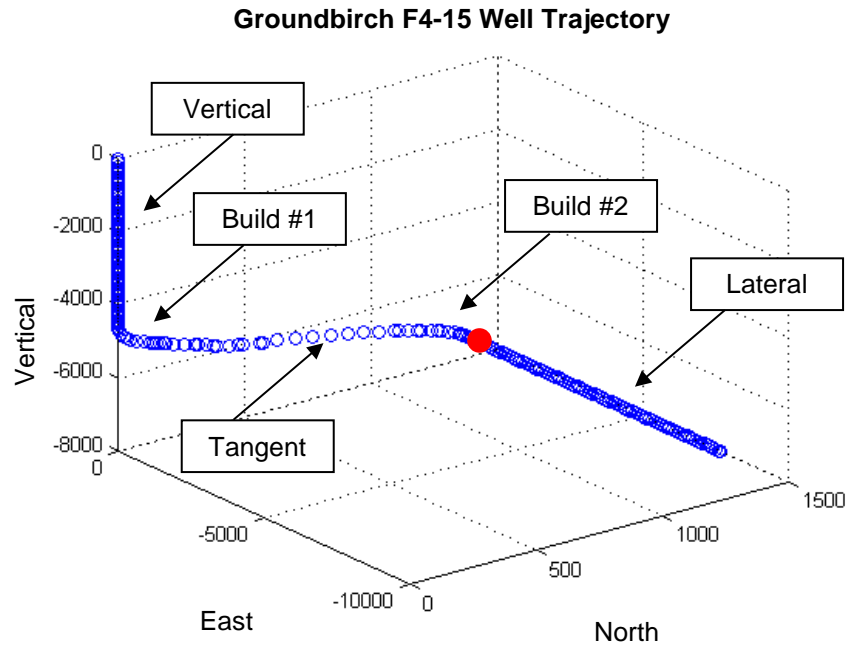
Primary objectives of this exercise include:

- Track progression of the torsional dead time and time constant in upper well sections, and compare the trend to analytical and real-time calculations
- Investigate the effectiveness of the SCADAdrill tool face control algorithm by comparing KPI's for two similar wells
- Comment on the learning curve pertaining to the SCADAdrill operator's ability to effectively tune the tool face controller in real-time by comparing tool face control performance for F4-15 vs. E4-15

Figure 5.3 illustrates the Groundbirch F4-15 well trajectory. Note the following features of this well design:

- Two build sections are separated by a tangent section, and the design includes an extended lateral section.
- The slim-hole design includes 4-inch drill pipe.
- F4-15 and E4-15 were drilled back-to-back with brand new rigs and novice SCADA-drill operators.
- Lateral sections were drilled with a RSS – SCADA did not operate in the lateral.

Because SCADA-drill does not operate in Groundbirch lateral sections at this time, there is no SCADA drilling data to directly compare to time constant results from Appalachia. Instead, key points in the Groundbirch well trajectories were chosen to simulate operations and capture how the torsional time constant progresses in upper-well sections, which were lacking from the Appalachia case study. Groundbirch results were projected into the lateral to investigate how the trend might continue if SCADA-drill were to continue drilling the lateral section with a down-hole motor. Table 5.2 includes key components of the F4-15 directional plan and relevant comments for each section of the well.



Note: The unit of depth is feet for both plots.

Figure 5.3: Groundbirch well plans include vertical, build, hold (tangent), and extended lateral sections. Note: F4-15 lateral step-out is 91 meters, where E4-15 is essentially a two-dimensional well. The red dots mark the transition between upper-well sections (regions of interest) and lateral sections (drilled with RSS).

Table 5.3: This table includes key components of the F4-15 directional plan and relevant comments for each section of the well. The highlighted sections are included in this analysis. A comprehensive, interpolated directional plan can be found in Appendix A.

MD (m)	INC (deg)	AZ (deg)	TVD (m)	Dogleg (°/30 m)	Build (°/30 m)	Turn (°/30 m)	Toolface (deg)	Comment
0	0	0	0	0.0	0.0	0.0	0.0	
90	0	0	90	0.0	0.0	0.0	0.0	SURFACE KICK: BUILD WITH 2°/30m
120	2	350	120	2.0	2.0	0.0	350.0	HOLD TANGENT
320	2	350	320	0.0	0.0	0.0	0.0	DROP TO VERTICAL
350	0	0	350	2.0	-2.0	0.0	180.0	HOLD VERTICAL
1,417	0	0	1,416	0.0	0.0	0.0	0.0	KOP#1: BUILD WITH 3.5°/30m
1,631	25	358	1,624	3.5	3.5	0.0	358.0	HOLD 25° TANGENT
1,791	25	358	1,769	0.0	0.0	0.0	0.0	KOP#2: BUILD WITH 5.8/30m
1,894	45	358	1,853	5.8	5.8	0.0	0.0	BUILD AND TURN WITH 5.8°/30m
2,241	75	286	2,043	5.8	2.6	-6.3	271.5	SHELL 170m HARD BOUNDARY
2,353	90	270	2,057	5.8	4.1	-4.2	313.0	HEEL (transition from build to lateral)
5,055	90	270	2,052	0.0	0.0	0.0	0.0	BH A4-15

A pre-drill-out analysis was completed for the F4-15 well in order to determine expected torsional dead time and time constant values in the sections highlighted in Table 5.3. These simulation results are shown in Figure 5.4:

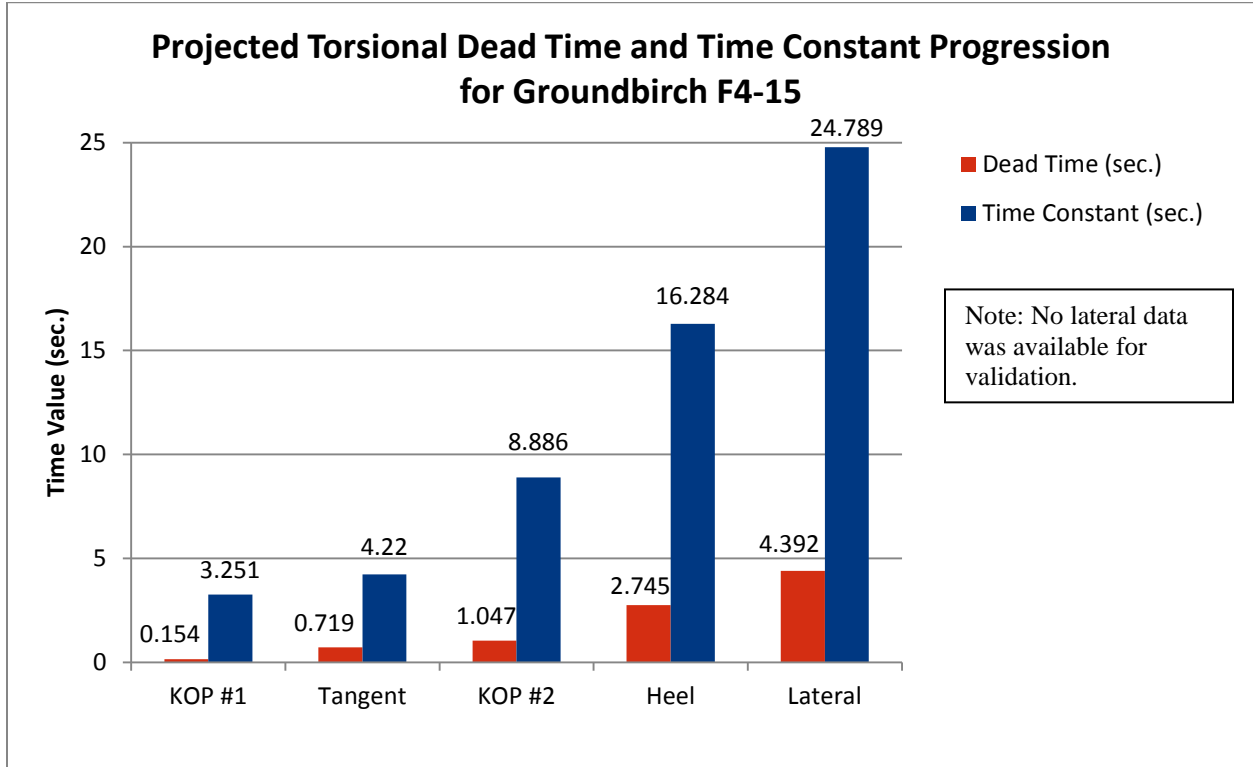


Figure 5.4: Projected torsional dead time and time constant values for Groundbirch F4-15 match the trend uncovered during the Appalachia case study.

When compared to MD from Appalachia, the torsional time constant calculated for Groundbirch F4-15 were consistently lower, and the sections exhibited 58, 105, 93, and 34% variance with increasing MD. It is interesting to note that the value calculated for the heel section has the lowest variance when compared to that MD from Appalachia. This behavior demonstrates the influence of well trajectory on the torsional time constant, which can be difficult to quantify without running detailed drill string dynamics simulations.

When comparing torsional time constant values at each section for wells F4-15 and E4-15, the % variance steadily increased from under 1% (KOP #1) to 11% (Heel) with MD. This

behavior demonstrates the effects of tortuosity on torsional time constant calculations, which is difficult to quantify when survey data is inconsistent or planned well trajectories are used for simulations rather than actual survey data. Simulation-based torsional time constant calculations averaged 12.4 and 40.1% variance from manually-entered values for F4-15 and E4-15, respectively.

Figure 5.5 provides a graphical comparison of torsional time constant values at various depths for the Groundbirch F4-15 and E4-15 wells. Note that F4-15 was used as the reference well, and each well section listed on the graph translates to an equivalent MD for E4-15 (for example, E4-15 does not have a well-defined tangent section). Results support trends established in the Appalachia case study, where simulation-based time constant calculations generally fall in-between analytical calculations and manually-entered values. Again, simulation results provided the highest torsional time constant calculated values at the deepest point of analysis – demonstrating the magnitude of influence that cumulative friction effects have on simulation results. Also note that the percent-variance between the manually-entered and simulation-based time constant values is, again, wide for smaller values before converging with increasing MD.

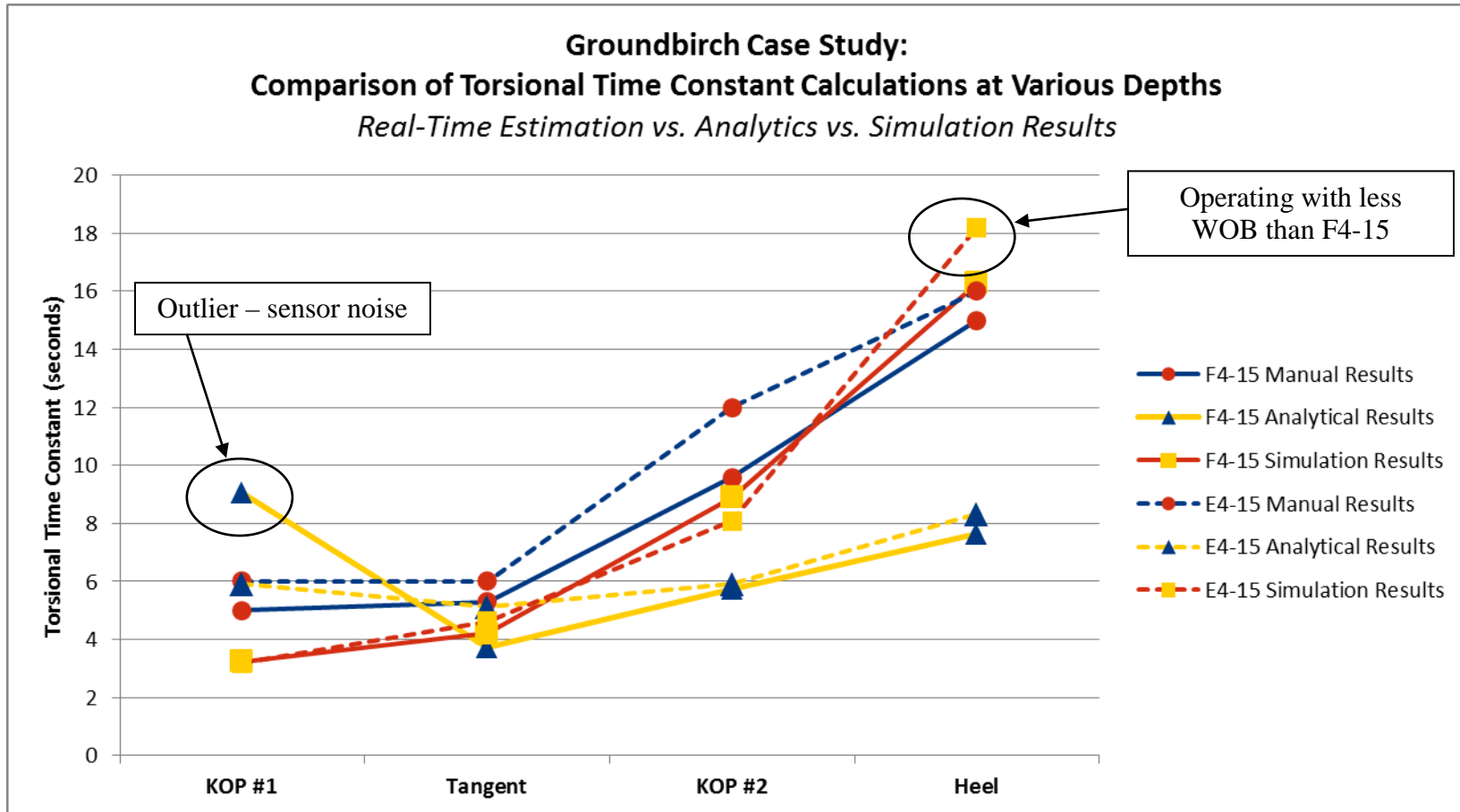


Figure 5.5: Experimental results from the Groundbirch case study were consistent with trends uncovered during the Appalachia case study, i.e. the simulation-based torsional time constant generally fell in-between the analytical and manually-entered values.

A total of 6 different SCADA operators were responsible for drilling wells F4-15 and E4-15, and none of these individuals drilled the well featured in the Appalachia case study. Further, 4 of these 6 SCADA operators in Groundbirch were using the system for the first time. Therefore, the manually-entered time constant values for the Groundbirch case study should not carry as much weight as those from Appalachia. Still, these parameters were manipulated in real-time while drilling in the upper-well sections in an attempt to achieve desired tool face control performance. Because the SCADA operators were inexperienced in using the system, the time constant entries were used on a trial-and-error basis while receiving intermittent coaching from experienced operators. Further, due to the challenges associated with commissioning SCADA in a new field, these wells were drilled using a combination of manual and SCADA-drilling operations. Therefore, it is not possible to confirm which time constant values yield superior tool face control performance with the data provided. This investigation should be re-visited after all wells on this pad have been drilled to TD and the new SCADA operators are fully-trained on the system.

The following pages compare tool face control performance while drilling with SCADA in each wellbore section for wells F4-15 and E4-15. Although the system was technically engaged, it is likely that the operator offered manual compensation during each slide drilling maneuver – introducing tool face bias based on reactive torque curves built during tare sequences. Note the variance between tool face set point and average values, as well as the reactive torque trends that dictate the maximum variance between tool face set point and maximum deviation values. Recall that reactive torque will introduce counter-clockwise rotation at the bit.

### Comparison of Tool Face Control Performance for F4-15 and E4-15 in the Upper-Build Section

Both F4-15 and E4-15 used a relatively-aggressive Halliburton MM64R PDC bit for the upper-build section – where bit aggressiveness is approximately 1.2 (Table 3.3).

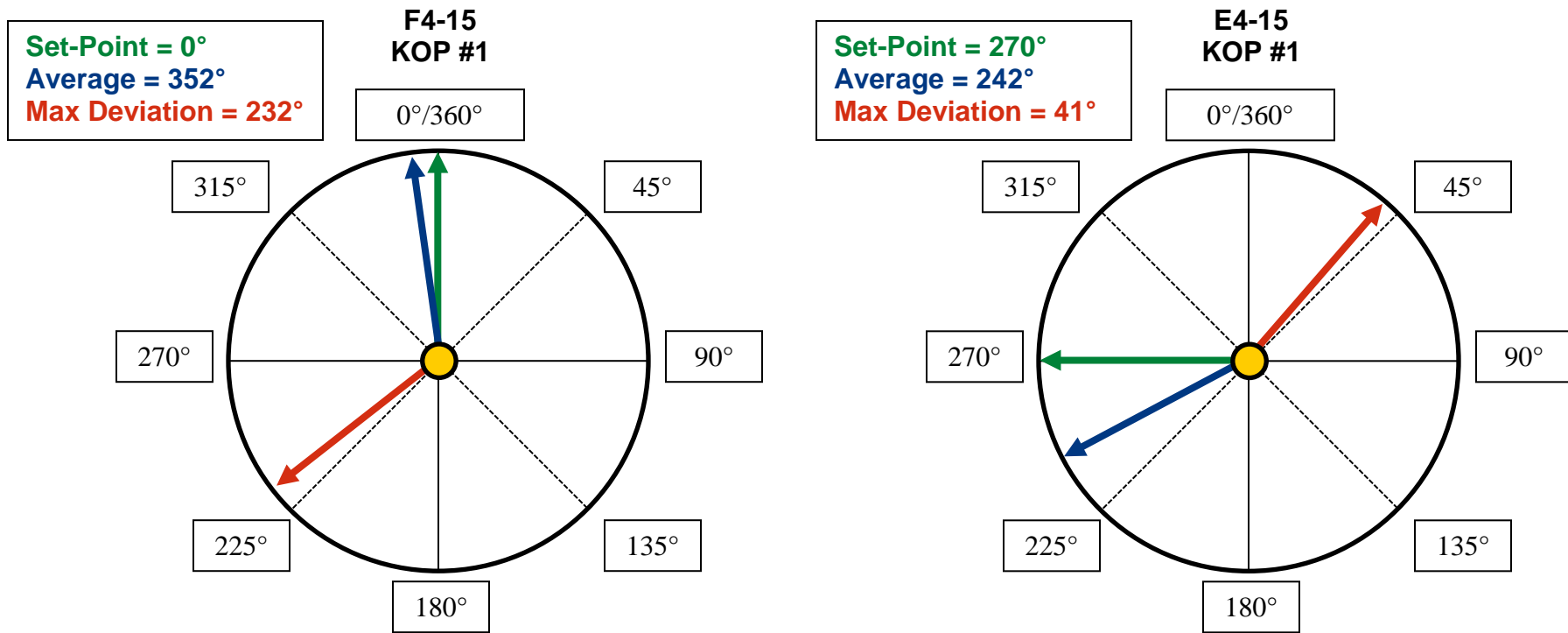


Figure 5.6: Tool face control performance comparison between two wells at the first kick-off point.

### Comparison of Tool Face Control Performance for F4-15 and E4-15 in the Tangent Section

The SCADA operator on E4-15 ran to bottom and applied WOB more aggressively than on F4-15, due to difficulties encountered within the formation and general operational technique, which leads to increased reactive torque spikes and accelerated bit wear. Note: E4-15 MD correlates with F4-15 section.

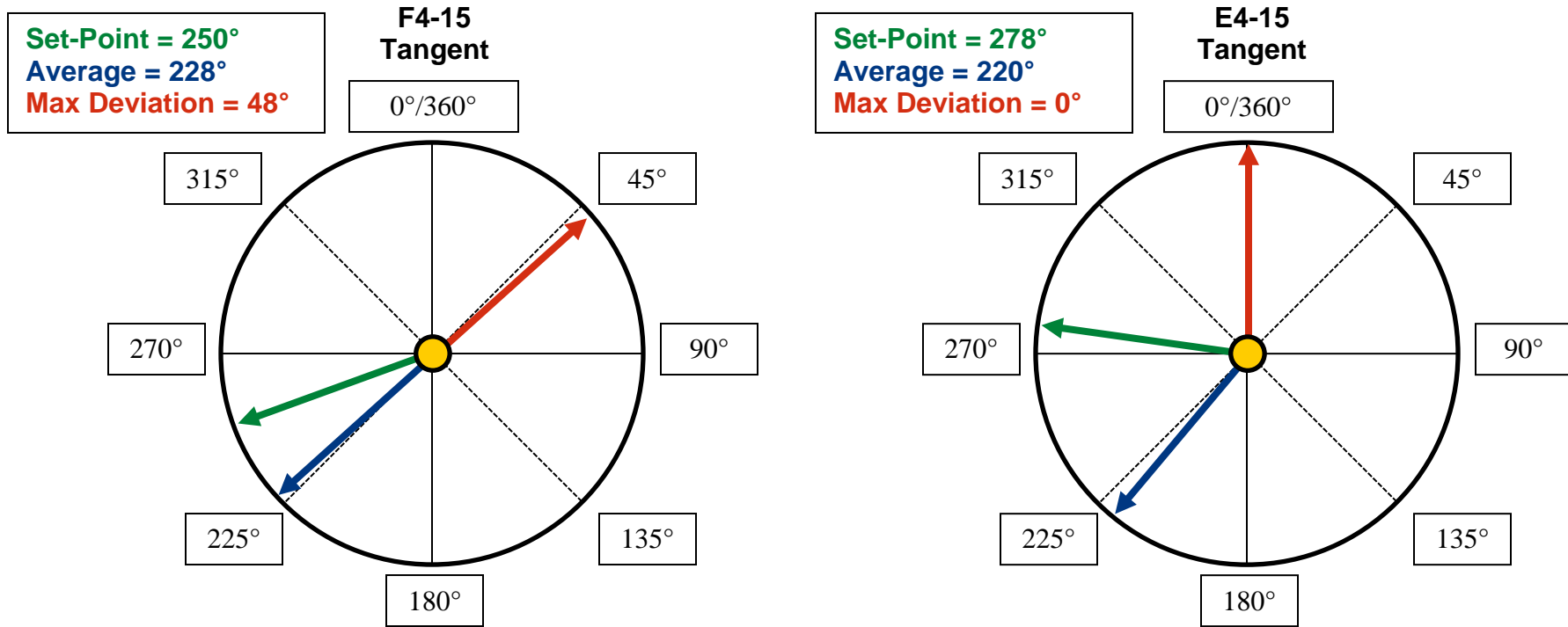


Figure 5.7: Tool face control performance comparison between two wells in the tangent section.

### Comparison of Tool Face Control Performance for F4-15 and E4-15 in the Lower-Build Section

Note that the reactive torque spikes for E4-15 grew progressively worse as more weight was stacked on the bit to achieve sufficient ROP. This slide was executed just prior to a bit trip, where the crew discovered that the bit was in poor condition (Appendix B). Note: E4-15 MD correlates with F4-15 section.

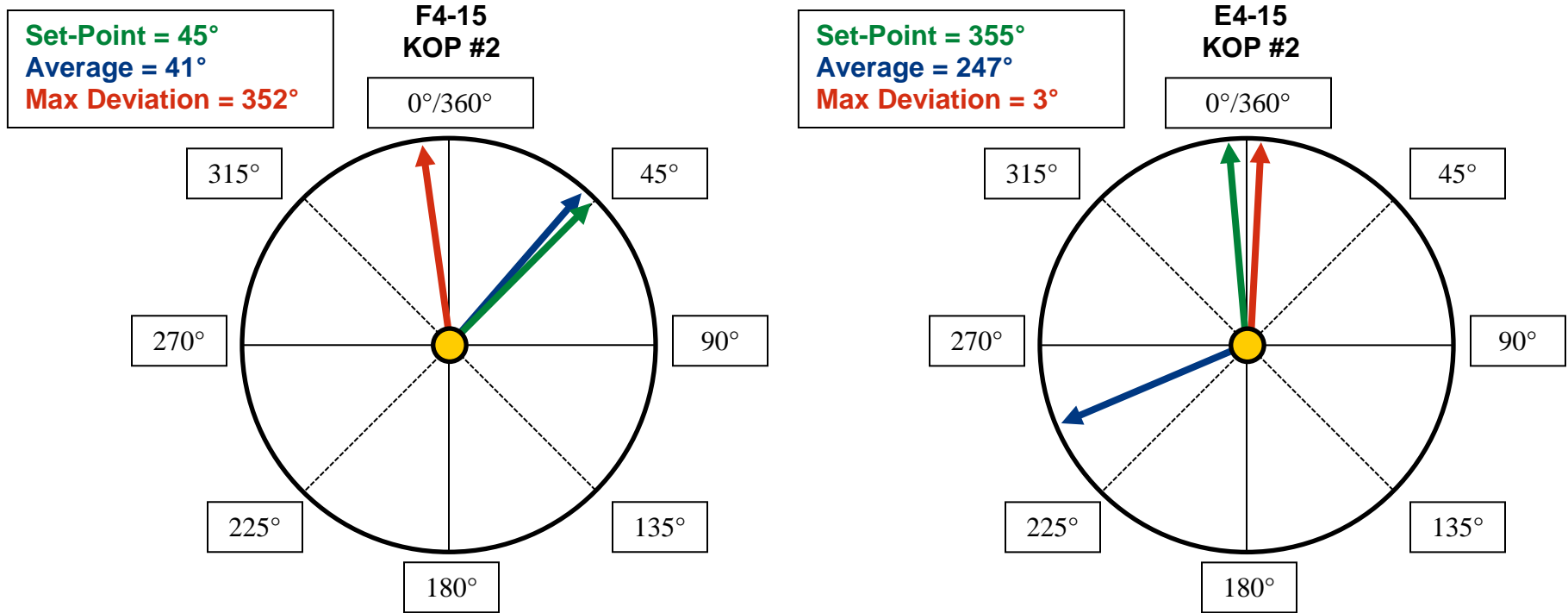


Figure 5.8: Tool face control performance comparison between two wells at the second kick-off point.

### Comparison of Tool Face Control Performance for F4-15 and E4-15 at Landing Point

F4-15 switched to a less-aggressive bit (MMD64DR) to drill this section, while E4-15 elected to replace the MM64R with another MM64R. Using Table 3.3 for reference, the MMD64DR bit aggressiveness is approximately 0.8 – compared to 1.2 for MM64R.

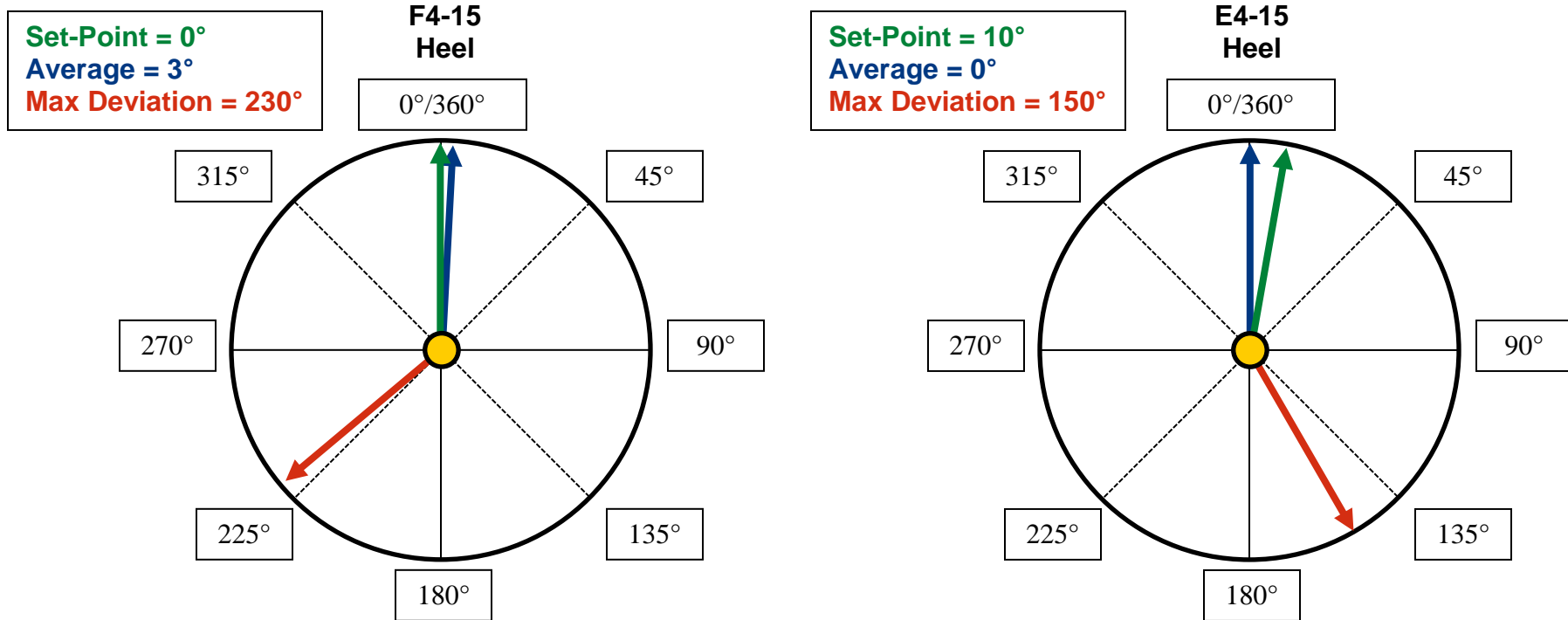


Figure 5.9: Tool face control performance comparison between two wells in the tangent section.

The tool face control schematics illustrate that reactive torque effects are consistently more significant in E4-15 than in F4-15 in each wellbore section. E4-15 was drilled by a more aggressive (and experienced) SCADA operator that understands how to manipulate the system to achieve higher ROP by manually stacking more weight on the bit. This practice includes manual implementation of a right-hand bias before lowering to bottom at a relatively-high axial velocity. The idea is that the reactive torque encountered when tagging bottom will correct the tool face to an appropriate value. Although this operator is experienced with the SCADA system, he is inexperienced in this field and was not aware that the formation characteristics encountered while drilling this well were relatively harsh. Differential pressure spikes and WOB fluctuations influenced drilling performance for the majority of this well, forcing operators to manually intervene in order to achieve sufficient tool face control performance. The F4-15 lower wellbore section was also drilled with less aggressive bit (MMD64DR vs. MM64R) (Appendix B) – a design feature that manifests itself in the following section, which addresses KPI and value assessment.

### **5.3 KEY PERFORMANCE INDICATORS AND VALUE ASSESSMENT**

The KPI's used to compare performance between wells F4-15 and E4-15 are shown in Table 5.4. While E4-15 included 6 more slides than F4-15, the total slide length was 150 meters less to reach a MD at landing that was 154 meters greater than F4-15. This correlation highlights the absence of step-out in E4-15. Increased build rates were achieved for E4-15 by applying more WOB during slide drilling maneuvers – the effects of which are further supported by the lesser percentage of slide drilling to well total length ratio and average slide length data for E4-15.

The total time spent sliding on-bottom and orienting tool face sums to 90 hours for F4-15 and 72 hours for E4-15. Results show that even though on-bottom slide drilling ROP is 4.5% greater for E4-15 than F4-15, the time spent orienting tool face before starting a slide sums to 9 additional hours. Tool face orientation data in Table 5.4

includes the time required to work pipe, ramp pumps, and complete system tare routines. It follows that in the case where rig rate is \$3,000 per hour, the \$81,000 savings gained from spending 27 fewer hours on-bottom sliding for E4-15 is reduced to a total savings of \$63,000 after considering the time required to complete off-bottom slide drilling requirements. Therefore, it would be beneficial to spend more time improving controller robustness so that sufficient tool face control could be achieved in the absence of precise off-bottom orientation and tare data.

There is potential upside in the average time required to orient tool face before starting a slide. One possibility is that new SCADA operators will become more comfortable lining up tool face using the same method employed on F4-15 and E4-15 (line up perfectly before lowering to bottom) and decrease the average time required to orient tool face per slide. Considering the time it takes for experienced operators to complete this process, a reasonable target is 10 minutes (or less), on average. Assuming the same \$3,000 per hour rig rate, this time savings translates to \$20,400 and \$42,750 on F4-15 and E4-15, respectively. Alternatively, the new SCADA operators may learn to adjust tool face on the fly – eliminating the requirement that tool face be perfectly aligned before lowering to bottom. In that case, a reasonable target is 5 minutes or less, on average, which translates to savings of \$33,150 and \$57,000 for F4-15 and E4-15, respectively. However, this technique often leads to increased wellbore tortuosity.

Table 5.4: Groundbirch wells F4-15 and E4-15 were compared using key performance indicators to assess tool face control performance metrics.

<b>Key Performance Indicator Analysis</b>		
<b>Item</b>	<b>F4-15</b>	<b>E4-15</b>
<b># Slides</b>	51	57
<b>Total Slide Length (m)</b>	529	379
<b>Measured Depth at Landing (m)</b>	2,221	2,375
<b>% Slide Drilling / Well Total Length</b>	23.8%	16.0%
<b>Average Slide Length (m)</b>	10.4	6.7
<b>Total Time - On-Bottom Sliding (hr)</b>	75	48
<b>Average ROP - On-Bottom Sliding (m/hr)</b>	7.1	7.9
<b>Total Time Orienting Tool Face (hr)</b>	15	24
<b>Average Time Orienting Tool Face / Slide (min)</b>	18	25
<b>General Comments</b>		
<ul style="list-style-type: none"> <li>• F4-15 pulled out of the hole to change the BHA during Build #2 (at risk of missing target).</li> <li>• E4-15 had no issues staying within target zone, despite formation-related challenges.</li> <li>• F4-15 reached TD in 27.5 days, and E4-15 reached TD in 22.5 days.</li> </ul>		

## 5.4 SUMMARY

Experimental results demonstrate that the first-principles directional drilling simulator is capable of consistently delivering torsional time constant calculations within 40% of manually-entered values. Because SCADA operators continually alternated between manual and automatic control while drilling with the system, it is not possible to carry out a meaningful analysis of tool face control performance based on the value of the

torsional time constant. Further, since each operator has different controller response preferences, it is not appropriate to base validation criteria upon manually-entered controller gain values. It is, however, possible to quantify the value of the learning curve progression as subsequent wells are drilled by comparing on-bottom sliding ROP and wellbore quality. Groundbirch E4-15 was drilled with 4.5% faster on-bottom ROP, drilled to TD in 5 fewer days, and encountered no directional issues from surface to TD, despite encountering formation-related challenges. A critical success factor for E4-15 was that an experienced SCADA operator was teamed with a new SCADA operator on each tower. Therefore, there was always someone available that was familiar with either the system or the field.

Field data shows that inaccurate torsional time constant values result in increased hole tortuosity – the nature of which is characterized by whether or not the value is over- or under-estimated. If the torsional time constant is under-estimated, the SCADA operator is required to chase the tool face over the course of a slide, because the system consistently over-corrects the tool face when a deviation is encountered. This behavior will increase the number of slides required to reach the target while introducing many micro-doglegs along the way. Over-estimation of the torsional time constant may result in deviation from the well plan in-between tool face value updates, which often take over 90 seconds to arrive. This scenario forces the SCADA operator to chase the well plan, weaving back and forth to stay within the target zone.

The first-principles directional drilling simulator is capable of executing case study simulations in real-time until torque and drag loads begin to delay convergence, i.e. a 30-second simulation takes 30 seconds to execute. However, in deep or highly-deviated wells, simulations begin to slow considerably. For example, the 30-second Appalachia

case study simulations increased in duration from 48 seconds at 5,000' to 422 seconds at 8,250'. Therefore, it would be appropriate to re-evaluate the integration interval and mesh size. Migration of the code from MATLAB to PLC would also speed up simulations.

## **6 Conclusions and Recommendations for Future Work**

### **OVERVIEW**

This project set out to establish a physically-meaningful directional drilling model and simulation platform – suitable for development of control algorithms that improve slide drilling performance. This was achieved through realization of the following objectives:

1. Development and validation of a physics-based drilling system model that captures the nature of drill string dynamics within a three-dimensional wellbore during rotary and slide drilling operations.
2. Creation of a simulation platform that utilizes realistic system inputs and captures transient system dynamics.
3. Completion of a sensitivity analysis to understand how drill string composition, well trajectory, operating parameters, friction effects, and formation characteristics affect system response.
4. Excellent quantitative comparison of the torsional time constant vs. manually-tuned values entered by SCADA operators while drilling in different formations.
5. Consideration of model and operational gaps encountered over the course of this study and their potential effect on control system design efforts.
6. Demonstration of consistent and repeatable calculations of the torsional time constant – not dependent upon the operator's experience with the system or knowledge of the field.

## 6.1 SUMMARY OF WORK

Both analytical and empirical results confirm that torsional dead time and time constant values increase as well trajectory complexity increases. In practice, wellbore tortuosity may increase or decrease torsional dead time and time constant values – depending on the degree and location of tortuosity. For example, if the lateral wellbore section contains relatively-minor, local tortuosity, increased drill string/wellbore interaction will give rise to higher normal forces, i.e. torque and drag. Alternatively, the semi-soft string model employed by the first-principles simulator is sensitive to wellbore tortuosity – given the assumption that the drill string conforms to the shape of the wellbore. Therefore, it is important to consider tortuosity effects in conjunction with well trajectory and scale wellbore friction factors accordingly when designing simulation routines to determine transient, torsional dynamics.

Although torsional dead time and time constant values are affected by drill string composition and operating parameters, the most influential model sensitivity is the friction profile used to characterize drill string/wellbore interaction. In fact, even well trajectory and tortuosity influences can be addressed through manipulation of coefficients of friction along the wellbore. This model formulation employed the Coulomb friction model to describe drill string/wellbore interaction, and results showed that the top drive PI-controller was highly sensitive to very high modeled, coefficients of friction with increasing depth and well trajectory complexity, as expected. Therefore, it is important to re-visit the friction model in order to ensure system stability in a wider range of simulation scenarios.

The user is currently able to manipulate any model parameter in order to create a simulation routine, based on well design parameters and offset well data, (e.g. empirical friction coefficients). In practice, the drilling engineer sets parameters that are monitored by field personnel. It was not an objective of this research to offer recommendations regarding well design or operating parameters. However, it is possible for drilling engineers to use knowledge gained from torque and drag simulations during the planning

phase to determine how the system will respond in various wellbore sections and operating scenarios. Therefore, there is an opportunity for drilling engineers to collaborate with SCADA operators during the planning phase in order to optimize drilling performance. This methodology would enable well delivery teams to circumvent gaps in system performance until controller robustness can be improved.

An essential part of future automated directional drilling routines will be the integration of ROP optimization and tool face control algorithms. If axial dead time and time constant values are tuned in conjunction with their torsional counterparts, it will be possible to develop a control scheme capable of optimizing ROP in real-time while performing complex slide drilling maneuvers. In this scenario, the draw-works would respond to WOB trends and optimize ROP to suit varying formation characteristics and operating parameters while oscillating the top drive to break friction forces along the wellbore to deliver sufficient WOB. Although not the focus of this study, this first-principles directional drilling simulator captures axial dynamics and is capable of calculating axial dead time and time constant values using the same methodology outlined for the study of torsional dynamics. The effort to achieve simultaneous optimization in the axial and torsional domains will require complex multi-variable control schemes. An additional feature of this automated drilling routine would involve utilization of geological data to determine optimal wellbore placement according to LWD data. Successful implementation of ROP optimization and wellbore placement algorithms in parallel would allow the industry to achieve the top tier of drilling automation proposed by Aldred et al. in Figure 1.7. This work delivers an important building block toward achieving that goal.

Experimental results show that the first-principles simulator is capable of consistently calculating torsional dead time and time constant values for comparison with analytical and manually-determined values. It is important to note that as MD and well trajectory increases, the time required to complete a simulation increases significantly. This behavior may improve when a more-refined friction model is implemented.

Migration of the simulation routine into a PLC-based program would also decrease simulation time.

After the simulation routine is translated to PLC code, it will be possible to transfer the first-principles model into existing SCADA architecture. Successful integration of this simulator with real-time SCADA operations would provide torsional dead time and time constant values that more closely match those determined by the SCADA operator than those currently calculated using system analytics. This would normalize SCADA operations and make the system less dependent upon experienced operators to achieve satisfactory tool face control performance. Further, the SCADA operator could dedicate more focus to drilling parameter optimization and other tasks that could increase ROP. Ongoing field experiments will track the ability of the simulator to replicate manually-chosen values and determine which methodology leads to optimal drilling performance.

The consequences of dead time/time constant inaccuracies vary according to whether the values are under- or over-predicted, considering true system values how they fit into the control system design. Because dead time and time constant values characterize top drive controller response to system dynamics and/or oscillation sequences employed while sliding, it is important to consider the extent to which non-optimal controller gains may affect operations in various wellbore sections. For example, if the torsional time constant is over-predicted in a critical build section, tool face could drift for too long without correction – potentially producing DLS values that make it difficult to run casing to bottom. Conversely, an under-predicted torsional time constant will introduce micro-doglegs that may cause a need to execute more slides than originally planned.

An accurate approximation of the torsional time constant would enable SCADA operators to drill the technical limit during slide maneuvers, given sufficient knowledge of the formation and ROP optimization techniques. Potential time savings calculated for the Groundbirch prospect are in excess of \$100,000 per well. Given the fact that the

Groundbirch is currently being drilled with brand new rigs, crews, SCADA operators, and well designs, it is conceivable that the value realized by drilling with optimized tool face controller gains will increase significantly over time. Based on the limited number of wells drilled with SCADA in Groundbirch, it is not yet possible to differentiate tool face control performance improvement gains achieved by drilling with more accurate dead time/time constant values, as opposed to those made possible by advancing the learning curve with the new rigs, crews, operators, and well design. The value of well-tuned tool face controller should be quantifiable by the end of the first pad – after drilling several wells. Using the quantifiable performance improvement gains realized between F4-15 and E4-15 as a standard (\$200,000 per well), the current estimation of this value is \$2,000,000 over the course of a 10 well pad – which validates the initial investment in the SCADA system.

## **6.2 FUTURE WORK**

Future work will include further model refinement before an attempt is made to develop advanced tool face control algorithms. Some suggestions for model refinement include:

- Incorporate a velocity-dependent (e.g. Stribeck) friction profile (Appendix C), which calculates friction coefficients as a function of relative angular velocity between the drill string and wellbore.
- Define various friction coefficients for different wellbore sections, especially those with distinguishing formation characteristics.
- Develop a real-time system identification or adaptive scheme that is capable of calculating effective friction coefficient values in real-time.
- Recall that drilling fluid viscosity, dynamic pressure effects, and hole cleaning were neglected in this model. Implementation of a more comprehensive fluid dynamics model would also affect drill

string/wellbore interaction – likely reducing the net coefficient of friction between the two surfaces.

An empirical study will be carried out – consisting of a back-to-back comparison of drilling performance achieved while using manually-calculated time constant values vs. those generated by the simulator. This experiment should include field data gathered from multiple wells in order to dilute human influences or extenuating circumstances that affect the outcome of drilling performance. Results from this study will improve the understanding of the applicability of the torsional time constant. It is important that objective standards are established using drilling efficiency optimization metrics combined with other drilling KPI's. An investigation into how axial and torsional dead time and time constant values relate to one another will provide a stepping stone to the development of automated control routines that optimize ROP in both rotary and slide drilling modes. From an industry perspective, it is also important to determine a faster method to take SCADA system tares and line up tool face before drilling, as these processes currently take up considerably more time than that required by a human driller. Finally, future work will include development of robust tool face control algorithms – capable of executing slide drilling maneuvers without manual intervention.

## Appendix A

### VERTICAL WELL TRAJECTORY

Measured Depth (ft)	Inclination (degrees)	Azimuth (degrees)
0	0	0
5000	0	0

### BUILD WELL TRAJECTORY

Measured Depth (ft)	Inclination (degrees)	Azimuth (degrees)
0	0	0
2000	0	0
2100	3	0
2200	6	0
2300	9	0
2400	12	0
2500	15	0
2600	18	0
2700	21	0
2800	24	0
2900	27	0
3000	30	0
3100	33	0
3200	36	0
3300	39	0
3400	42	0
3500	45	0
3600	48	0
3700	51	0
3800	54	0
3900	57	0
4000	60	0
4100	63	0
4200	66	0

4300	69	0
4400	72	0
4500	75	0
4600	78	0
4700	81	0
4800	84	0
4900	87	0
5000	90	0

### SLANT WELL TRAJECTORY

Measured Depth (ft)	Inclination (degrees)	Azimuth (degrees)
0	0	0
1000	0	0
1100	3	0
1200	6	0
1300	9	0
1400	12	0
1500	15	0
1600	18	0
1700	21	0
1800	24	0
1900	27	0
2000	30	0
5000	30	0

### LATERAL WELL TRAJECTORY

Measured Depth (ft)	Inclination (degrees)	Azimuth (degrees)
0	0	0
1000	0	0
1100	3	0
1200	6	0

1300	9	0
1400	12	0
1500	15	0
1600	18	0
1700	21	0
1800	24	0
1900	27	0
2000	30	0
2100	33	0
2200	36	0
2300	39	0
2400	42	0
2500	45	0
2600	48	0
2700	51	0
2800	54	0
2900	57	0
3000	60	0
3100	63	0
3200	66	0
3300	69	0
3400	72	0
3500	75	0
3600	78	0
3700	81	0
3800	84	0
3900	87	0
4000	90	0
5000	90	0

**APPALACHIA**

Measured Depth (ft)	Inclination (degrees)	Azimuth (degrees)
0	0	0
1400	0	0
1500	3	150

1600	6	150
1700	9	150
1800	12	150
1900	15	150
2000	18	150
3200	18	150
3300	15	150
3400	12	150
3500	9	150
3600	6	150
3700	3	150
3800	0	150
3900	0	0
4000	4	0
4100	12	0
4200	20	335
4300	28	335
4400	36	335
4500	44	335
4600	52	335
4700	60	335
4800	68	335
4900	76	335
5000	84	335
5100	92	335
9300	92	335

**GROUND BIRCH F4-15**

Measured Depth (ft)	Inclination (degrees)	Azimuth (degrees)
0	0	0
90	0	0
120	2	350
150	2	350
180	2	350
210	2	350

240	2	350
270	2	350
300	2	350
320	2	350
330	1	350
350	0	0
1417	0	0
1440	3	358
1469	6	358
1470	6	358
1498	10	358
1500	10	358
1520	12	358
1530	13	358
1560	17	358
1563	17	358
1590	20	358
1610	23	358
1620	24	358
1631	25	358
1791	25	358
1800	27	358
1830	33	358
1851	37	358
1860	38	358
1890	44	358
1891	44	358
1894	45	358
1920	45	351
1950	46	343
1980	48	335
2010	50	328
2040	52	321
2070	55	315
2100	58	309
2130	61	303
2142	63	301
2160	65	298
2182	67	295

2190	68	293
2190	68	293
2220	72	289
2241	75	286
2250	76	284
2280	80	280
2310	84	276
2340	88	272
2353	90	270
5055	90	270

### GROUND BIRCH E4-15

Measured Depth (ft)	Inclination (degrees)	Azimuth (degrees)
0	0	0
1417	0	0
1440	3	358
1469	6	358
1470	6	358
1498	10	358
1500	10	358
1520	12	358
1530	13	358
1560	17	358
1563	17	358
1590	20	358
1610	23	358
1620	24	358
1631	25	358
1791	25	358
1800	27	358
1830	33	358
1851	37	358
1860	38	358
1890	44	358
1891	44	358

1894	45	358
1920	45	351
1950	46	343
1980	48	335
2010	50	328
2040	52	321
2070	55	315
2100	58	309
2130	61	303
2142	63	301
2160	65	298

2182	67	295
2190	68	293
2190	68	293
2220	72	289
2241	75	286
2250	76	284
2280	80	280
2310	84	276
2340	88	272
2353	90	270
5055	90	270

## Appendix B

Table B.1: This table outlines the BHA model used in the Appalachia case study.

Component type	# Jts	Length (ft)	OD (in)	Max OD (in)	ID (in)
Drill Pipe	109	4,852.32	5.000		4.276
Heavy Weight Drill Pipe	5	276.84	4.000		3.000
Crossover	1	2.90	6.125		2.937
Drill Collar	3	90.73	6.500		
Flexible Non-Mag Drill Collar	1	30.57	6.500		2.812
Flexible Non-Mag Drill Collar	1	29.29	6.125		2.812
Pulser Sub	1	10.20	6.125		2.750
MWD Tool	1	19.47	6.250		3.250
Crossover	1	2.14	6.187		3.000
Pony Drill Collar	1	14.29	6.375		2.875
Bent Housing	1	27.50	6.625		
Polycrystalline Diamond Bit	1	0.75	7.875	7.880	

### Groundbirch F4-15 Long-Lateral, Slim-Hole Design

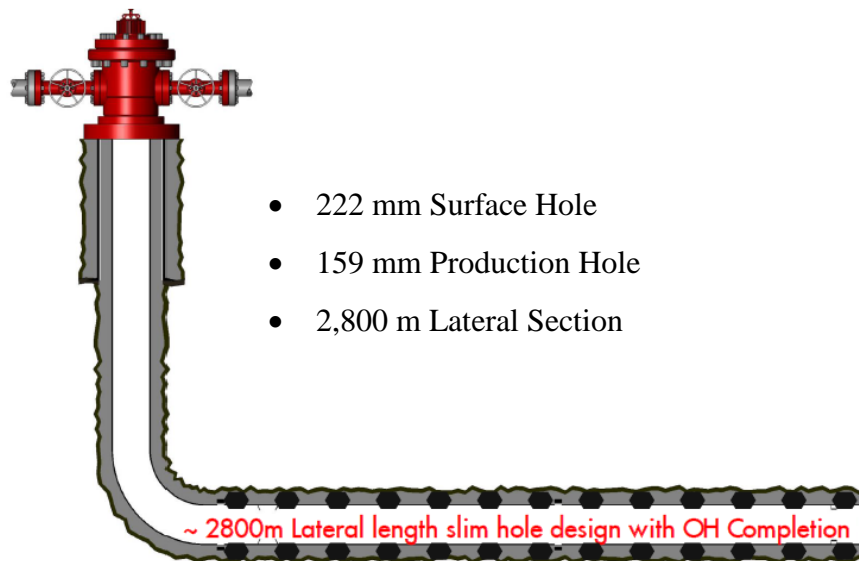


Figure B.1: Groundbirch elected to drill long, slim-hole laterals with open-hole completions on the 4-15 pad.

## **Groundbirch F4-15 BHA Summary**

1. Drill-out to Cecil
  - Motor: 4.75" 7/8 3.7 1.83<sub>o</sub> MBTB
  - ABH Stabilized and NM motor top, EM MWD
  - 4" HWDP and 4" DP
2. Cecil to 30m into DOIG
  - Motor: 4.75" 7/8 3.7 1.83<sub>o</sub> MBTB
  - ABH Stabilized and NM motor top, EM MWD
  - 4" HWDP and 4" DP
3. Base of DOIG to land
  - Motor: 4.75" 5/6 8.3 1.83<sub>o</sub> MBTB
  - ABH Stabilized and NM motor top, EM MWD
4. Lateral – Rotary Steerable System
  - PowerDrive X6 Stabilized
  - Drive Motor: 4.75" 7/8 3.7 Straight
  - Stabilized BHA, EM MWD

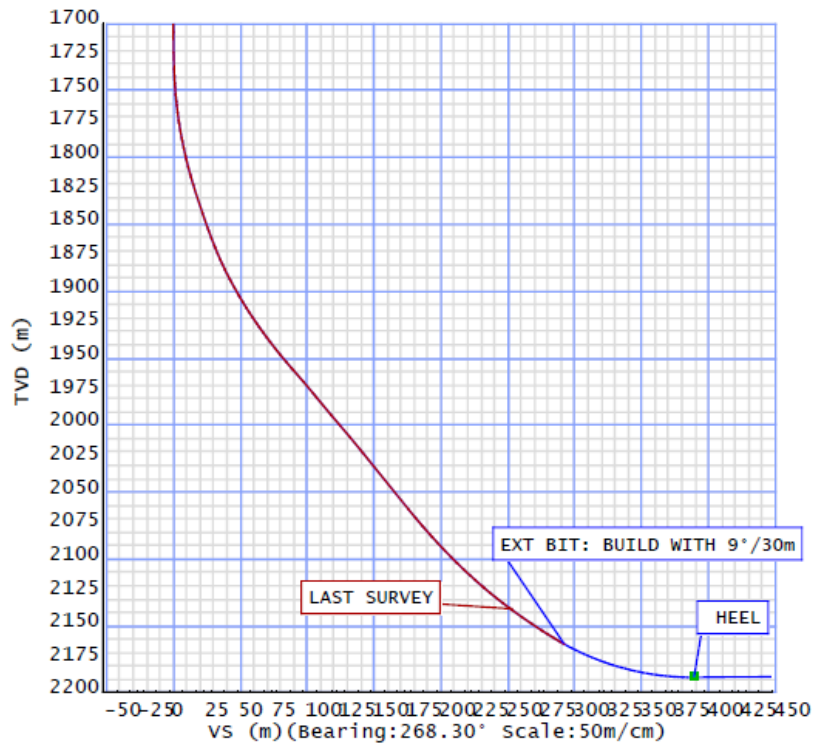
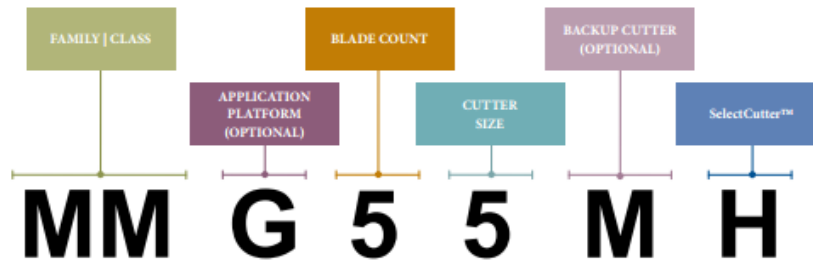


Figure B.2: Groundbirch F4-15 required an extra bit trip and aggressive build rate near the heel, due to directional issues encountered while drilling the build and turn section.

F4-15 Bits & Run	E4-15 Bits & Run
<p data-bbox="451 359 740 422"><b>MM64R</b> 425mm<sup>2</sup> TFA Graded: 2-4-WT-S-X-I-CT-PR</p> <p data-bbox="391 459 802 522">5" (4.75") 7/8 3.7 <b>Adj at 1.83deg</b> Med BTB 1.44m, Stabilized NB &amp; on Top</p> <p data-bbox="456 590 737 617">POOH for PR at 1861m MD</p>	<p data-bbox="878 359 1167 422"><b>MM64R</b> 425mm<sup>2</sup> TFA Graded: 5-6-BT-A-X-1-CT-PR</p> <p data-bbox="818 459 1229 522">5" (4.75") 7/8 3.7 <b>Adj at 1.50deg</b> Med BTB 1.44m, Stabilized NB &amp; on Top</p> <p data-bbox="883 590 1159 617">POOH for PR @ 1856m MD</p> <p data-bbox="992 690 1057 718"><b>Notes</b></p> <p data-bbox="812 724 1203 814">A less-aggressive motor bend was required, since E4-15 did not include a build and turn section.</p> <p data-bbox="812 854 1229 1079">This bit was in poor shape compared with the same bit pulled at nearly the same depth for F4-15. Drillers reported that this well was "ratty" - where several hard, interbedded formations were encountered that caused significant differential pressure spikes.</p>
<p data-bbox="428 1152 761 1306"><b>MMD64DR</b> 504.7mm<sup>2</sup> TFA 5" (4.75") 7/8 3.7 Adj at 1.83deg Med BTB 1.44m, Stabilized NB POOH for Builds @ 2275m Graded: 2-3-WT-S-0-0-ER-BHA</p>	<p data-bbox="857 1152 1190 1243"><b>MM64R</b> 504.7mm<sup>2</sup> TFA 5" (4.75") 7/8 3.7 Adj at 1.83deg Med BTB 1.44m, Stabilized NB</p>

Figure B.3: F4-15 and E4-15 were drilled using the same bit model but different motor bends (1.5 degrees compared to 1.83 degrees, respectively) to approximately 1,850 m MD. Then, F4-15 drilled the heel with a less aggressive bit.

## MegaForce™ Drill Bits Nomenclature



FAMILY   CLASS	CUTTER SIZE	OPTIONAL FEATURES
<b>MegaForce™ Drill Bits</b>	The cutter size digit describes the size of the PDC cutters on the bit. On bits with multiple cutter sizes, the predominant size is described. 2 = 8 mm   3/8" 3 = 10.5 mm   13/32" 4 = 13 mm   1/2" 5 = 16 mm   5/8" 6 = 19 mm   3/4" 8 = 25 mm   1"	Not listed in nomenclature but found on marketing spec sheet. For more information, please contact your local Halliburton Drill Bits representative. b = Backreaming c = Carbide Reinforcement e = SE - Highly Spiraled f = Full PDC Gauge Trimmers k = Kerfing - Scribe Cutters p = PDC Gauge Reinforcement u = Updrill
APPLICATION PLATFORM (OPTIONAL)	BACKUP CUTTER (OPTIONAL)	SelectCutter™
D = Directional (all other directional systems) G = Geo-Pilot™ Rotary Steerable E = Geo-Pilot™ EDL Rotary Steerable T = Turbine High Rotational Speed	D = Dual Row Backup M = Modified Diamond Round R = R1™ Backup Cutters I = Impreg Backup Discs C = Carbide Impact Arrestor	H = Hard and abrasive
BLADE COUNT		
The blade count describes the number of blades on the bit. 3 = Three Blades 4 = Four Blades 5 = Five Blades 6 = Six Blades 7 = Seven Blades 8 = Eight Blades 9 = Nine Blades		

Figure B.4: The Halliburton MegaForce bit is a more aggressive, matrix-body bit used to drill upper-well sections on both F4-15 and E4-15. This bit was also used to drill the lower-well section on E4-15.

Table B.5: The less-aggressive, conventional Halliburton FX bit was used to drill the lower-build section on F4-15.

Bit Details										
Bit no.	Size (mm)	Manufacturer	Model no.	Class	IADC code	Serial no.	Size (mm)	MD in (m)	MD out (m)	IADC Dull Grade
3	159.00	HALLIBURTON	MMD64DR		M333	12373763	6x11.1	1,856.00	2,374.00	1-2-CT-N-X-1-FC-BHA

## Appendix C

The Stribeck friction model proposed by Li [2013] was considered for this first-principles directional drilling simulator, because of the potential capability to more accurately capture velocity-dependent friction effects.

$$T_b(\dot{\theta}_b) = T_c \cdot \frac{2}{\pi} \left[ \alpha_1 \cdot \dot{\theta}_b \cdot e^{-\alpha_2 |\dot{\theta}_b|} + \arctan(\alpha_3 \cdot \dot{\theta}_b) \right]$$

$$T_c = 350 \text{ ft-lbf}$$

$$\alpha_1 = 10$$

$$\alpha_2 = 2$$

$$\alpha_3 = 35$$

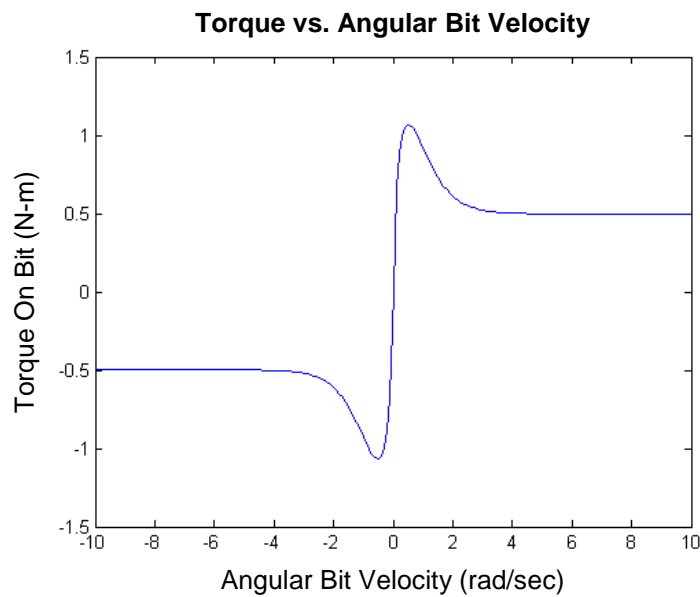


Figure C.1: The Stribeck friction model calculates TOB as a function of bit RPM.

Rayleigh damping coefficients influence the amount of overshoot seen at various drill string locations after a step change is introduced.

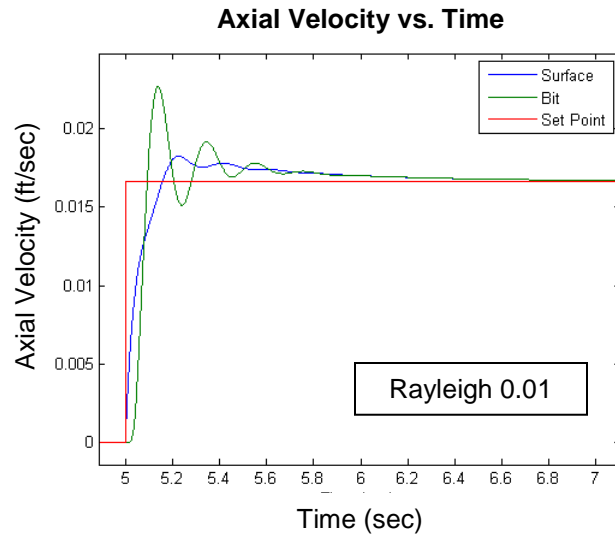


Figure C.2: This plot shows how a lower Rayleigh damping constant affects axial response to a step change.

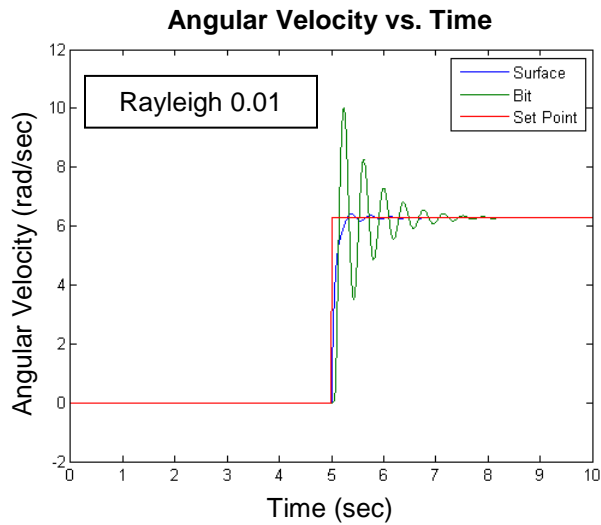


Figure C.3: This plot shows how a lower Rayleigh damping constant affects torsional response to a step change.

## Nomenclature

$\alpha$	Newmark Beta integration constant
$\alpha_{0-7}$	Newmark Beta solution coefficient
$A_{dc}$	cross-sectional area of drill collars (in <sup>2</sup> )
$A_{dp}$	cross-sectional area of drill pipe [in <sup>2</sup> ]
$\alpha_C$	Rayleigh damping coefficient
ASME	American Society of Mechanical Engineers
$\beta_C$	Rayleigh damping coefficient
BEM	Boundary Element Method
BHA	Bottom-Hole Assembly
[C]	damping matrix
CD	contact diameter [in.]
CSF	Compressive Strength of Formation [psi]
CV	Control Variable
DLS	Dog Leg Severity [degrees/100-ft]
DOF	Degrees-Of-Freedom
$E$	Young's Modulus of steel [psi]
{ $F$ }	general equation of motion force vector – sum of $F_0$ , $F_c$ , $F_{dyn}$
{ $F_0$ }	steady-state force vector
{ $F_c$ }	controller force vector
{ $F_{eff}$ }	Newmark- $\beta$ effective force vector
{ $F_{dyn}$ }	dynamic force vector
$F_D$	damping force acting on drill string element [lbf]
$F_G$	gravitational force acting on drill string element [lbf]
$F_N$	normal force acting on drill string element [lbf]
$F_T$	tension force acting on drill string element [lbf]

FEM	Finite Element Method
HWDP	heavy-weight drill pipe
$I$	mass moment of inertia [lbf-in <sup>2</sup> ]
$ID$	element inner diameter [in.]
IEEE	Institute of Electrical and Electronics Engineers
$J$	polar moment of inertia [in <sup>4</sup> ]
$[K]$	stiffness matrix
$K_A$	axial stiffness contribution [lbf/ft]
$K_T$	torsional stiffness contribution [lbf/rad]
$K_{eff}$	Newmark- $\beta$ effective stiffness matrix
$K_i$	integral gain
$K_p$	proportional gain
KPI	Key Performance Indicator
$L$	element length [ft]
$\mu_{rock}$	rock friction coefficient
$[M]$	mass matrix
$M_A$	axial mass contribution [lbm]
$M_T$	torsional mass contribution [lbm]
MCM	Minimum Curvature Method
MSE	Mechanical Specific Energy
MWD	Measurement While Drilling
$\phi$	well trajectory inclination [degrees]
$\Phi$	internal force matrix
$\varphi$	well trajectory azimuth [degrees]
$OD$	element outer diameter [in.]
$P$	axial load acting on drill string node [lbf]
PI	Proportional-Integral (control)
PLC	Programmable Logic Controller

PV	Process Variable
ROP	Rate Of Penetration [ft/hr]
RPM	Rotations Per Minute
RSS	Rotary Steerable System
SCADA	Supervisory Control And Data Acquisition
SDT	String Delta Torque [ft-lbf]
SP	Set-Point
SPE	Society of Petroleum Engineers
$\tau$	time constant [sec.]
$T$	torque acting on drill string element [ft-lbf] / potential energy
$T_d$	dead time [sec.]
$T_P$	tension [lbf]
$T_\phi$	torsion [lbf]
$\theta$	angular position [rad]
$\dot{\theta}$	angular velocity [rad/sec]
$\ddot{\theta}$	angular acceleration [rad/sec <sup>2</sup> ]
$u$	axial position [ft]
$\dot{u}$	axial velocity [ft/sec]
$\ddot{u}$	axial acceleration [ft/sec <sup>2</sup> ]
$U$	nodal displacement matrix
$\dot{U}$	nodal velocity matrix
$\ddot{U}$	nodal acceleration matrix
$V$	kinetic energy
$W$	dry pipe weight [lbf] / Work
WOB	Weight On Bit [lbf]

## References

1. Al-Hiddabi, S.A., Samanta, B., and Seibi, A. 2003. Non-Linear Control of Torsional and Bending Vibrations of Oilwell Drillstrings. *Journal of Sound and Vibration* **265** (2): 401-415. DOI: 10.1016/S0022-460X(02)01456-6.
2. Allen, M.B. 1987. BHA Lateral Vibrations: Case Studies and Evaluation of Important Parameters. Paper SPE 16110 presented at the SPE/IADC Drilling Conference, new Orleans, 15-18 March. DOI:10.2118/16110-MS.
3. Apostal, M.C., Haduch, G.A., and Williams, J.B. 1990. A Study To Determine the Effect of Damping on Finite-Element Based, Forced-Frequency-Response Models for Bottomhole Assembly Vibration Analysis. Paper SPE 20458 presented at the SPE Annual Technical Conference and Exhibition, new Orleans, 23-26 September. 10.2118/20458-MS.
4. Bailey, J.J. and Finnie, I. 1960. An Analytical Study of Drill-String Vibration. *Trans., ASME, Journal of Engineering for Industry* **82B** (May): 122-128
5. Bathe, K.-J. 1982. *Finite Element Procedures in Engineering Analysis*. Englewood Cliffs, new Jersey: Prentice-Hall.
6. BelokobylPrent, S. and Prokopov, V. 1982. Friction-Induced Self-Excited Vibrations of Drill Rig With Exponential Drag Law. *International Applied Mechanics* **18** (12): 1134-1138. DOI: 10.1007/BF00882226.
7. Belayev, A., Brommundt, E., and Palmov, V.A. 1995. Stability Analysis of Drillstring Rotation. *Dynamics and Stability of Systems: an International Journal* **10**(2): 99-110.
8. Besaisow, A.A. and Payne, M.L. 1988. A Study of Excitation Mechanisms and Resonance Inducing Bottomhole-Assembly Vibrations. *SPEDE* **3** (1): 93-101. SPE-15560-PA. DOI: 10.2118/15560-PA.

9. Booer, A.K. and Meehan, R.J. 1993. Drillstring Imaging - An Interpretation of Surface Drilling Vibrations. *SPEDC* **8** (2): 93-98. SPE-23889-PA. DOI: 10.2118/23889-PA.
10. Bradbury, R. and Wilhoit, J. 1963. Effect of Tool Joints on Passages of Plane Longitudinal and Torsional Waves Along a Drill Pipe. *Trans., ASME, Journal of Engineering for Industry* **85** (May): 156-162.
11. Brakel, J.D. and Azar, J.J. 1989. Prediction of Wellbore Trajectory Considering Bottom Hole Assembly and Drillbit Dynamics. *SPEDE* **4** (2): 109-118. SPE-16172-PA. DOI: 10.2118/16172-PA.
12. Brebbia, C.A., Telles, J.C.F., and Wrobel, L.C. 1984. *Boundary Element Techniques*. Berlin: Springer-Verlag.
13. Brett, J.F. 1992. The Genesis of Torsional Drillstring Vibrations. *SPEDE* **7** (3): 168-174. SPE-21943-PA. DOI: 10.2118/21943-PA.
14. Burgess, T.M., McDaniel, G.L., and Das, P.K. 1987. Improving BHA Tool Reliability With Drillstring Vibration Models: Field Experience and Limitations. Paper SPE 16109 presented at the SPE/IADC Drilling Conference, New Orleans, 15-18 March. DOI: 10.2118/16109-MS.
15. Burnett, D.S. 1987. *Finite Element Analysis From Concepts to Applications*. Reading, Massachusetts: Addison-Wesley.
16. Chen, G. and Zhou, J. 1992. *Boundary Element Methods*. London: Academic Press.
17. Chen, S.L. and Geradin, M. 1995. An Improved Transfer Matrix Technique as Applied to BHA Lateral Vibration Analysis. *Journal of Sound and Vibration* **185** (1): 93-106. DOI: 10.1006/jsvi.1994.0365.
18. Chen, Smith, and LaPierre. 2003. Advanced Drillstring Dynamics System Integrates Real-Time Modeling and Measurements. SPE 81093-MS.
19. Chevallier, A.M. 2000. Nonlinear Stochastic Drilling Vibrations. PhD dissertation, Rice University, Houston, Texas.

20. Chin, W.C. 1994. *Wave Propagation in Petroleum Engineering*. Houston: Gulf Publishing Company.
21. Christoforou, A.P. and Yigit, A.S. 1997. Dynamic Modelling of Rotating Drillstrings With Borehole Interactions. *Journal of Sound and Vibration* **206** (2): 243:260. DOI: 10.1006/jsvi.1997.1091.
22. Christoforou, A.P. and Yigit, A.S. 2003. Fully Coupled Vibration of Actively Controlled Drillstrings. *Journal of Sound and Vibration* **267** (5): 1029-1045. DOI: 10.1016/S0022-460X(03)00359-6.
23. Close, D.A., Owens, S.C., and Macpherson, J.D. 1988. Measurement of BHA Vibration Using MWD. Paper SPE 17273 presented at the IADC/SPE Drilling Conference, Dallas, 28 February-2 March. DOI: 10.2118/17273-MS.
24. Coomer, J., Lazarus, M., Tucker, R.W., Kershaw, D., and Tegman, A. 2001. A Non-Linear Eigenvalue Problem Associated With Inextensible Whirling Strings. *Journal of Sound and Vibration*. **239** (5): 969-982. DOI: 10.1006/jsvi.2000.3190.
25. Craig, R.R. Jr. 1981. *Structural Dynamics: An Introduction to Computer Methods*. New York: John Wiley and Sons.
26. Crandall, S.H. 1961. Random Vibration of a Nonlinear System With a Set-Up Spring. Technical Report No. AFOSR709, Accession No. AD0259320, Massachusetts Institute of Technology, Cambridge, Massachusetts (June 1961).
27. Cull, S. and Tucker, R. 1999. On the Modelling of Coulomb Friction. *Journal of Physics A: Math. Gen.* **32** (11): 2103-2113. DOI: 10.1088/0305-4470/32/11/006.
28. Cunningham, R.A. 1968. Analysis of Downhole Measurements of Drill String Forces and Motions. *Trans., ASME, Journal of Engineering for Industry* **90** (May): 208-216.
29. Dareing, D.W. 1983. Rotary Speed, Drill Collars Control Drillstring Bounce. *Oil & Gas Journal* **81** (23): 63-68.
30. Dareing, D.W. 1984a. Drill Collar Length Is a Major Factor in Vibration Control. *JPT* **36** (4): 637-644. SPE-11228-PA. DOI: 10.2118/11228-PA.

31. Dareing, D.W. 1984b. Guidelines for Controlling Drill String Vibrations. *Journal of Energy Resources Technology* **106** (June): 272-277.
32. Dareing, D.W. and Livesay, B.J. 1968. Longitudinal and Angular Drillstring Vibrations With Damping. *Trans., ASME, Journal of Engineering for Industry* **90B** (4): 671-679.
33. Dareing, D.W., Tlusty, J., and Zamudio, C. 1990. Self-Excited Vibrations Induced by Drag Bits. *Trans., ASME Journal of Energy Resources Technology* **112** (March): 54-61.
34. Dawson, R., Lin, Y., and Spanos, P. 1987. Drill String Stick-Slip Oscillations. *Proc., 1987. SEM Spring Conference on Experimental Mechanics, Houston, 14-19 June, 590-595.*
35. Deily, F.H., Dareing, D.W., Paff, G.H., Ortolff, J.E., and Lynn, R.D. 1968. Downhole Measurements of Drill String Forces and Motions. *Trans., ASME, Journal of Engineering for Industry* **90** (May): 217-225.
36. Dekkers, E. 1992. The Soft Torque Rotary Soft Industry and Motions. Twente, Enschede, The Netherlands.
37. Hatch, A., Shepherd, N., Diepeveen, P., and Affleck, G. 2011. Wired drill pipe, motorized RSS improve drilling performance in North Sea wells. *World Oil*. April 2011: 33-38.
38. de Vries, H.M. 1994. The Effect of Higher Order Resonance modes on the Damping of Torsional Drillstring Vibrations. PhD dissertation, University of Twente, Enschede, The Netherlands.
39. Dubinsky, V.S.H., Henneuse, H.P., and Kirkman, M.A. 1992. Surface Monitoring of Downhole Vibrations: Russian, European and American Approaches. Paper SPE 24969 presented at the European Petroleum Conference, Cannes, France, 16-18 November. DOI: 10.2118/24969-MS.

40. Dufeyte, M-P/ and Henneuse, H. 1991. Detection and Monitoring of the Slip-Stick Motion: Field Experiments. Paper SPE 21945 presented at the SPE/IADC Drilling Conference, Amsterdam, 11-14 March. DOI: 10.2118/21945-MS.
41. Dunayevsky, V.A., Abbassian, F., and Judzis, A. 1993. Dynamic Stability of Drillstrings Under Fluctuating Weight on Bit. *SPEDC* **8** (2): 84-92. SPE-14329-PA. DOI: 10.2118/14329-PA.
42. Dykstra, M. 1996. Nonlinear Drill String Dynamics. PhD dissertation, University of Tulsa, Tulsa, Oklahoma.
43. Dykstra, M.W., Chen, D.C.-K., Warren, T.M., and Zannoni, S.A. 1994. Experimental Evaluations of Drill Bit and Drill String Dynamics. Paper SPE 28323 presented at the SPE Annual Technical Conference and Exhibition, New Orleans, 25-28 September. DOI: 10.2118/28323-MS.
44. Elsayed, M.A., Dareing, D.W., and Vonderheide, M. 1997. Effect of Torsion on Stability, Dynamic Forces, and Vibration Characteristics in Drillstrings. *Trans., ASME, Journal of Energy Resources Technology* **119** (March): 11-19.
45. Ertas, D., Bailey, J.R., Wang, L., Pastusek, P.E. 2013. Drillstring Mechanics Model for Surveillance, Root Cause Analysis, and Mitigation of Torsional and Axial Vibrations. SPE/IADC 163420.
46. Finnie, I. and Bailey, J.J. 1960. An Experimental Study of Drill-String Vibration. *Trans., ASME, Journal of Engineering for Industry* **82B** (May): 129-135.
47. Frohrib, D. and Plunkett, R. 1967. The Free Vibrations of Stiffened Drill Strings With Static Curvature. *Trans., ASME, Journal of Engineering for Industry* **89** (February): 23-30.
48. Gatlin, C. 1957. How Rotary Speed and Bit Weight Affect Rotary Drilling Rate. *Oil & Gas Journal* **55** (May): 193-198.
49. Halsey, G.W., Kyllingstad, A., Aarrestad, T.V., and Lysne, D. 1986. Drillstring Torsional Vibrations: Comparison Between Theory and Experiment on a Full-Scale

- Research Drilling Rig. Paper SPE 15564 presented at the SPE Annual Technical Conference and Exhibition, New Orleans, 5-8 October. DOI: 10.2118/15564-MS.
50. Inglis, T.A. 1988. *Directional Drilling*, Petroleum Engineering and Development Studies Vol. 2. London: Graham and Trotman.
51. Jansen, J.D. 1991. Non-Linear Rotor Dynamics as Applied to Oilwell Drillstring Vibrations. *Journal of Sound and Vibrations* **148** (1): 114-134. DOI: 10.1016/0022-460X(91)90687-F.
52. Jansen, J. and van den Steen, L. 1995. Active Damping of Self-Excited Torsional Vibrations in Oil Well Drillstrings. *Journal of Sound and Vibration* **179** (26): 637-668. DOI: 10.1006/jsvi.1995.042.
53. Javanmardi, K. and Gaspard, D. 1992. Soft Torque Rotary System Reduces Drillstring Failures. *Oil & Gas Journal* **90** (41): 68-71.
54. Kane, J. 1984. Dynamic Lateral Bottom Hole Forces And Drilling. *Drilling* **11** (August): 43-47.
55. Kardestuncer, H., Norrie, D.H., and Brezzi, F. eds. 1987. *Finite Element Handbook*. New York: McGraw-Hill.
56. Karkoub, M. June 2011. Robust Control of the Elastodynamic Vibrations of a Flexible Rotor System With Discontinuous Friction. *Journal of Vibration and Acoustics*. Vol. 133. 034501-1.
57. Khulief, Y. and Al-Naser, H. 2005. Finite Element Dynamic Analysis of Drillstrings. *Finite Elements in Analysis and Design* **41** (13): 1270-1288. DOI: 10.1016/j.finel.2005.02.003.
58. Khulief, Y.A., Al-Sulaiman, F.A., and Bashmal, S. 2007. Vibration Analysis of Drillstrings With Self-Excited Stick-Slip Oscillations. *Journal of Sound and Vibration* **299** (3): 540-558. DOI: 10.1016/j.jsv.2006.06.065.
59. Kotsonis, S.J. 1994. Effects of Axial Forces on Drillstring Lateral Vibrations. MS thesis, Rice University, Houston, Texas.

60. Kreisle, L.F. and Vance, J.M. 1970. Mathematical Analysis of the Effect of a Shock Sub on the Longitudinal Vibrations of an Oilwell Drill String. *SPEJ* **10** (4) 349-356. SPE-2778-PA. DOI: 10.2118/2778-PA.
61. Kyllingstad, A. and Halsey, G.W. 1988. A Study of Slip/Stick Motion of the Bit. *SPEDE* **3** (4): 369-373. SPE-16659-PA. DOI: 10.2118/16659-PA.
62. Lear, W.E. and Dareing, D.W. 1990. Effect of Drillstring Vibrations on MWD Pressure Pulse Signals. *Journal of Energy Resources Technology* **112** (2): 84-89. DOI: 10.1115/1.2905727.
63. Lee, C.W. and Kim, Y.D. 1986. Finite Element Analysis of Rotor Bearing Systems Using a Modal Transformation Matrix. *Journal of Sound and Vibration* **111** (3): 441-456.
64. Leine, R.I. 1997. Literature Survey on Torsional Drillstring Vibrations. Internal report No. WFW 97.069, Division of Computational and Experimental Mathematics, Eindhoven University of Technology, Eindhoven, The Netherlands.
65. Leine, R.I., van Campen, D.H., and van de Vrande, B.L. 2000. Bifurcations in Nonlinear Discontinuous Systems. Department of Mechanical Engineering, Eindhoven University of Technology, Eindhoven, The Netherlands.
66. Ligrone, A., Botto, G., and Calderoni, A. 1995. Reliability Methods Applied to Drilling Operations. Paper SPE 29355 presented at the SPE/IADC Drilling Conference, Amsterdam, 28 February-2 March. DOI: 10.2118/29355-MS.
67. Lin, Y.K. 1976. *Probabilistic Theory of Structural Dynamics*. Melbourne, Florida: Krieger Publishing.
68. Lin, Y.K. and Cai, G.Q. 1995. *Probabilistic Structural Dynamics: Advanced Theory and Applications*. McGraw-Hill Education (ISE Editions), New York.
69. Lin, Y-Q. and Wang, Y-H. 1990. New Mechanism in Drillstring Vibration. Paper OTC 6225 presented at the Offshore Technology Conference, Houston, 7-10 May.
70. Lin, Y-Q. and Wang, Y-H. 1991. Stick-Slip Vibration of Drill Strings. *Trans., ASME, Journal of Engineering for Industry* **113** (February): 38-43.

71. Macpherson, J.D., Mason, J.S., and Kingman, J.E.E. 1993. Surface Measurement and Analysis of Drillstring Vibrations While Drilling. Paper SPE 25777 presented at the SPE/IADC Drilling Conference, Amsterdam, 23-25 February. DOI: 10.2118/25777-MS.
72. Mason, J. and Sprawls, B. 1998. Addressing BHA Whirl: The Culprit in Mobile Bay 1998. *SPEDC* **13** (4): 231-236. SPE-52887-PA. DOI: 10.2118/52887-PA.
73. Massimiliano Vassallo, Giancarlo Bernasconi, Dipartimento di Elettronica e Informazione, POLIMI; Vittorio Rampa, I.E.I.I.T.-MI, CNR, 2003. Bit Bounce Detection Using Neural Networks. SEG Conference Paper, 2004-0348.
74. McCann, R.C. and Suryanarayana, P.V.R. 2001. Horizontal Well Path Planning and Correction Using Optimization Techniques. *Journal of Energy Resources Technology* **123** (3): 187-193. DOI: 10.1115/1.1386390.
75. Melakhessou, H., Berlioz, A., and Ferraris, G. 2003. A Nonlinear Well-Drillstring Interaction Model. *Journal of Vibration and Acoustics* (January): 46-52.
76. Millheim, K.K. and Apostal, M.C. 1981. The Effect of Bottomhole Assembly Dynamics on the Trajectory of a Bit. *JPT* **33** (12): 2323-2338. SPE-9222-PA. DOI: 10.2118/9222-PA.
77. Mitchell, R.F. 2008. Tubing Buckling - The Rest of the Story. *SPEDE* **23** (2): 112-122. SPE-96131-PA. DOI: 10.2118/96131-PA.
78. Murtha, J. 1997. Monte Carlo Simulation: Its Status and Future. *JPT* **49** (4): 361-370. SPE-37932-PA. DOI: 10.2118/37932-PA.
79. Narasimhan, S. 1987. A Phenomenological Study of Friction Induced Torsional Vibrations of Drill Strings. MS thesis, Rice University, Houston.
80. Navarro-Lopez, E.M. and Cortes, D. 2007. Avoiding Harmful Oscillations in a Drillstring Through Dynamical Analysis. *Journal of Sound and Vibration* **307** (1-2): 152-171. DOI: 10.1016/j.jsv.2007.06.037.

81. Nicholson, J.W. 1994. An Integrated Approach to Drilling Dynamics Planning, Identification, and Control. Paper SPE 27537 presented at the IADC/SPE Drilling Conference, Dallas, 15-18 February. DOI: 10.2118/27537-MS.
82. Paidoussis, M.P., Luu, T.P., and Prabhakar, S. 2007. Dynamics of a Long Tubular Cantilever Conveying Fluid Downwards, Which Then Flows Upwards Around the Cantilever as a Confined Annular Flow. *Journal of Fluids and Structures* **24** (1): 111-128. DOI: 10.1016/j.jfluidstructs.2007.07.004.
83. Paslay, P.R. and Bogy, D.B. 1963. Drill String Vibrations Due to Intermittent Contact of Bit Teeth. *Trans ASME, Journal of Engineering for Industry* **85B** (May): 187-194.
84. Payne, M.L. 1992. Drilling Bottom-Hole Assembly Dynamics. PhD dissertation, Rice University, Houston.
85. Payne, M.L., Abbassian, F., and Hatch, A.J. 1995. Drilling Dynamic Problems and Solutions for Extended-Reach Operations. In *Drilling Technology 1995*, PD-Volume 65, ed. J.P. Vozniak, 191-203. New York: ASME.
86. Peterson, S.K., Murtha, J.A., and Roberts, R.W. 1995. Drilling Performance Predictions: Case Studies Illustrating the Use of Risk Analysis. Paper SPE 29364 presented at the SPE/IADC Drilling Conference, Amsterdam, 28 February-2 March. DOI: 10.2118/29364-MS.
87. Placido, J.C.R., Santos, H.M.R., and Galeano, Y.D. 2002. Drillstring Vibration and Wellbore Instability. *Journal of Energy Resources Technology* **124**: 217-222. DOI: 10.1115/1/1.1501302.
88. Plunkett, R. 1967. Static Bending Stresses in Catenaries and Drill Strings. *Trans., ASME, Journal of Engineering for Industry* **89B** (1): 31-36.
89. Poletto, F. and Bellezza, C. 2006. Drill-Bit Displacement-Source Model: Source Performance and Drilling Parameters. *Geophysics* **71** (5): 121-129. DOI: 10.1190/1.2227615.
90. Politis, N.P. 2002. An Approach for Efficient Analysis of Drill-String Random Vibrations. MS thesis, Rice University, Houston.

91. Przemieniecki, J.S. 1968. *Theory of Matrix Structural Analysis*. New York: McGraw-Hill Book Company.
92. Puebla, H. and Alvarez-Ramirez, J. 2008. Suppression of Stick-Slip in Drillstrings: A Control Approach Based on Modeling Error Compensation. *Journal of Sound and Vibration* **310** (4-5): 881-901. DOI: 10.1016/j.jsv.2007.08.020.
93. Raftoyiannis, J. and Spyrakos, C. 1997. *Linear and Nonlinear Finite Element Analysis in Engineering Practice*. Pittsburgh, Pennsylvania: ALGOR.
94. Reddy, J.N. 1993. *An Introduction to the Finite Element Method*, second edition. New York: McGraw-Hill Science/Engineering/Math.
95. Richard, T., Germa, C., and Detournay, E. 2004. Self-Excited Stick-Slip Oscillations of Drill Bits. *Comptes Rendus Mecanique* **332** (8): 619-626. DOI: 10.1016/j.crme.2004.01.016.
96. Richard, T., Germa, C., and Detournay, E. 2007. A Simplified Model To Explore the Root Cause of Stick-Slip Vibrations in Drilling Systems With Drag Bits. *Journal of Sound and Vibration* **305** (3): 432-456. DOI: 10.1016/j.jsv.2007.04.015.
97. Roberts, J.B. and Spanos, P.D. 1990. *Random Vibration and Statistical Linearization*. New York: John Wiley and Sons.
98. Sampaio, R., Piovan, M., and Lozano, G.V. 2007. Coupled Axial/Torsional Vibrations of Drill-Strings by Means of Non-Linear Model. *Mechanics Research Communications* **34** (September): 497-502. DOI: 10.1016/j.mechrescom.2007.03.005.
99. Sengupta, A. 1993. Dynamic Modeling of Roller Cone Bit Lift-Off in Rotary Drilling. PhD dissertation, Rice University, Houston.
100. Serrarens, A.F.A., van de Molengraft, M.J.G., Kok, J.J., and van den Steen, L. 1998. H<sub>∞</sub> Control for Suppressing Stick-Slip in Oil Well Drillstrings. *IEEE Control System* **18** (2): 19-30. DOI: 10.1109/37.664652.
101. Shell International Exploration and Production. 2012-2014. Internal Reports.

102. Shivers, R.M. III and Comangue, R.J. 1993. Operational Decision Making for Stuck-Pipe Incidents in the Gulf of Mexico: A Risk Economics Approach. *SPEDC* **8** (2): 125-130. SPE-21998-PA. DOI: 10.2118/21998-PA.
103. Shyu, R-J. 1989. Bending Vibration of Rotating Drill Strings. PhD dissertation. MIT Department of Ocean Engineering, Cambridge, Massachusetts.
104. Smit, A. 1995. Using Optimal Control Techniques To Dampen Torsional Drillstring Vibrations. PhD dissertation, University of Twente, Enschede, The Netherlands.
105. Spanos, P.D., Sengupta, A.K., Cunningham, R.A., and Paslay, P.R. 1995. Modeling of Roller Cone Bit Lift-Off Dynamics in Rotary Drilling. *Journal of Energy Resources Technology* **117** (3): 197-207. DOI: 10.1115/1.2835341.
106. Spanos, P.D., Payne, M.L., and Secora, C.K. 1997. Bottom-Hole Assembly Modeling and Dynamic Response Determination. *Journal of Energy Resources Technology* **119** (3): 153-158. DOI: 10.1115/1.2794983.
107. Spanos, P.D., Chevallier, A.M., and Politis, N.P. 2002. Nonlinear Stochastic Drill-String Vibrations. *Journal of Vibration and Acoustics* **124** (4): 512-518. DOI: 10.1115/1.1502669.
108. Spanos, P.D., Chevallier, A.M., Politis, N.P., and Payne, M.L. 2003. Oil and Gas Well Drilling: A Vibrations Perspective. *Shock & Vibration Digest* **35** (March 2003): 85-103. DOI: 10.1177/0583102403035002564.
109. Thoft-Christensen, P. and Murotsu, Y. 1986. *Application of Structural Systems: Reliability Theory*. New York: Springer-Verlag.
110. Thomson, W.T. and Dahleh, M.D. 1997. *Theory of Vibration With Applications*, fifth edition. Upper Saddle River, New Jersey: Prentice-Hall.
111. Trindade, M.A., Wolter, C., and Sampaio, R. 2005. Karhunen-Loeve Decomposition of Coupled Axial/Bending Vibrations of Beams Subject to Impacts. *Journal of Sound and Vibration* **279** (3-5): 1015-1036. DOI: 10.1016/j.jsv.2003.11.057.

112. Tucker, W.R. and Wang, C. 1999. On the Effective Control of Torsional Vibrations in Drilling Systems. *Journal of Sound and Vibration* **224** (1): 101-122. DOI: 10.1006/jsvi.1999.2172.
113. van den Steen, L. 1997. Suppressing Stick-Slip-Induced Drillstring Oscillations: A Hyperstability Approach. PhD dissertation, University of Twente, Enschede, The Netherlands.
114. Van Der Heijden, G.H. 1993. Bifurcation and Chaos in Drillstring Dynamics. *Chaos, Solitons & Fractals* **3** (2): 219-247. DOI: 101016/0960-0779(93)90068-C.
115. Vandiver, K.J., Nicholson, J.W., and Shyu, R.-J. 1990. Case Studies of the Bending Vibration and Whirling Motion of Drill Collars. *SPEDE* **5** (4): 282-290. SPE-18652-PA. DOI: 10.2118/18652-PA.
116. Vas, M.A. and Patel, M.H. 1995. Analysis of Drill Strings in Vertical and Deviated Holes Using the Galerkin Technique. *Engineering Structures* **17** (6): 437-442. DOI: 10.1016/0141-0296(95)00098-R.
117. Viguie, R., Kerschen, G., Golinval, J.-C., McFarland, D.M., Bergman, L.A., Vakakis, A.F., and van de Wouw, N. 2009. Using Passive Nonlinear Targeted Energy Transfer To Stabilize Drill-String Systems. *Mechanical Systems and Signal Processing: Special Issue on Nonlinear Structural Dynamics* **23** (January): 148-169. DOI: 10.1016/j.ymssp.2007.07.001.
118. Warren, T.M., Brett, J.F., and Sinor, L.A. 1990. Development of a Whirl-Resistant Bit. *SPEDE* **5** (4): 267-274; *Trans., AIME*, **289**. SPE-19572-PA. DOI: 10.2118/19572-PA.
119. Williams, A.N. June 1984. Nonlinear Inertia Forces on Slender Cylindrical Members. *Journal of Energy Resources Technology*. Volume 106.
120. Wise, J.L., Mansure, A.J., and Blankenship, D.A. 2005. Hard Rock Field Performance of Drag Bits and a Downhole Diagnostics-While-Drilling (DWD) Tool. *GRC Transactions* **29** (September).

121. Wolf, S.F., Zacksenhouse, M., and Arian, A. 1985. Field Measurements of Downhole Drillstring Vibrations. Paper SPE 14330 presented at the SPE Annual Technical Conference and Exhibition, Las Vegas, Nevada, USA, 22-26 September. DOI: 10.2118/14330-MS.
122. Yigit, A.S. and Christoforou, A.P. 1998. Coupled Torsional and Bending Vibrations of Drillstrings Subject to Impact With Friction. *Journal of Sound and Vibration* **215** (1): 167-181. DOI: 10.1006/jsvi.1998.1617.
123. Yigit, A.S. and Christoforou, A.P. 2000. Coupled Torsional and Bending Vibrations of Actively Controlled Drillstrings. *Journal of Sound and Vibration* **234** (1): 67-83. DOI: 10.1006/jsvi.1999.2854.
124. Yigit, A.S. and Christoforou, A.P. 2006. Stick-Slip and Bit-Bounce Interaction in Oil-Well Drillstrings. *J. Energy Resour. Technol.* 128(4), 268-274 (Feb 19, 2006) (7 pages); DOI:10.1115/1.2358141
125. Zamanian, M., Khadem, S.E., and Ghazavi, M.R. 2007. Stick-Slip Oscillations of Drag Bits by Considering Damping of Drilling Mud and Active Damping System. *Journal of Petroleum Science and Engineering* **59** (3-4): 289-299. DOI: 10.1016/j.petrol.007.04.008.
126. Zhenhai. 2009. From Vibration to Bouncing: The Introduction of Stress Wave Transmitting Theory., SPE 123839-MS.

## **Vita**

Rebecca Leigh Leonard was born in Fort Smith, Arkansas. After graduating from Southside High School in 2006, she took a gap year before attending Hendrix College in Conway, Arkansas. Rebecca studied Physics at Hendrix for two years before transferring into the College of Engineering at the University of Arkansas. Rebecca graduated from the University of Arkansas in December 2011 with a Bachelor of Science in Mechanical Engineering and entered the Graduate School at The University of Texas at Austin in January 2011. In September 2013, Rebecca accepted a position in the Drilling Mechanics Technology department at Shell Oil Company – hired to develop and deploy drilling automation technology on a global scale.

Address: Rebecca.L.Leonard@gmail.com

This thesis was typed by the author.